International
Progress Report

IPR-03-03

Äspö Hard Rock Laboratory

Äspö Pillar Stability Experiment

Design of heaters and preliminary results from coupled 2D thermo-mechanical modelling

Anders Fredriksson
Isabelle Staub
Thomas Janson

Golder Associates AB

February 2003
Reviewed February 2003
Revised version May 2003

Svensk Kärnbränslehantering AB
Swedish Nuclear Fuel
and Waste Management Co
Box 5864
SE-102 40 Stockholm Sweden
Tel +46 8 459 84 00
Fax +46 8 661 57 19

Äspö Hard Rock
Laboratory

Report no.	No.
IPR-03-03	F86K
Author	Date
Anders Fredriksson Isabelle Staub Thomas Janson	2003-05-09
Checked by	Date
Christer Andersson	2003-05-13
Approved	Date
Christer Svemar	2003-05-21

Äspö Hard Rock Laboratory

Äspö Pillar Stability Experiment

Design of heaters and preliminary results from coupled 2D thermo-mechanical modelling

Anders Fredriksson
Isabelle Staub
Thomas Janson

Golder Associates AB

February 2003
Reviewed February 2003
Revised version May 2003

Keywords: Äspö Pillar Stability Experiment, spalling, 2D thermo-mechanical modelling, JobFem, deformation, stresses, sensitivity analysis

Abstract

A site scale Pillar Stability Experiment is planned in the Äspö Hard Rock Laboratory. One of the experiment's aim is to demonstrate the possibilities of predicting spalling in the fractured rock mass.

In order to investigate the probability and conditions for spalling in the pillar preliminary numerical simulations have been undertaken. This report presents the results obtained from 2D coupled thermo-mechanical numerical simulations that have been done with the Finite Element based programme JobFem.

The optimal number and location of heaters were determined by numerical simulations, and the layout of the experiment was defined. The suggested heating system is composed of 4 heaters, located 2 on each side of the pillar.

Complementary simulations were conducted to achieve the evolution of temperature, deviatoric stresses and total stresses during the experiment. A sensitivity analysis of input parameters (deformation's modulus, thermal conductivity, in situ stresses) have been conducted in order to catch the potential range of stresses and temperature in the rock mass during the experiment.

The results of the simulations point out that the required level of stress for spalling can be reached in the pillar even when accounting for the "lowest" combination.

Sammanfattning

Ett fullskaleförsök angående pelarstabilitet planeras vid Äspö laboratoriet. En av målsättningarna med experiment är att demonstrera möjligheten att prediktera risken för smällberg i en uppsprucken bergmassa.

För att undersöka sannolikheten och förutsättningarna till smällberg i bergmassan genomfördes preliminära numeriska simuleringar. Denna rapport redovisar resultaten från 2D - kopplade, termomekaniska numeriska beräkningar som utfördes med det finita element - baserade programmet JobFem.

Det optimala antalet värmare och deras utplacering bestämdes med hjälp av numeriska beräkningar. Den föreslagna experimentuppsättningen innefattar 4 värmare som placeras parvis på var sida av pelaren.

Den numeriska modellen byggdes upp utifrån denna experimentuppsättning och ytterligare simuleringar genomfördes. Utvecklingen av temperatur och spänningar registrerades och studerades under olika steg av experimentet. En känslighetsanalys för några ingångsparametrar (deformationsmodul, termisk konduktivitet, initiala spänningar) utfördes för att bedöma spridningen av beräkningsutfallet och spannet av förväntade temperatur- och spänningsförändringar i bergmassan.

Simuleringarna visade att förutsättningarna för smällberg i berget nås även för den parameterskombination som ger den lägsta temperatur- och spänningsökningen.

Contents

1 Introduction

1.1 Background

SKB is planning a full-scale rock mechanics experiment. The experiment will study pillar stability. The main objectives with the pillar stability experiment are summarized in /Andersson, 2003/:

1. Demonstrate the capability to predict spalling in a fractured rock mass
2. Demonstrate the effect of backfill (confining pressure) on the rock mass response
3. Comparison of 2D and 3D mechanical and thermal predicting capabilities

The experiment will be performed in the Äspö Hard Rock Laboratory (HRL) at level –450 m. Three alternative locations are studied, alternative 1 is located north of the F-tunnel, alternative 2 is located south of the TBM-tunnel and alternative 3 180° from alternative 2, see Figure 1-1. A new tunnel will be excavated with start from the F-tunnel or TBM-tunnel and from the floor of the new tunnel two vertical holes will be drilled. The pillar between the holes will be heated and the additional thermal stresses shall force the rock in the holes walls to spall.

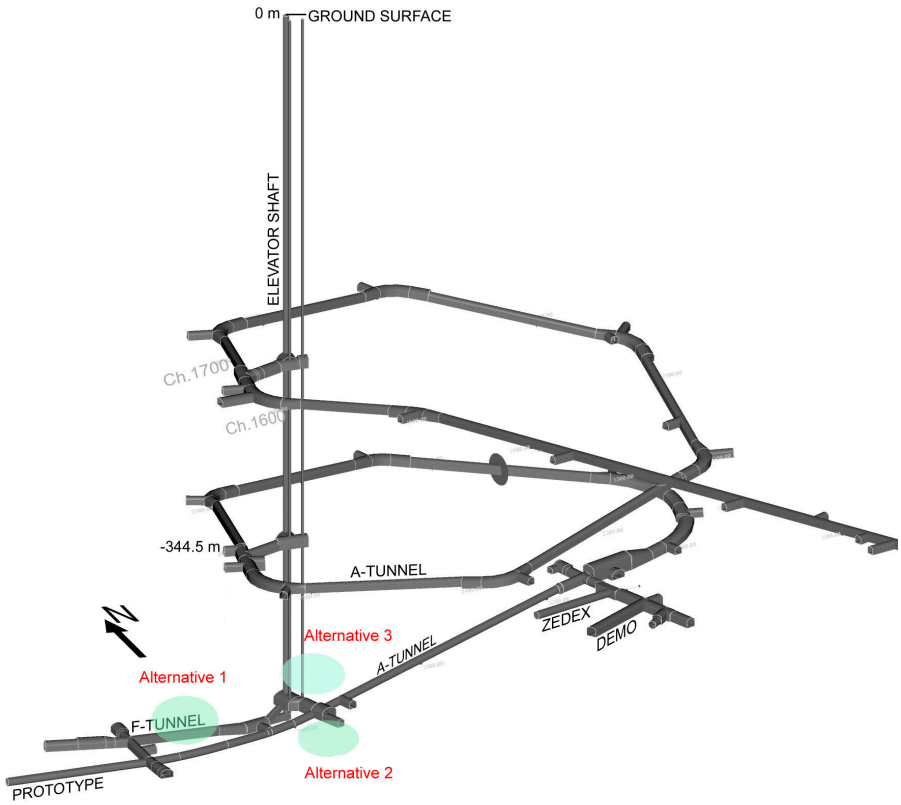

Figure 1-1. *3D view of the tunnel-system. Localization of the of the experiment volumes.*

1.2 Objective

In order to achieve the best possible results during the experiment the optimal number and location of heaters have been determined by means of numerical simulations. Several alternatives have been run and their outcome compared and analyzed. The results are presented in section 2.

This study had to take into consideration the location of the acoustic emission system, and the maximum temperature the emitters could stand, as well as the level of stresses estimated to be optimal for the initiation of spalling in the pillar.

After having determined the optimal layout for the experiment, coupled 2D thermo-mechanical simulations have been run. The preliminary mechanical and thermal properties assigned to the rock mass are estimated in Staub *et al.*, 2003. The results of the 2D modeling are presented in section 3.

2 Determination of the optimal layout for heaters

This section reports the numerical analysis conducted to determine the influence of the number and position of the heaters in the proximity of the pillar. The assessed optimal layout is illustrated and discussed in sections 2.4 and 2.5.

2.1 Material data

The following input data have been used for the modeling:

- Initial temperature 13.2 ^{o}C
- Thermal conductivity, rock 2.56 W/m, K
- Volume heat capacity, rock 2.09 MJ/m^3,K
- Volume heat capacity, water 4.18 MJ/m^3,K
- Volume heat capacity, air 0.00129 MJ/m^3, K
- Coefficient of linear expansion 7.0 E-06 l/K
- Young's modulus 68 GPa
- Poisson's ratio 0.2
- Initial stresses σ_1 = 30 MPa (310/30) (Äspö96)

  σ_2 = 15 MPa (082/53) (Äspö96)

  σ_3 = 10 MPa (210/20) (Äspö96)
- Heater ϕ: 32 mm; effect: 100 – 500 W/m

N.B. it should be stressed that the input data used for defining the layout of the experiment are not exactly reflecting the input data defined in the report "Geology and properties of the rock mass around the experiment volume" /Staub *et al.*, 2003/. The modeling for the layout started before the complete evaluation of mechanical and thermal properties of rock and fractures was achieved. Hence input data for the thermo-mechanical modeling should be taken from the aforementioned report, and not from this section.

This does not influence the results of the thermal modeling as the study focuses on relative changes and comparisons between different alternatives, all models being run with the input data as stated in this section.

2.2 Method of analysis

Heat flow and temperature induced stresses have been calculated under plain strain condition. The finite element code JobFem was used.

The heaters were modeled as a point heat source in the plain strain model with a given effect. A maximum temperature of 200 °C was specified at the heater. If the temperature at the heater reached 200 °C the effect was reduced to keep the temperature at 200 °C. The effects of the heaters were varied from 100 – 500 W/m.

One of the large holes is filled with water and the other with air. This was considered in the transient heat calculation.

The temperature increase and temperature induced stresses after 60 days of heating were compared between the different alternatives and for different heater effects.

The size of the model was chosen large enough to avoid influence of the boundary. Figure 2-1 illustrates the whole model for one alternative and the temperature situation after 60 days of heating. The figure illustrates that the temperature increase has not reached the boundary of the model, and validates the size of the model chosen for further modeling.

The stress changes due to excavation of tunnel, holes and slots were given by SKB. The boundary element code Examine 3D was used to calculate the stress changes.

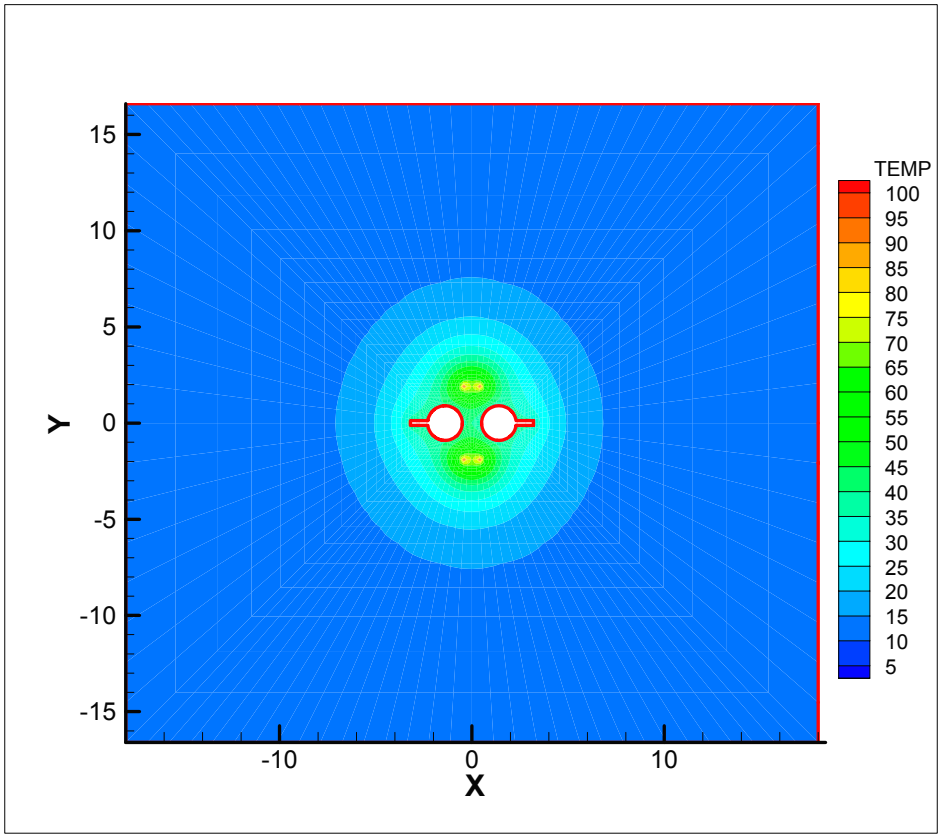

Figure 2-1. *Illustration of the zone of influence of heating compared to the size of the model.*

2.3 Analysis of different alternatives

2.3.1 Geometry of the alternatives

Three different alternatives based on varying number and location of the heaters have been tested, see Figure 2-2 to Figure 2-4. To compare the different alternatives the temperature and temperature induced stresses are registered in three points A, B and C, located as illustrated in Figure 2-5.

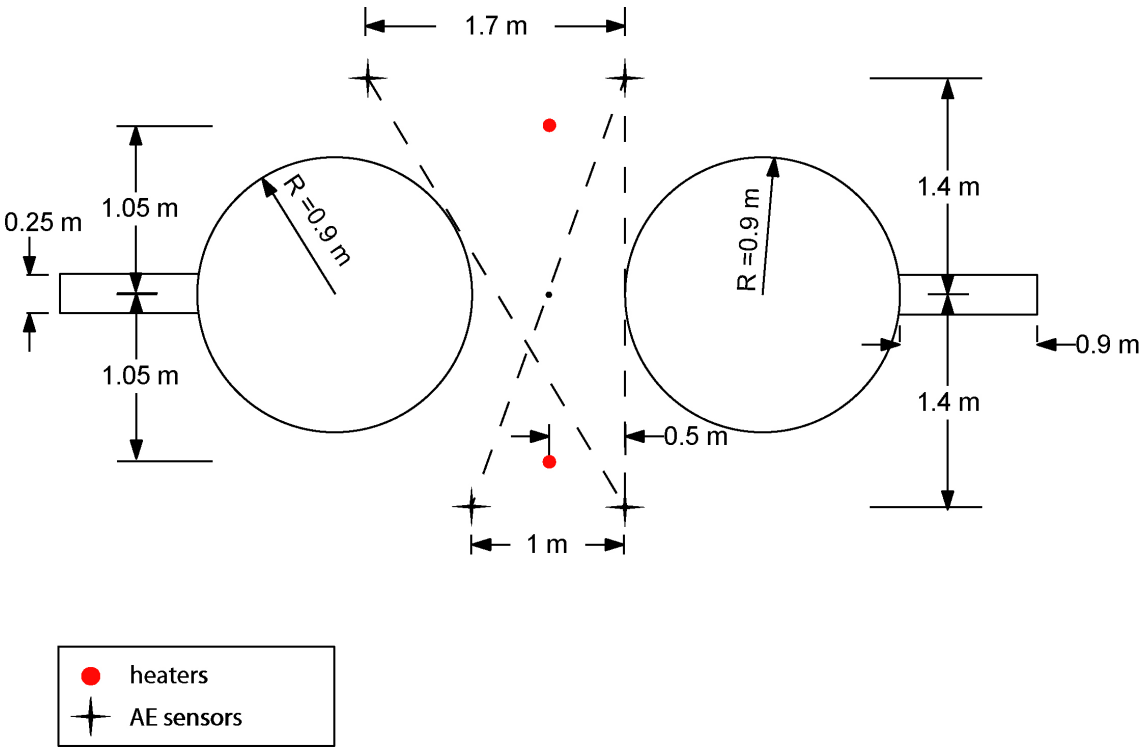

Figure 2-2. *Alternative 1, with two heaters.*

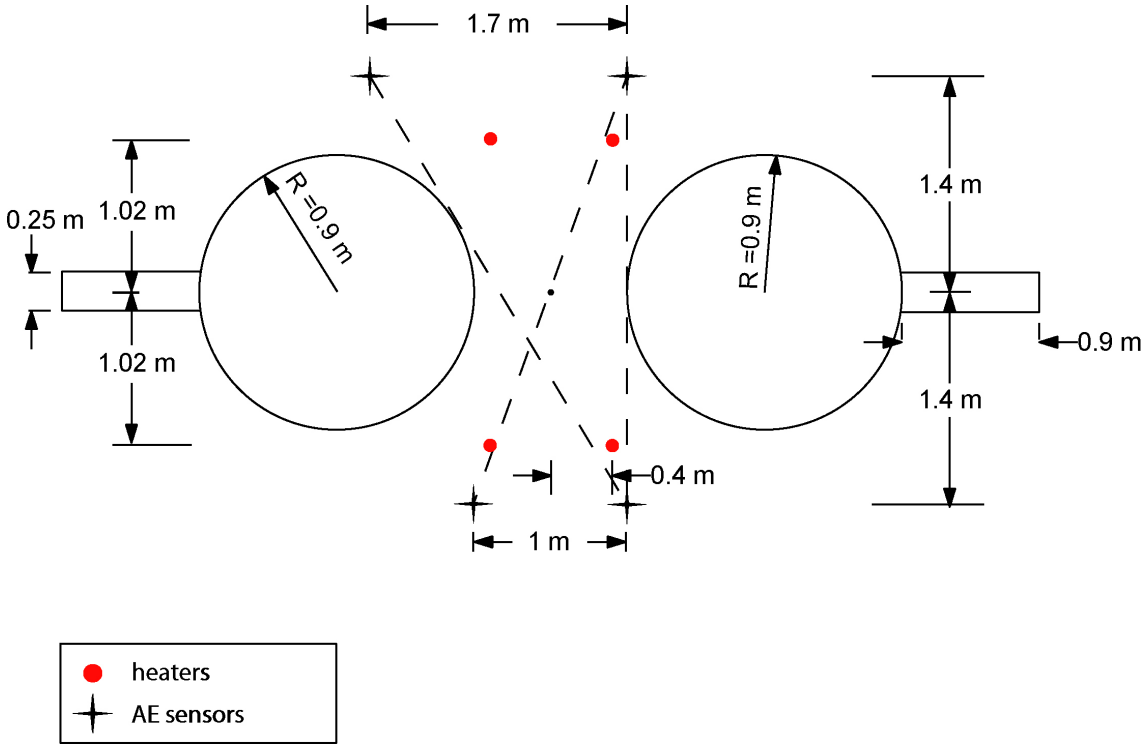

Figure 2-3. *Alternative 2, with four heaters inside the volume defined by the AE-sensors.*

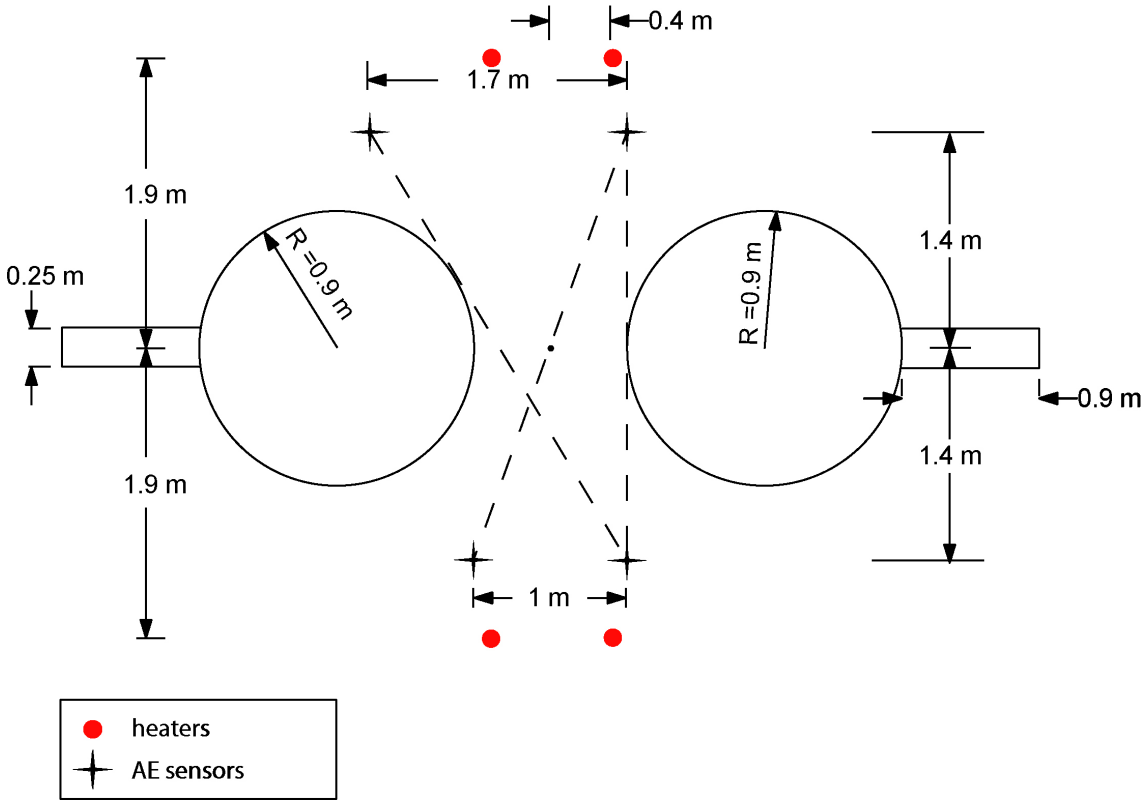

Figure 2-4. *Alternative 3, with four heaters outside the volume defined by the AE-sensors.*

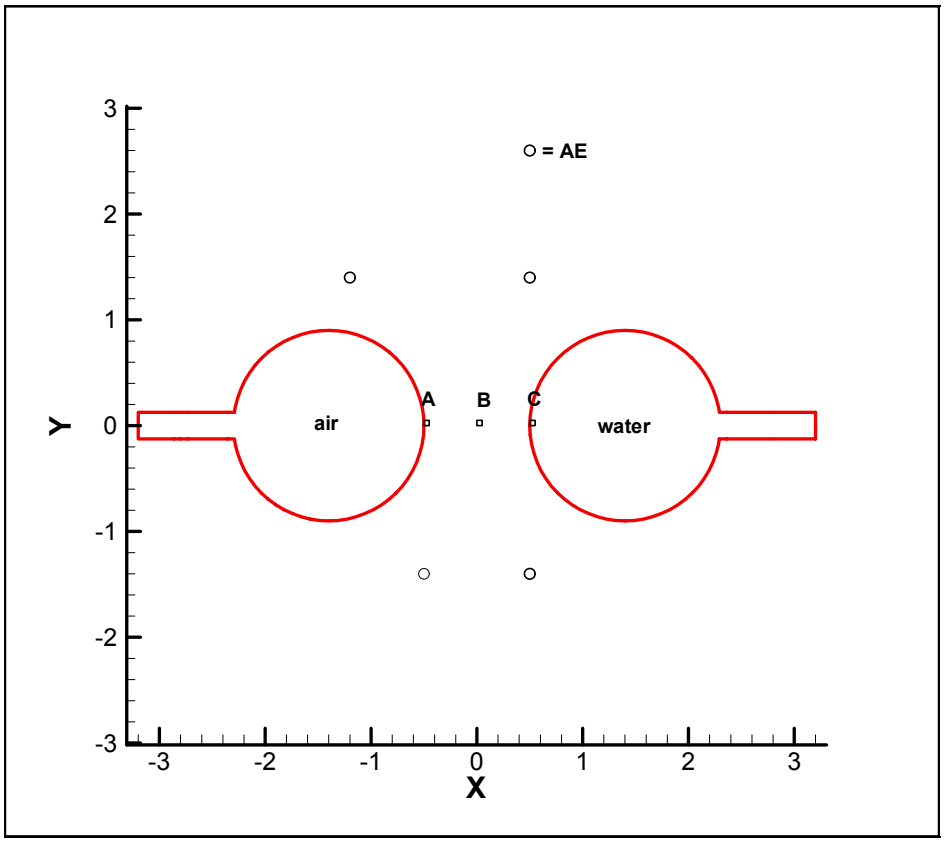

Figure 2-5. *Location of the recording points A, B and C.*

2.3.2 Presentation of the results

Alternative 1

The temperature increase and temperature induced stresses in the measuring points A - C after 60 days of heating for alternative 1 are presented in Figure 2-6 and Figure 2-7. In Appendix A the results from the heater effects of 200 and 400 W/m are presented as contour maps. The effect to the heaters has been varied from 100 – 500 W/m.

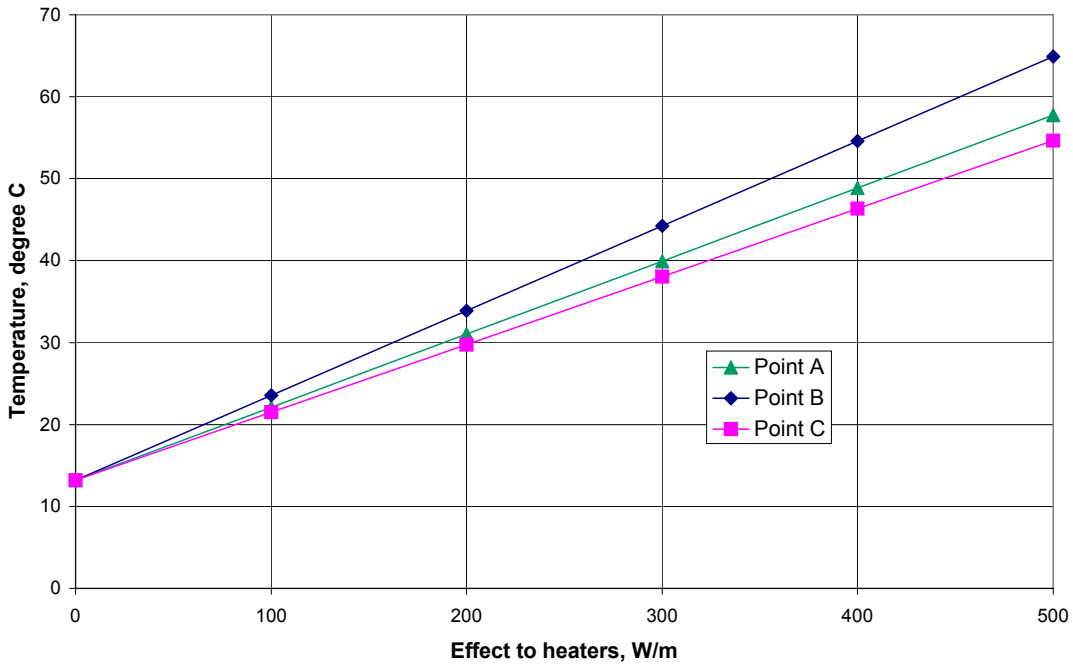

Figure 2-6. *Temperature increase after 60 days of heating, alternative 1.*

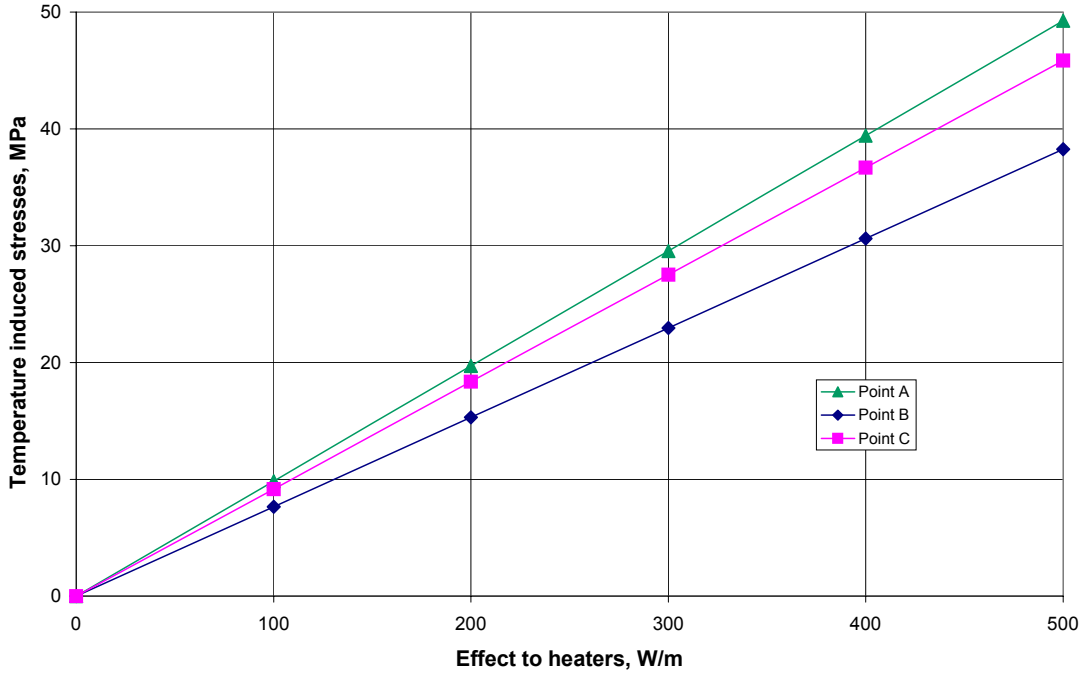

Figure 2-7. *Temperature induced stresses after 60 days of heating, alternative 1.*

Alternative 2

The temperature increase and temperature induced stresses in the measuring points A-C after 60 days of heating for alternative 2 with four heaters are presented in Figure 2-8 and Figure 2-9. In Appendix B the results are presented as contour maps. The effect to the heaters has been varied from 100 – 500 W/m.

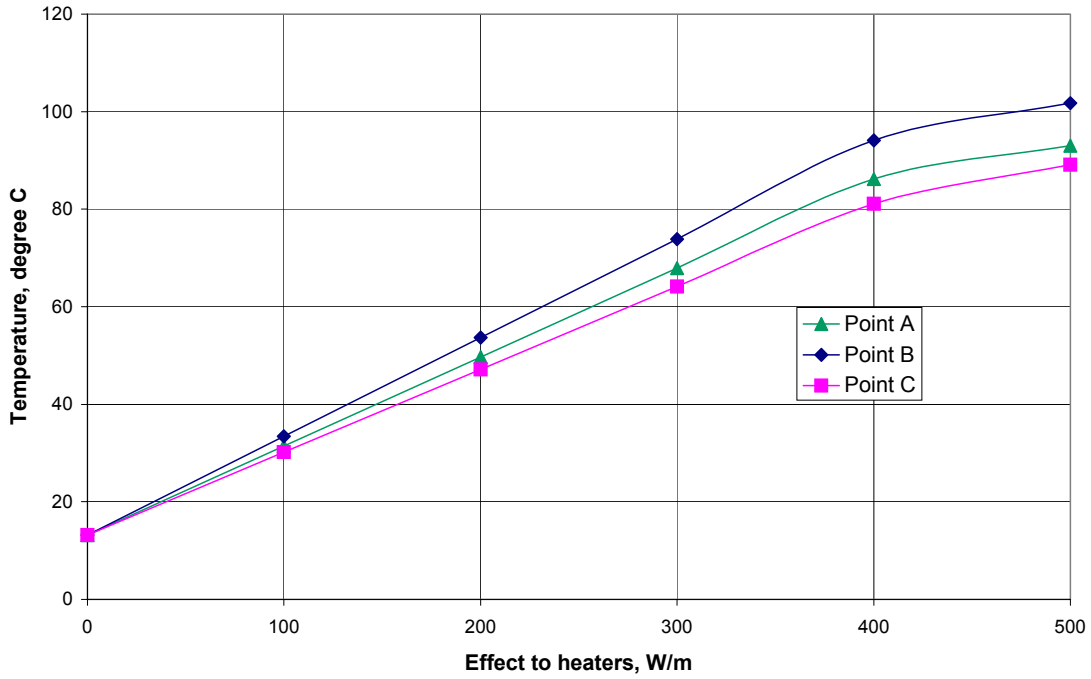

Figure 2-8. *Temperature increase after 60 days of heating, alternative 2.*

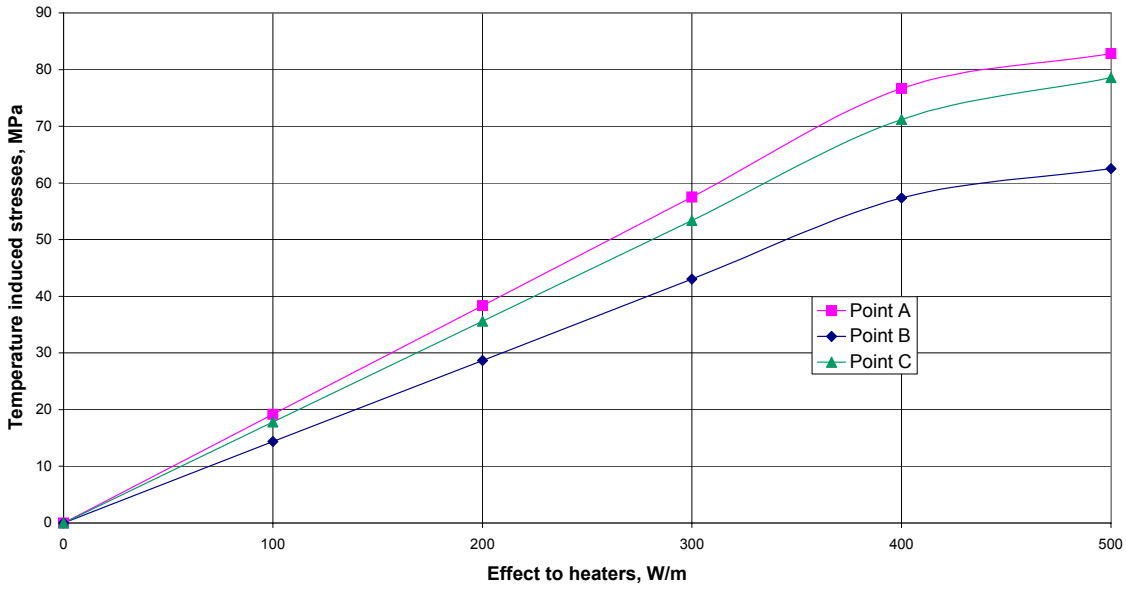

Figure 2-9. *Temperature induced stresses after 60 days of heating, alternative 2.*

Note: the non-linear behavior of the curves at high effect of the heaters is due to the constraint of a maximal temperature of 200° applied at the heaters. This does also have an impact on the temperature evolution in the monitoring points.

Alternative 3

The temperature increase and temperature induced stresses in the measuring points A-C after 60 days of heating for alternative 3 with four heaters are presented in Figure 2-10 and Figure 2-11. In Appendix C the results are presented as contour maps. The effect to the heaters has been varied from 100 – 500 W/m.

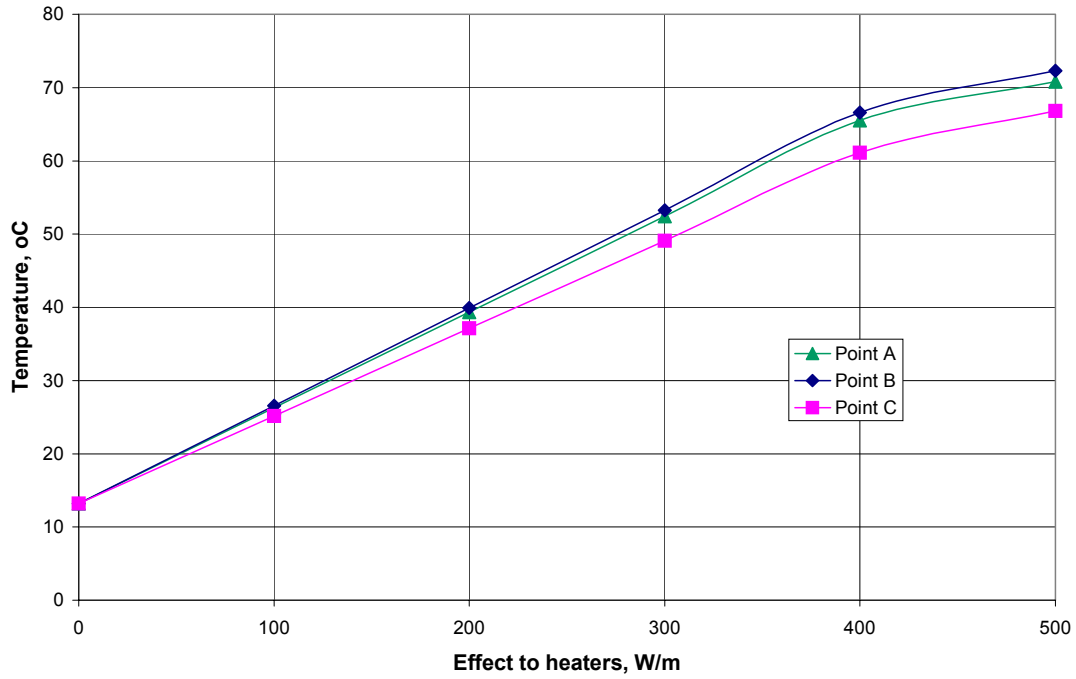

Figure 2-10. *Temperature increase after 60 days of heating, alternative 3.*

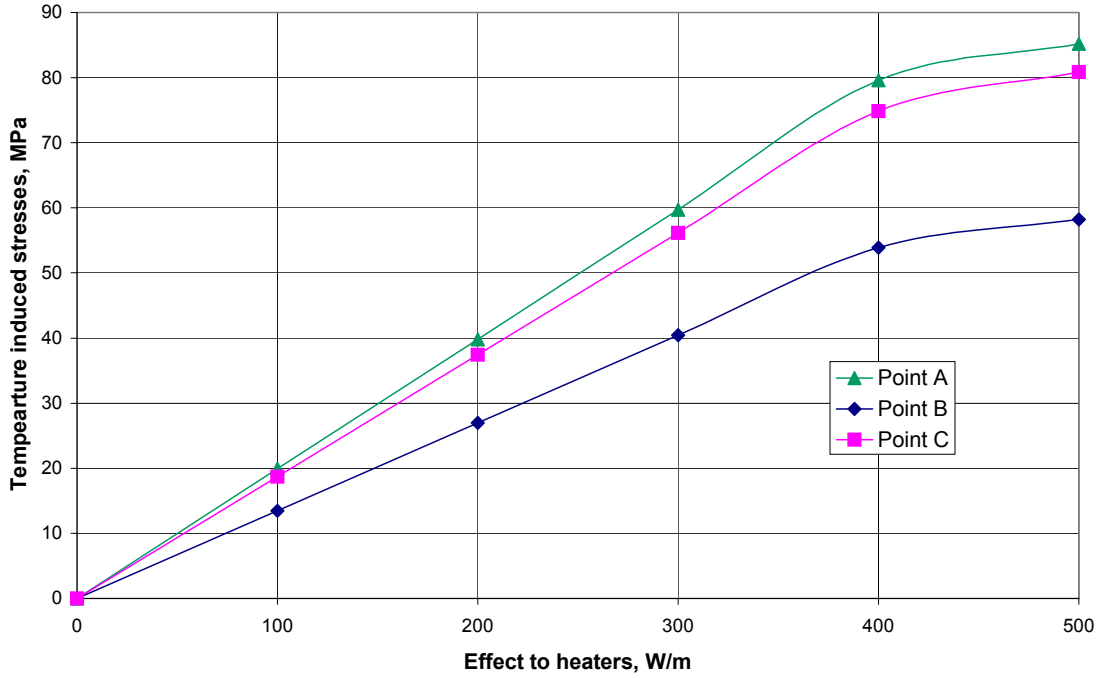

Figure 2-11. *Temperature induced stresses after 60 days of heating, alternative 3.*

2.3.3 Discussion

The magnitude of temperature induced stresses in the pillar is in about the same range for both alternatives 2 and 3, maximum 40 MPa at 200 W/m. Alternative 1 gives only half the stress increase. An advantage with alternative 3 is that the heaters are located outside the volume defined by the AE-monitoring holes, and this alternative is therefore recommended. An effect around 200 W/m will give a size of the heaters that is practical to handle.

2.4 Proposed layout for the experiment

Recommendations for location of the acoustic emission system, the heaters and holes for recording temperature during the experiment are presented in Figure 2-12. The effect of the heaters shall be variable from 100 to 300 W/meter. The heaters shall be at least 0.5 m longer than the 1.8 m diameter boreholes.

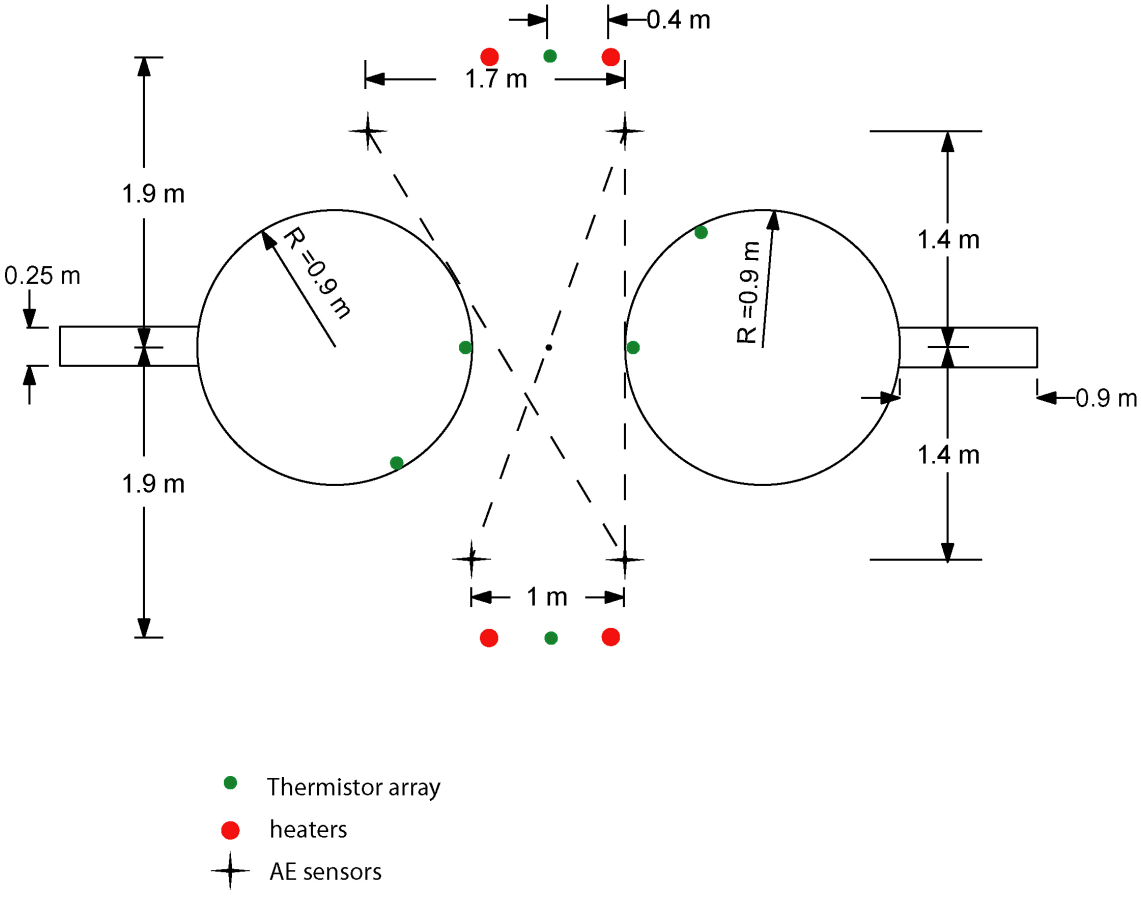

Figure 2-12. *The proposed layout of the experiment.*

The installation of thermistor arrays to monitor the evolution of temperature in the rock mass during the experiment is recommended and the suggested position of these arrays is illustrated in Figure 2-12.

2.5 Analysis of the proposed layout

Further simulations have been run on the proposed layout. For this layout, illustrated in Figure 2-12, the temperature increase and temperature induced stresses have been calculated during 120 days of heating with a heater effect of 200 W/m. The temperature induced stresses have been added to the stresses calculated with the 3D boundary element program Examine 3D. Two horizontal sections located 0.5 m and 1.5 m below the tunnel floor have been studied.

The calculated temperature increase in the measuring points A – C is shown in Figure 2-13. In Appendix D the results are presented as contour maps.

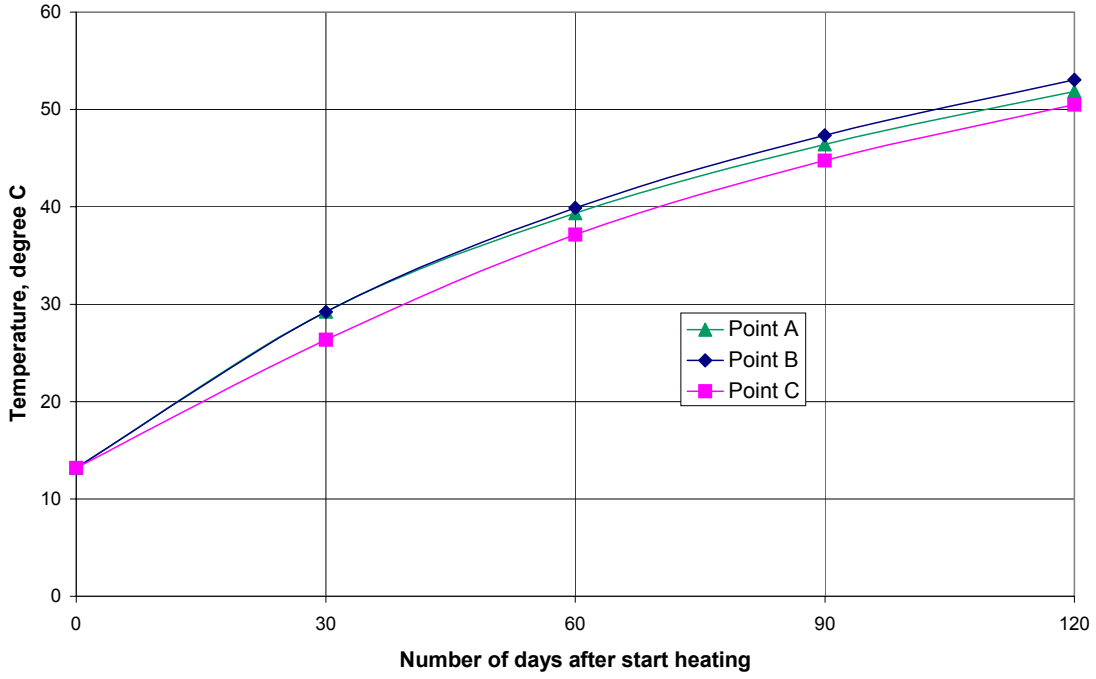

Figure 2-13. *Temperature increase during 120 days of heating, 200 W/m.*

The major stress reached in the rock mass after heating is illustrated in the measuring points A – C, 1.5 m and 0.5 m below the tunnel floor, see Figure 2-14 and Figure 2-15. In Appendix D the results are presented as contour maps.

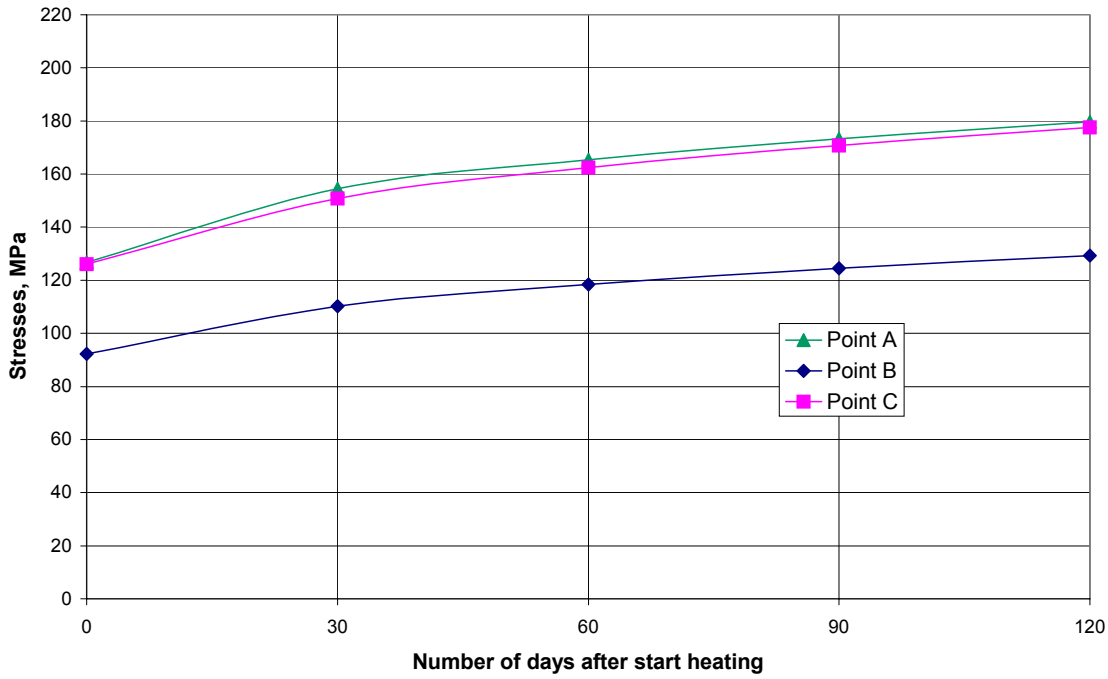

Figure 2-14. *Major stress increase in measuring points A – C, 1.5 m below the tunnel floor during 120 days of heating.*

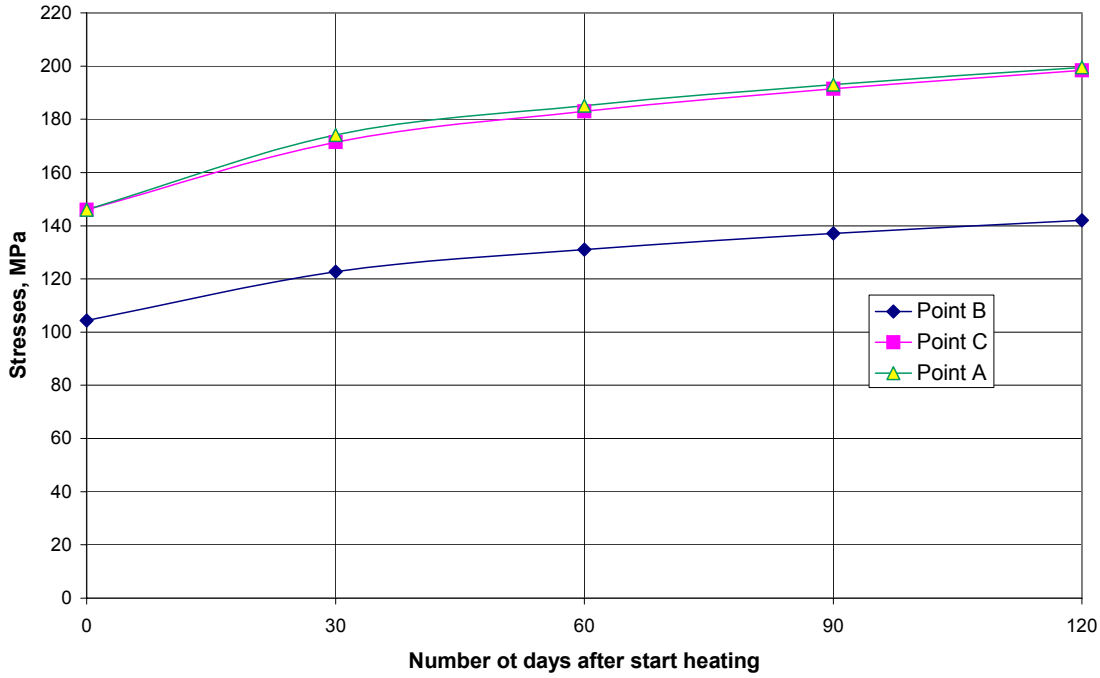

Figure 2-15. *Major stress increase in measuring points A – C, 0.5 m below the tunnel floor during 120 days of heating.*

2.6 Conclusions

The aim of the modeling was to determine the optimal layout for heaters during the experiment, in order to get temperature induced stresses high enough to initiate spalling in the pillar's wall. For the recommended layout 4 heaters are required, see Figure 2-4. The effect of the heaters shall be variable from 100 to 300 W/meter, and the heaters shall be 0.5 m longer than the 1.8 diameter boreholes. It is recommended to set monitoring equipment for the following-up of heating of the rock mass in 6 locations, with thermosensors located every meter along the holes (Figure 2-16). Four of these equipments are on the boreholes walls, and two are on specific holes located between the heaters on both sides of the pillar.

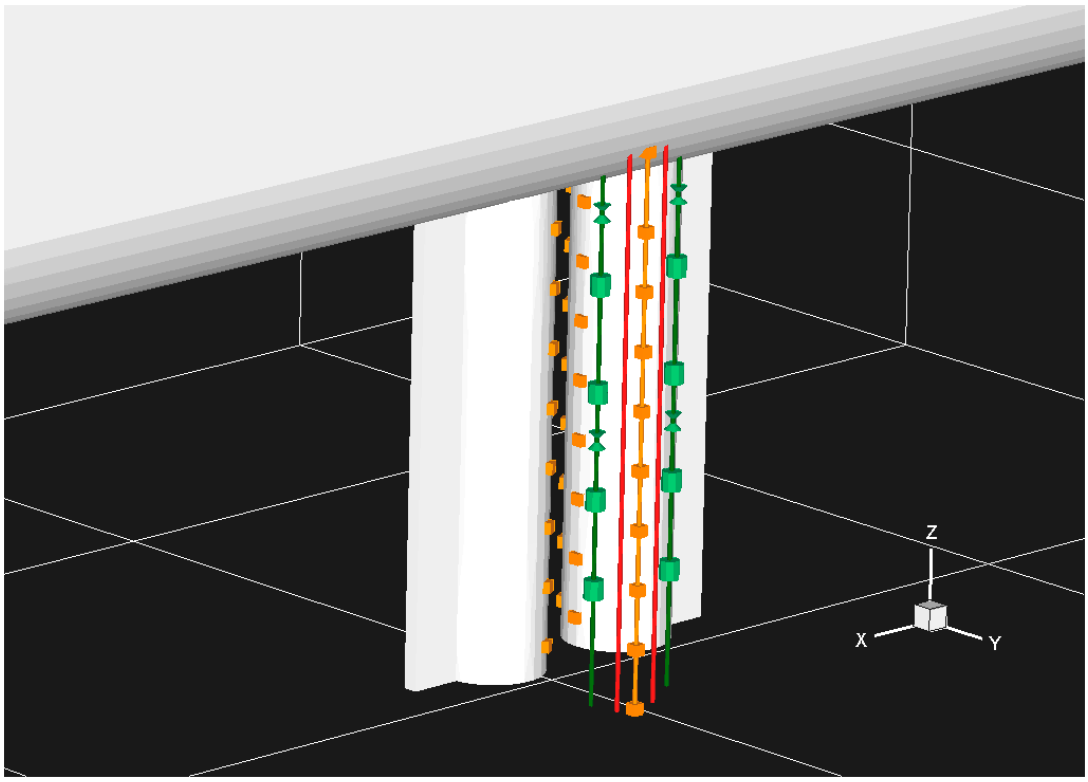

Figure 2-16. *Vertical view of the monitoring system at the proximity of the pillar. The thermistor arrays are the orange squares, the AE transmitters the green cones, the AE receivers the green cylinders, and the red vertical lines are the heaters.*

The results presented in this report are valid for the range of input data applied and listed in section 2.1. Based on the mechanical and thermal properties used as input in the model the temperature increase and temperature induced stresses are as expected to initiate spalling in the holes walls.

The variation of input parameters, mechanical as well as thermal, will influence the results of the modeling and the magnitude of temperature induced stresses. It can anyhow be stated without further modeling that the range of increase in temperature induced stresses is linearly dependent to the value of the coefficient of expansion. For the same value of Young's modulus, a decrease of 10% of the coefficient of expansion will induce a decrease of 10% of the magnitude of temperature induced stresses.

A sensitivity analysis will be carried out on the influence of input parameters on the outcome of modeling.

3 2D coupled thermo-mechanical modeling

This section presents the preliminary results of the coupled 2D thermo-mechanical modeling with the numerical code JobFem. The modeling has been conducted in order to determine the temperatures and level of stresses reached in the pillar as a function of heating time. Both models with slots and without slots have been simulated to check if the presence of slots was necessary. A sensitivity analysis has been conducted on the value of in-situ stresses, deformation modulus and thermal conductivity.

3.1 Modeling strategy

The aim of the modeling is to predict the thermo-induced stresses and the resulting total stresses in the pillar. The predictions of thermo-induced stresses were made by simulations with Flac3D /Wanne and Johansson, 2003/ and in 2D with the numerical code JobFem. Two horizontal sections, 0.5m and 1.5m below the tunnel floor were designed as a reference for comparisons between results obtained in 2D and 3D.

A short presentation of JobFem is presented in section 3.1.1. The input parameters and assumptions made for this project are presented in section 3.1.2.

3.1.1 The numerical code: JobFem

The numerical code JobFem is based on the Finite Element Method. The programme has been available for 20 years and used for different applications in the construction sector. The module for coupled thermo-mechanical modeling has been developed and validated in the frame of the hot water cavern project in Avesta /Rehbinder G. and Stille H., 1985/.

The quality and relevance of the results are related to the assumptions made on the rock mass behavior and properties. The agreement of the theoretical thermo-induced stresses to the measured stresses increases in correlation with the knowledge of rock mass fracturing and properties.

3.1.2 Set-up of the model for the experiment

Preliminary simulations have been conducted with JobFem in order to set-up the layout of the experiment, see section 2. The characteristics and position of heaters used in this report are based on the conclusions of this preliminary study.

Heat flow and temperature induced stresses have been calculated under plain strain conditions. The effect of the heater is set to 200 W/m, with a maximal temperature of 200°C specified at the heaters.

The temperature increase and thermo-induced stresses are monitored at different stages of the modeling:

– before heating after excavation of the holes, and after applying the confining stress of 1 MPa,

– during heating after 30, 60, 90 and 120 days of heating.

The total stresses at each stage are achieved by adding for each node of the element mesh stress values after excavation to thermo-induced stresses.

Three types of input parameters are required to build the model:

- mechanical and thermal properties of the rock mass
- stresses after excavation
- geometry and layout of the experiment

Mechanical and thermal rock mass properties

In the first stage of modeling the rock mass is assumed to be elastic and homogeneous.

Preliminary study of the fracturing and mechanical and thermal properties of the rock mass are presented in sections 2 and 4 /Staub et al, 2003/. The parameters chosen for the experiment are listed in Table 3-1.

Table 3-1. Input mechanical and thermal properties for the rock mass

Parameter	Value	Unit
Young's modulus, intact rock	68	GPa
Young's modulus, rock mass	47	GPa
Poisson's ratio, intact rock	0.24	-
Poisson's ratio, rock mass	0.26	-
Thermal conductivity	2.83	W/m, K
	2.4	
Volume heat capacity	2.10	MJ/m^3, K
Linear expansion	7.9E-06	l/K
Density	2.71	g/cm^3
Initial temperature of the rock mass	15	°C

The analysis of in-situ stresses in the experiment volumes is presented in section 3 /Staub *et al.*, 2003/, and the most probable values are listed in Table 3-2.

Table 3-2. In-situ stresses

σ_1 [MPa]	σ_2 [MPa]	σ_3 [MPa]	Trend [Äspö 96]	Dip [°]
25 / 30 / 35			310	30
	15		090	53
		10	208	20

The parameters are evaluated for the dominant rock type in the experiment volume, which is Diorite (see section 2 and 5 /Staub *et al.*, 2003/. The values chosen for the Young's modulus and Poisson's ratio can be interpreted as the minimal and maximal values that the simulated rock mass can reasonably take considering its fracturing degree.

In the same way the two values used for thermal conductivity can be interpreted as extreme values of this parameter, on the basis of the analysis of calculated thermal properties in the four drilled boreholes in the experiment volumes, see section 5 /Staub *et al.*, 2003/. No range is given for volume heat capacity as the values are almost the same in the 4 boreholes.

Stresses after excavation

The calculations of stresses along the new tunnel are achieved with the 3D numerical model built with Examine3D. Table 3-2 lists the stress tensors that have been used for the calculations of the new tunnel. Stress values along the tunnel and in the rock mass around the pillar are monitored at different stages of excavation: after tunnel excavation, after excavation of the slots, and after drilling of the boreholes.

The coordinates of the nodes of the element mesh of the 2D sections modeled in JobFem have been imported to the Examine3D model in order to obtain the stress tensor at each node of the element mesh of both horizontal 2D sections. These stress values were then transformed to fit a 2D model and the recalculated values are the one used for the evaluation of total stresses after heating. The procedure is to add the stress values to the thermo-induced stresses monitored during the JobFem's modeling.

Layout of the experiment

The geometry of the pillar and the layout of heaters and AE sensors is illustrated in Figure 3-1. Confinement pressure of 1 MPa is achieved with water in one hole. The geometry of the boreholes and of the slots has been optimized on the basis of stress calculations in Examine3D. The position of the AE sensors is optimal for the monitoring of microseismic events. The position of the heaters is based on preliminary modeling results with JobFem, see section 2.

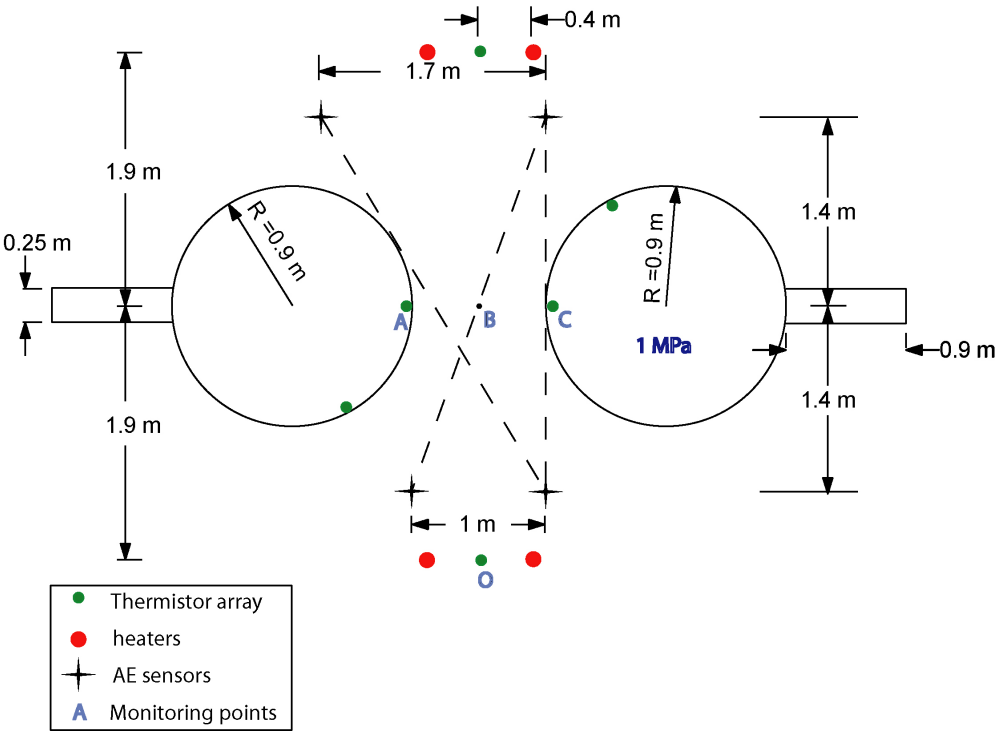

Figure 3-1. *Experiment layout.*

3.2 Modeling results

Simulations have been conducted for the three different values of σ_1, the values for σ_2 and σ_3 are constant, see Table 3-2. This gives a range of potential thermo-induced stresses and total stresses in the pillar in the consideration of the potential in-situ stresses at the experiment volume. These combinations are conducted with E=68 GPa and λ=2.83 W/m, K.

For each value of σ_1 the simulations have been conducted with and without slots. These combinations are conducted with E=68 GPa and λ=2.83 W/m, K.

Each combination of parameters was simulated at the both depth levels, named in the graphs level a (1.5m below the tunnel floor) and level b (0.5m below the tunnel floor).

The results are presented as sections across the pillar, from x=-0.5 (hole with air) to x=0.5m (hole with confining pressure). 20 measurement sections along this 1m "fictive" line are plotted in the graphs.

The graphs for all realized simulations are presented in appendix E. In the following sections some realizations have been chosen to illustrate the influence of slots, depth level and in-situ stresses.

3.2.1 Influence of the depth level

The results presented in Figure 3-2 and Figure 3-3 illustrate the influence of depth level on temperatures and total stresses reached in the pillar at different stages of modeling.

These values are obtained for a model without slots, σ_1=30 MPa, E=68 GPa and λ=2.83 W/m, K.

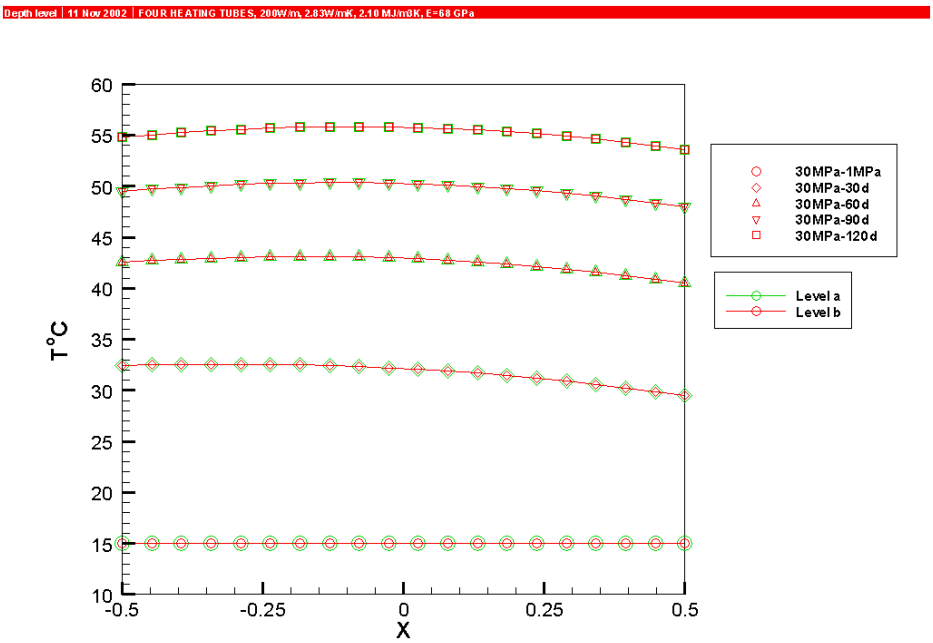

Figure 3-2. *Temperature monitored in the pillar at different stages of modeling, depth levels a and b.*

As illustrated in Figure 3-2 temperatures reached at different stages of modeling are identical for both levels. This is an implication of the plain strain assumptions made on the model: the tunnel will have no effect on the temperature flow in the rock mass. However the tunnel has a strong influence on the stress level, and the stresses reached in the section closed to the tunnel floor (level b) are very high, see Figure 3-3.

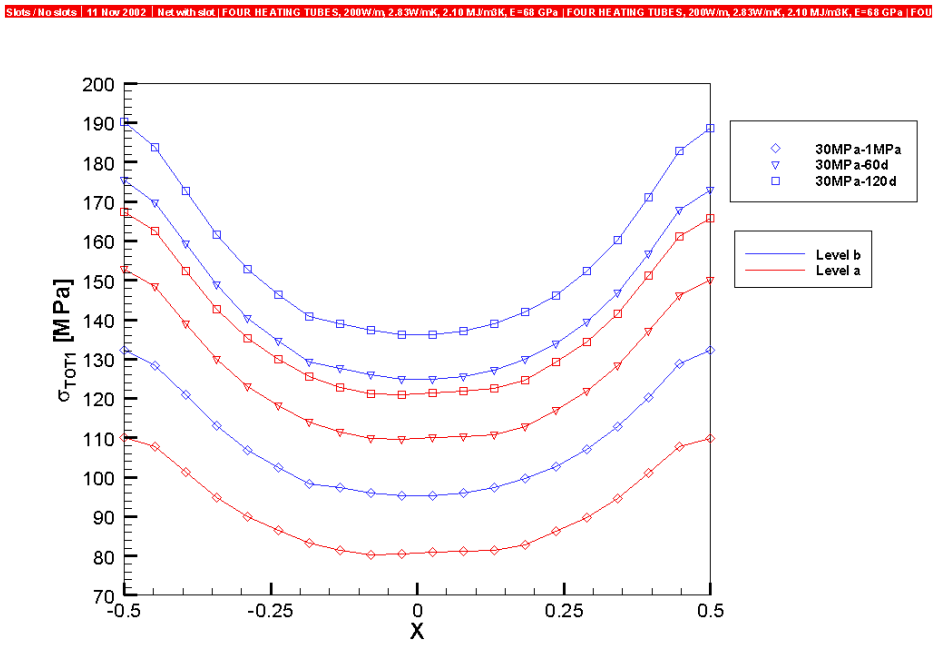

Figure 3-3. *Total major stress at different stages of the modeling, levels a and b.*

As a consequence the results from the 2D section located 0.5 m below the tunnel floor (level b) are not considered in the following.

3.2.2 Influence of the slots

The results presented in Fifure 3-4 and Figure 3-5 illustrate the influence of the slots on the temperatures and total stresses reached in the pillar at different stages of modeling. The results are presented for depth level a, σ_1=30 MPa, E=68 GPa and λ=2.83 W/m, K.

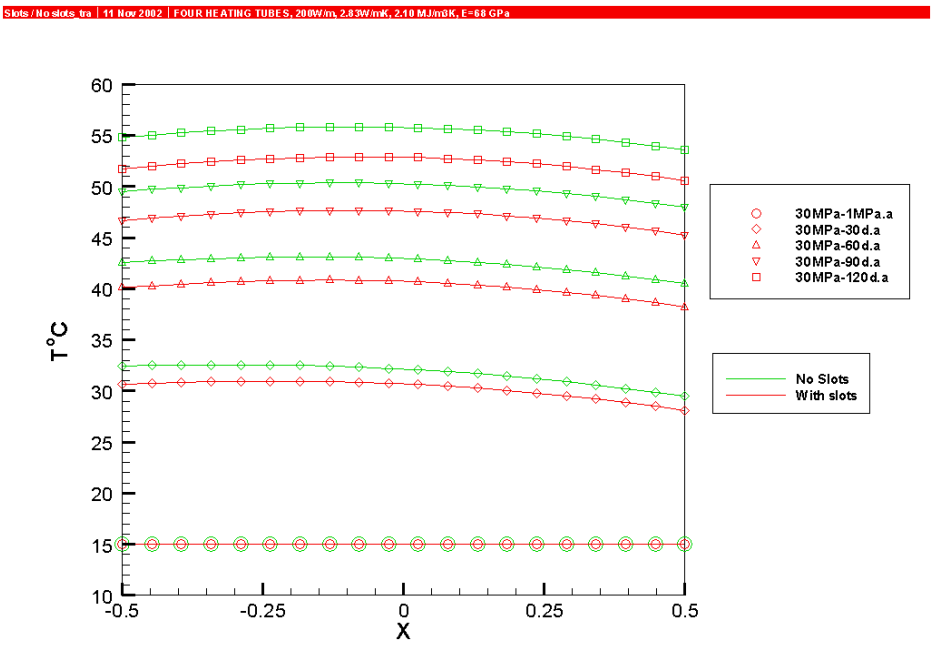

Figure 3-4. *Temperature reached in the pillar, with and without slots, for different stages of modeling, σ_1=30 MPa.*

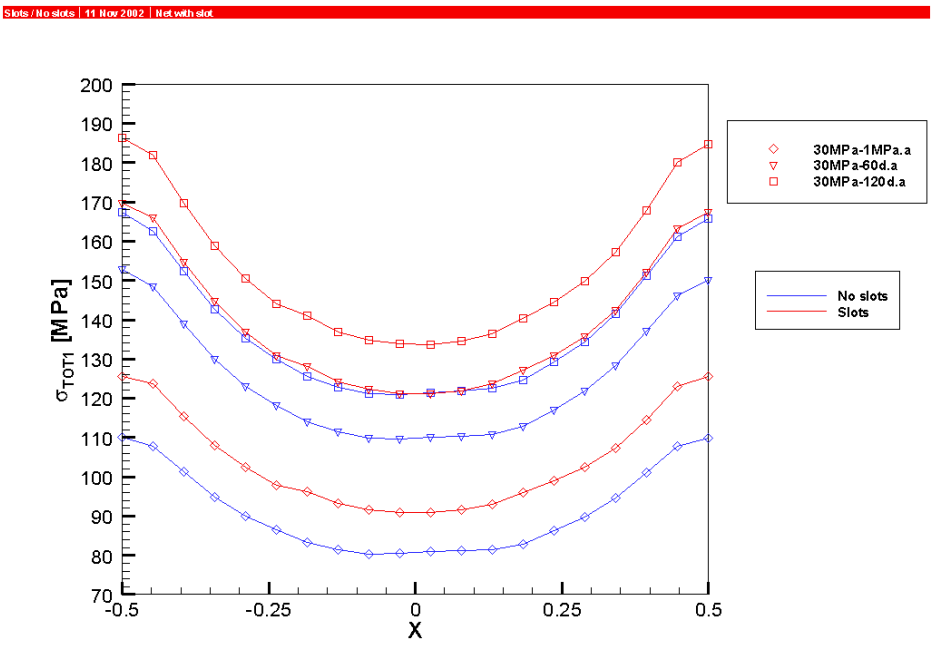

Figure 3-5. *Total major stress at different stages of the modeling, with and without slots.*

Figure 3-6 illustrates the evolution of temperature with time in two monitoring points, with and without slots (their position is shown in Figure 3-1).

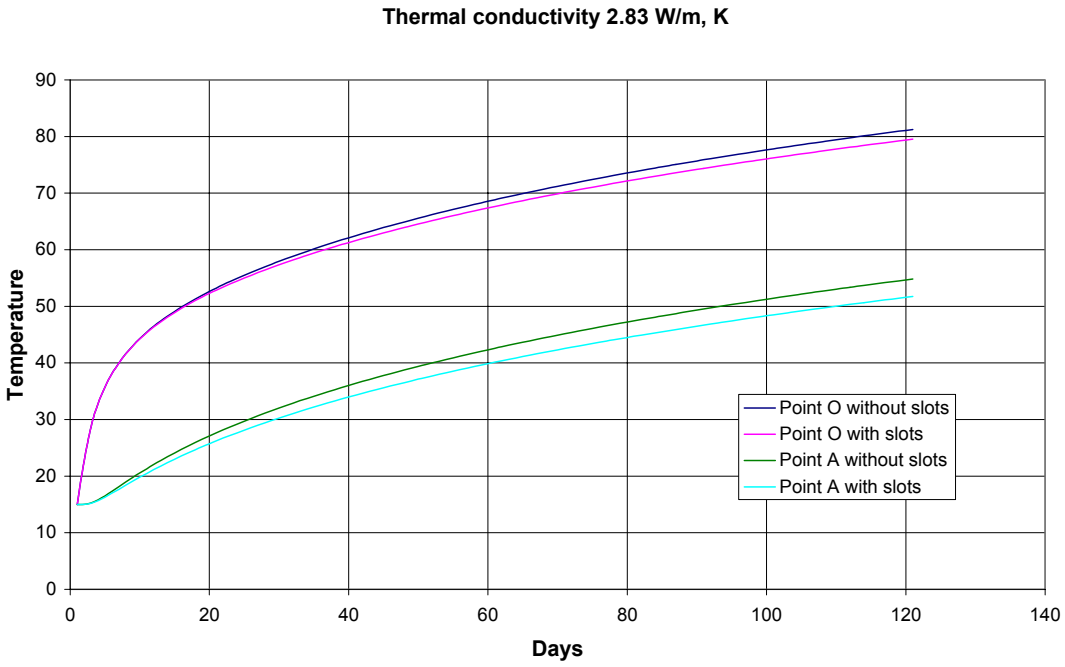

Figure 3-6. *Evolution as a function of time of the temperature in two monitoring points.*

3.3 Sensitivity analysis

The outcome of the modeling is subjected to the value of input parameters. The confidence in the modeling results is related to the quality and certainty in the input data. In order to better estimate the range of stresses that can be achieved in the pillar sensitivity analysis on input parameters has been conducted. The tested parameters are in-situ stresses, deformation modulus and thermal conductivity.

The different combinations that have been modeled are listed in Table 3-3.

Table 3-3. List of parameter combinations used for the sensitivity analysis

σ_1, MPa	Depth level	Slots (Yes or No)	E (GPa)	λ (W/m, K)	Number of combinations
25	a / b	Y / N	68	2.83	4
30	a / b	Y / N	68	2.83	4
35	a / b	Y / N	68	2.83	4
30	a / b	N	47 / 68	2.4 / 2.83	8

Processed data are presented in the following sections. The curves for all combinations are found in appendix E.

3.3.1 Influence of in-situ stresses

The model has been run for the three different values of σ_1. A comparison of the obtained total major stress after 120 days of heating is illustrated in Figure 3-7 for depth level a. These results are for a model without slots, E=68GPa and λ=2.83 W/m, K.

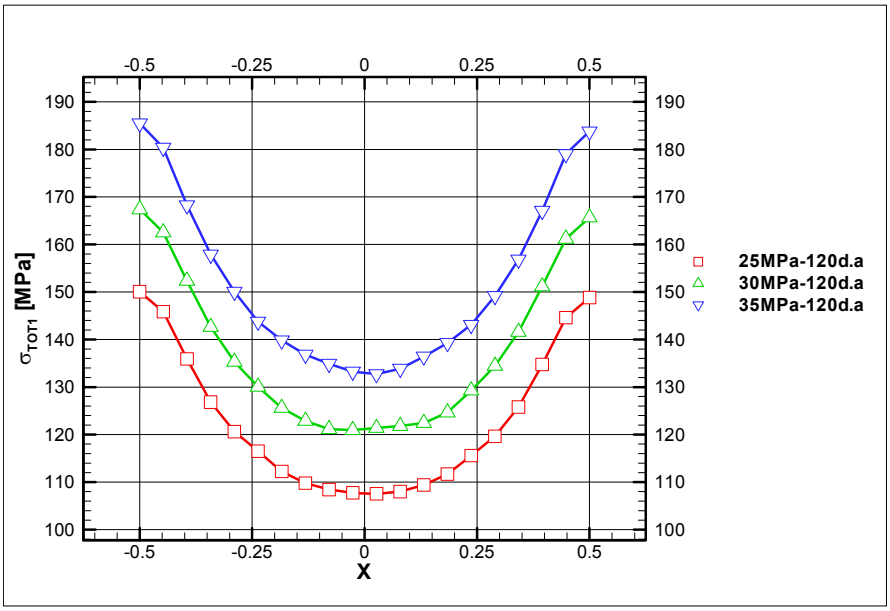

Figure 3-7. *Total stresses after 120 days of heating, level a, different values of σ_1.*

3.3.2 Influence of the deformation modulus

The influence of deformation modulus is illustrated in two different sections, one when modeling with a thermal conductivity of 2.83 W/m, K, and the second when applying a thermal conductivity of 2.4 W/m, K.

The results are presented for depth level a, σ_1=30 MPa, model without slots.

λ=2.83 W/m, K

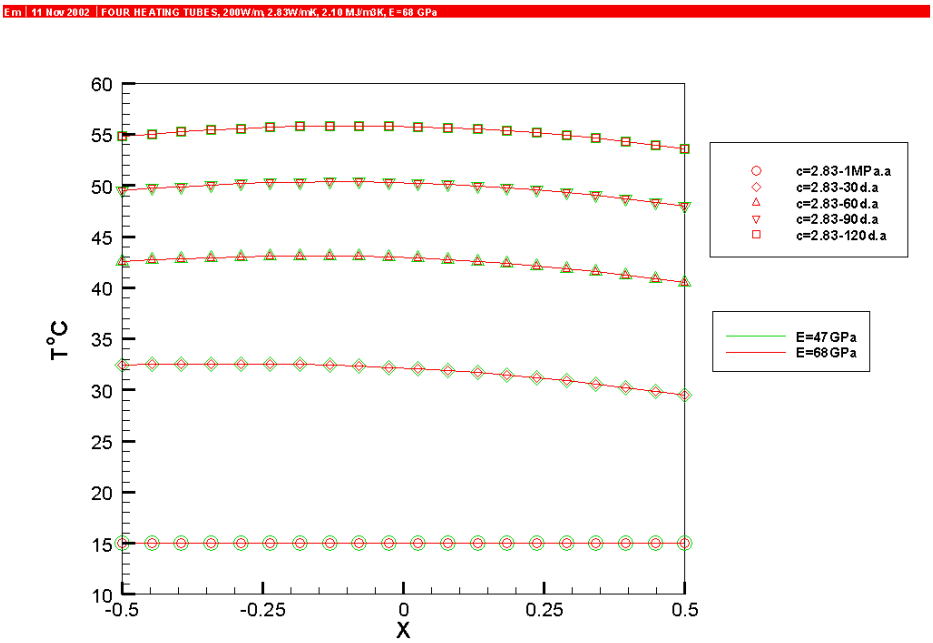

Figure 3-8. *Temperature monitored in the pillar at different stages of modeling, depth level a, E=47GPa and E=68GPa.*

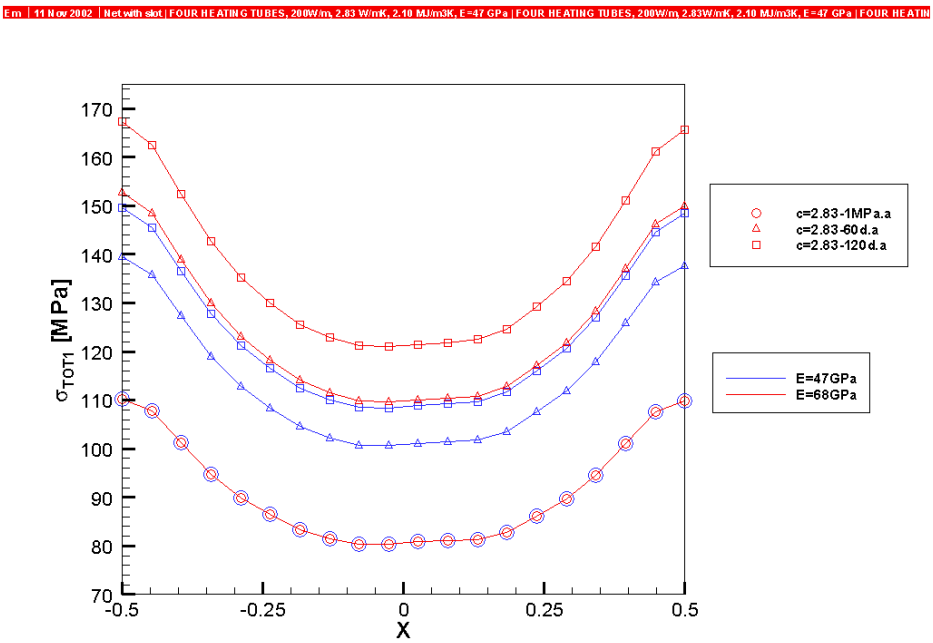

Figure 3-9. *Total major stress at different stages of the modeling, depth level a, E=47GPa and E=68GPa.*

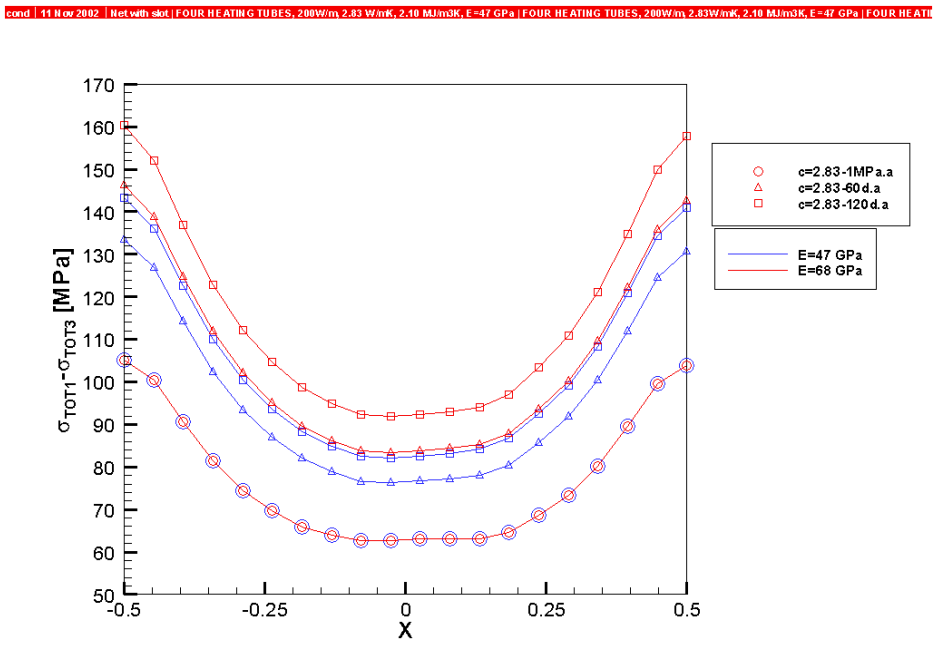

Figure 3-10. *Deviatoric stresses at different stages of the modeling, depth level a, E=47GPa and E=68GPa.*

λ=2.4 W/m, K

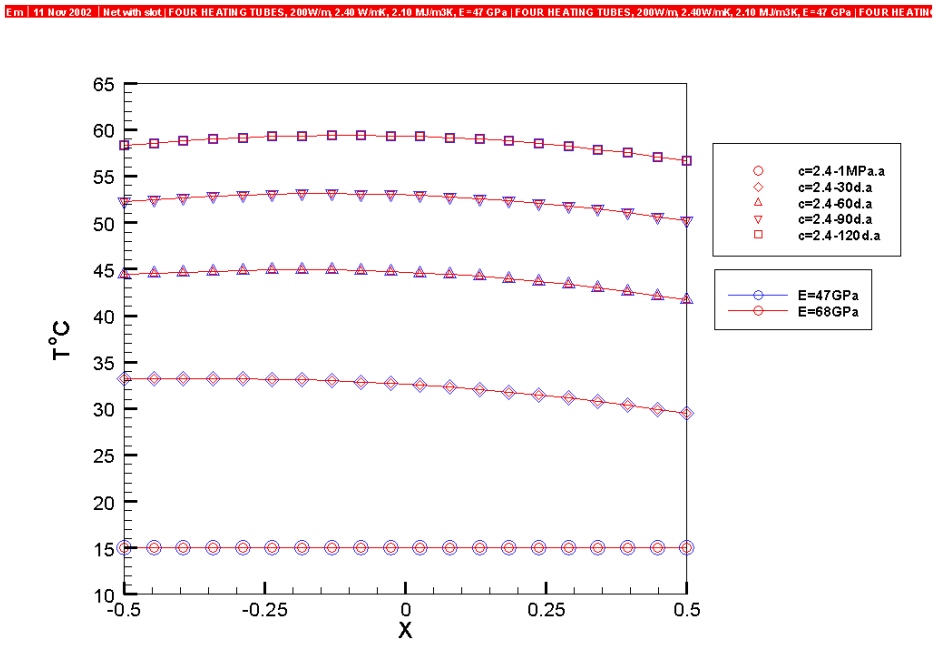

Figure 3-11. *Temperature monitored in the pillar at different stages of modeling, depth level a, E=47GPa and E=68GPa.*

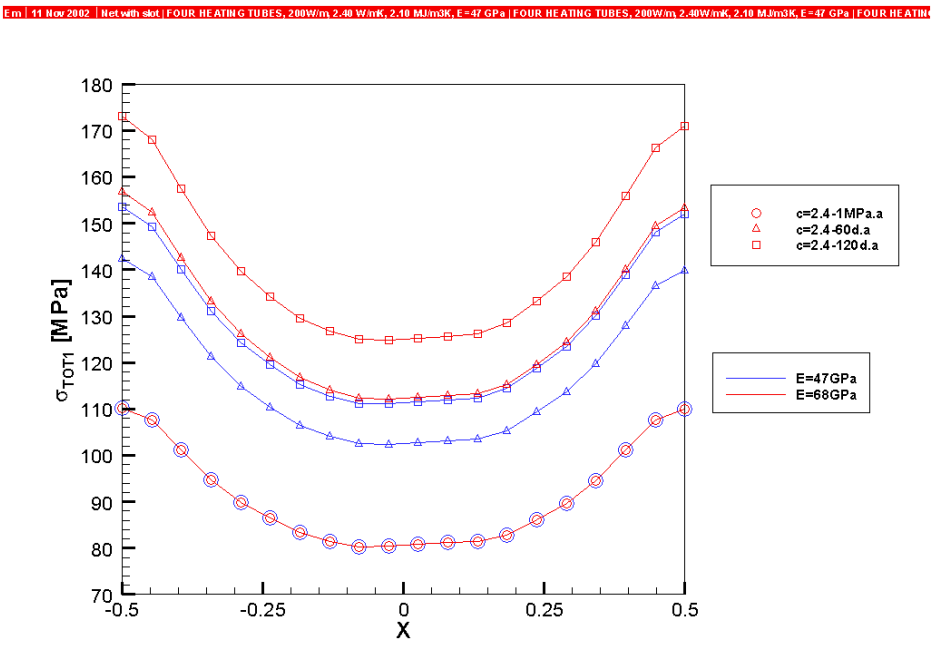

Figure 3-12. *Total major stress at different stages of the modeling, depth level a, E=47GPa and E=68GPa.*

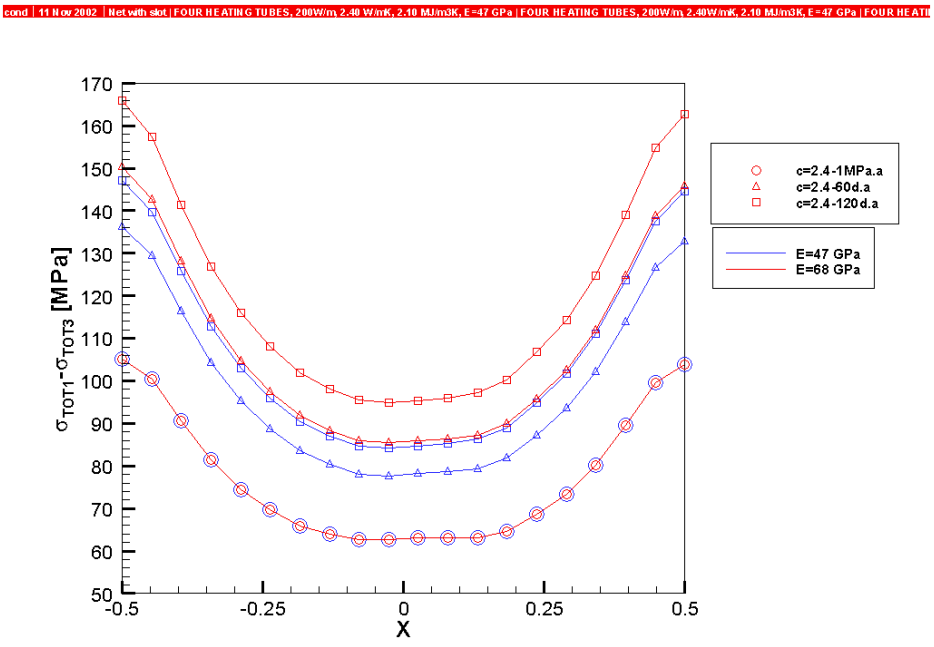

Figure 3-13. *Deviatoric stresses at different stages of the modeling, depth level a, E=47GPa and E=68GPa.*

3.3.3 Influence of the thermal conductivity

The influence of thermal conductivity is illustrated in two different sections, one when modeling with a deformation modulus of 47 GPa, and the second when applying a deformation modulus of 68 GPa.

The results are presented for depth level a, σ_1=30 MPa, model without slots.

E=47 GPa

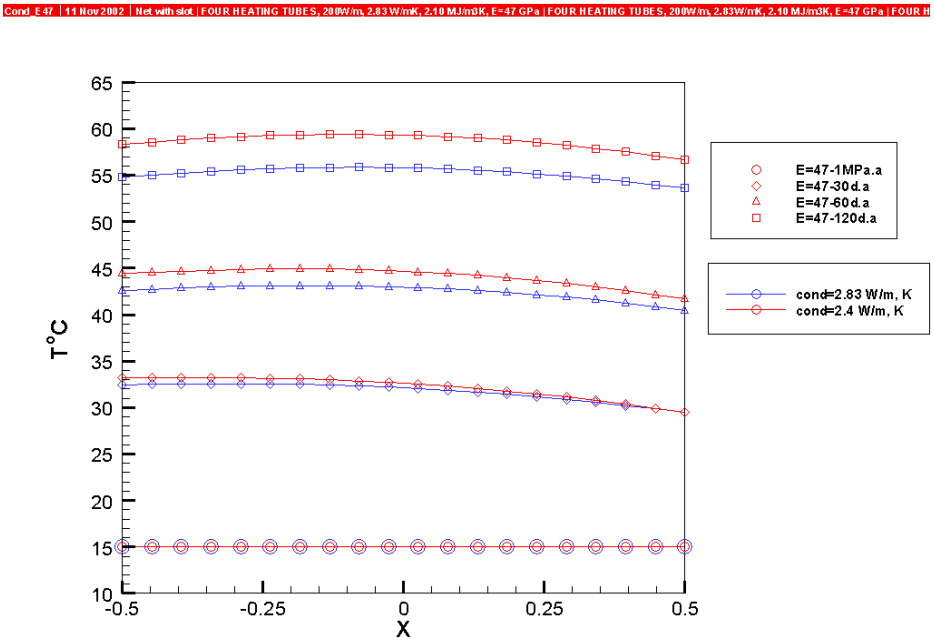

Figure 3-14. *Temperature monitored in the pillar at different stages of modeling, depth level a, λ=2.4 W/m, K and λ=2.83W/m, K.*

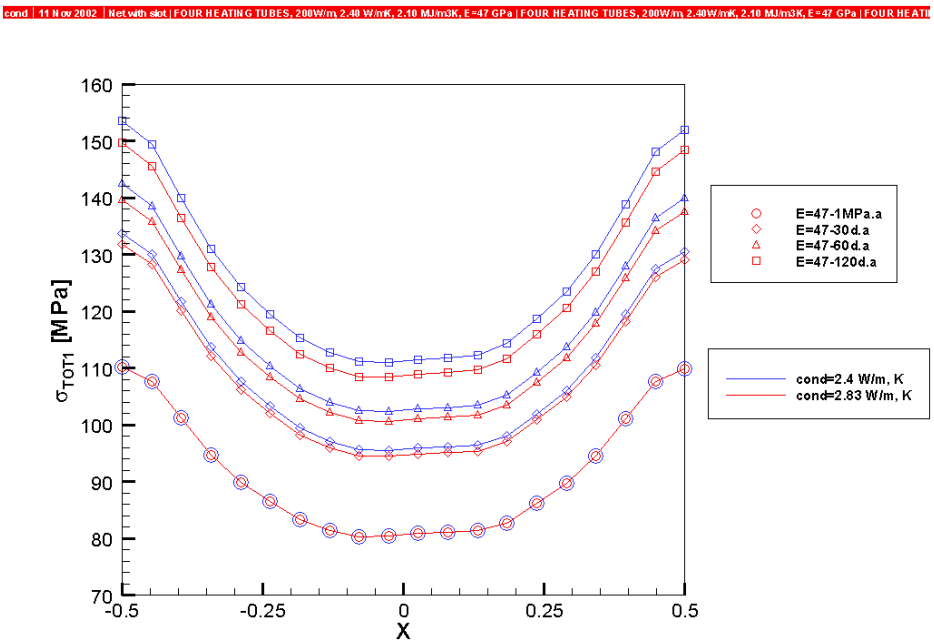

Figure 3-15. *Total major stress at different stages of the modeling, depth level a, λ=2.4 W/m, K and λ=2.83W/m,K.*

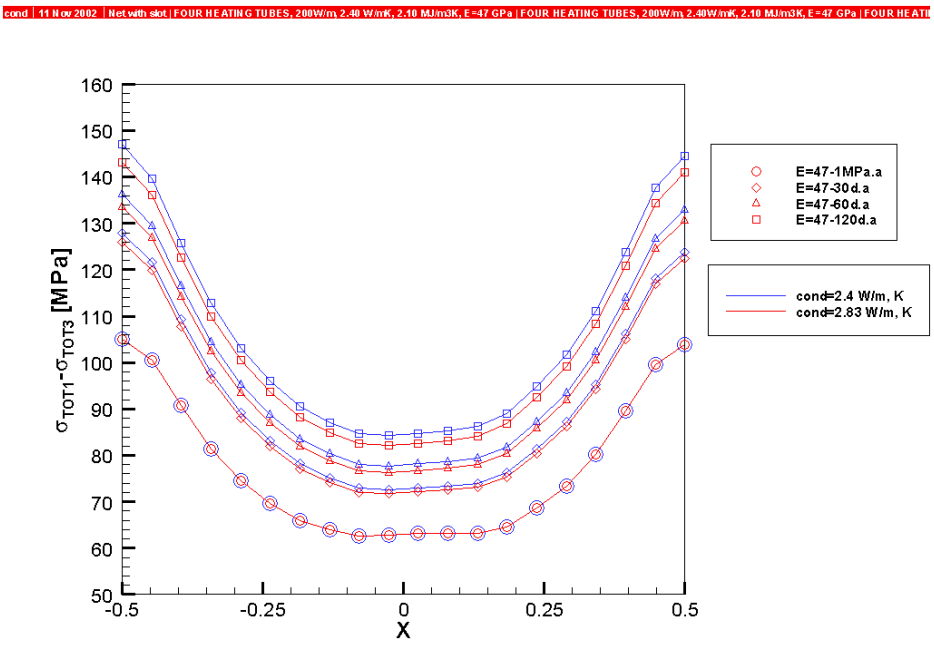

Figure 3-16. *Deviatoric stresses at different stages of the modeling, depth level a, λ=2.4 W/m, K and λ=2.83W/m,K.*

E=68 GPa

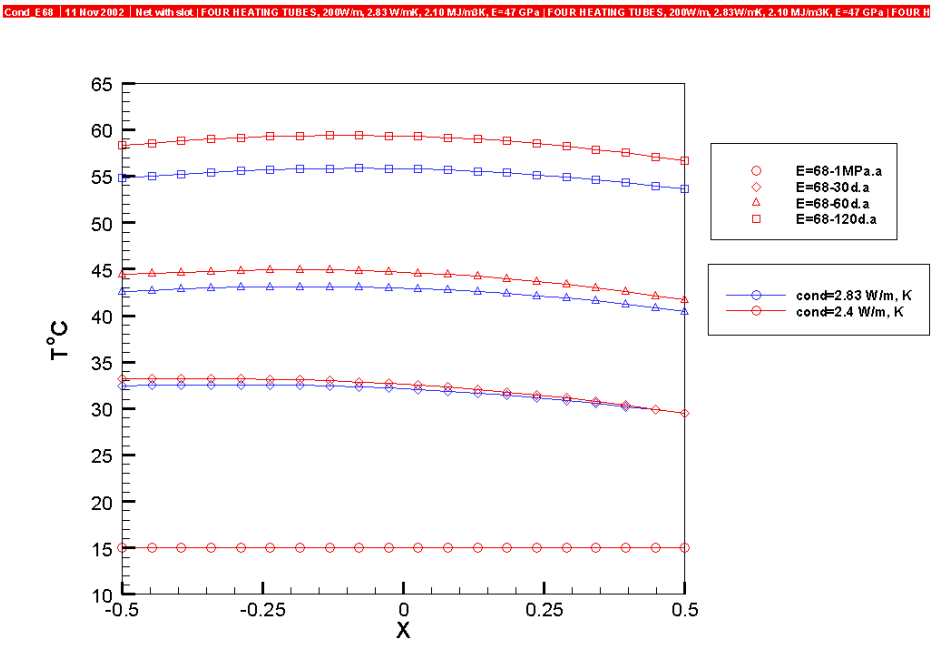

Figure 3-17. *Temperature monitored in the pillar at different stages of modeling, depth level a, λ=2.4 W/m, K and λ=2.83W/m,K.*

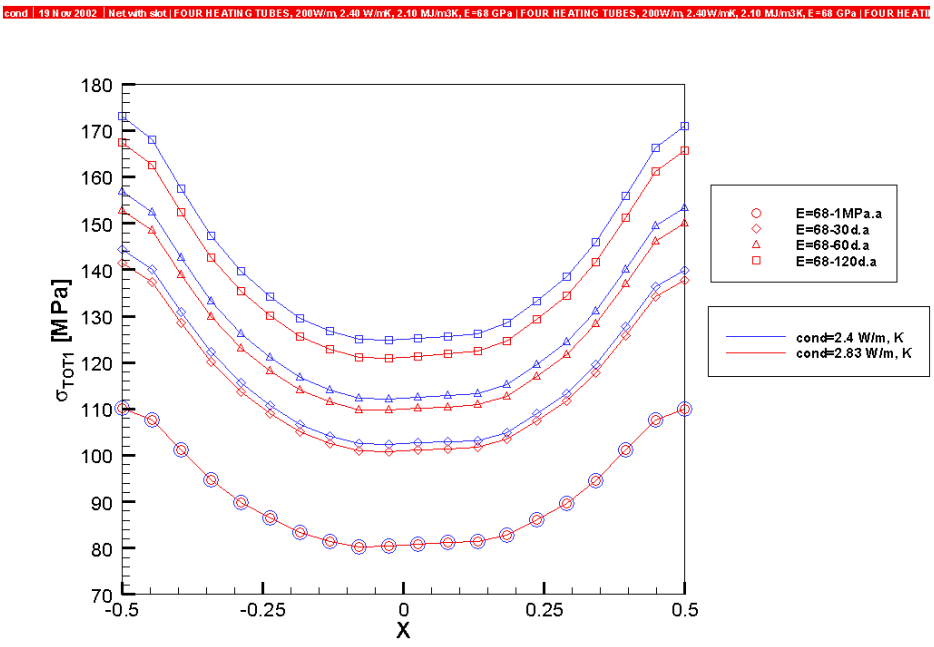

Figure 3-18. *Total major stress at different stages of the modeling, depth level a, λ=2.4 W/m, K and λ=2.83W/m,K.*

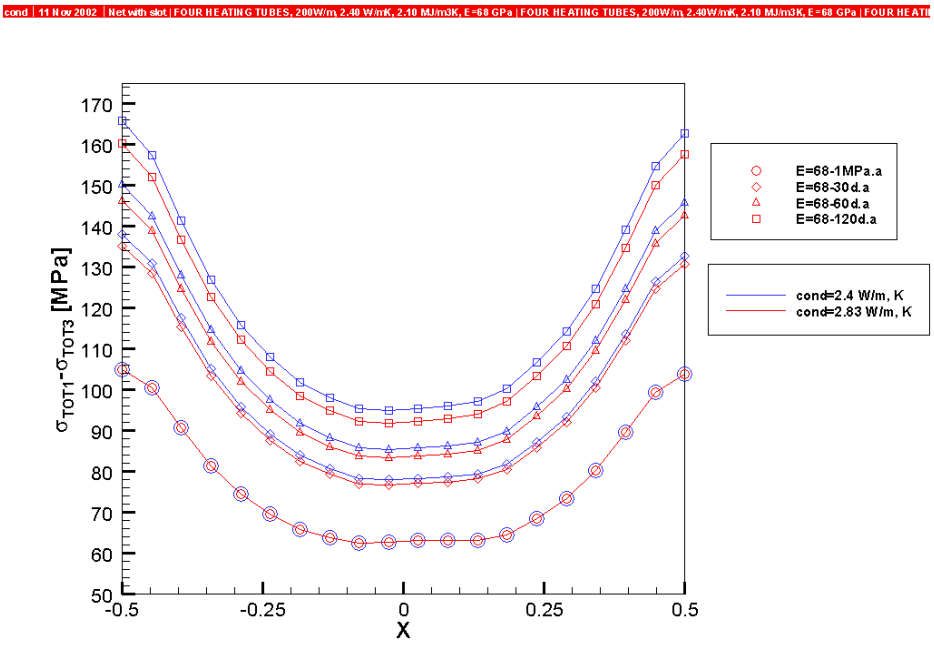

Figure 3-19. *Deviatoric stresses at different stages of the modeling, depth level a, λ=2.4 W/m, K and λ=2.83W/m,K.*

Figure 3-20 illustrates the influence of thermal conductivity on the evolution of temperature with time in two monitoring points, A and O (localized in Figure 3-1).

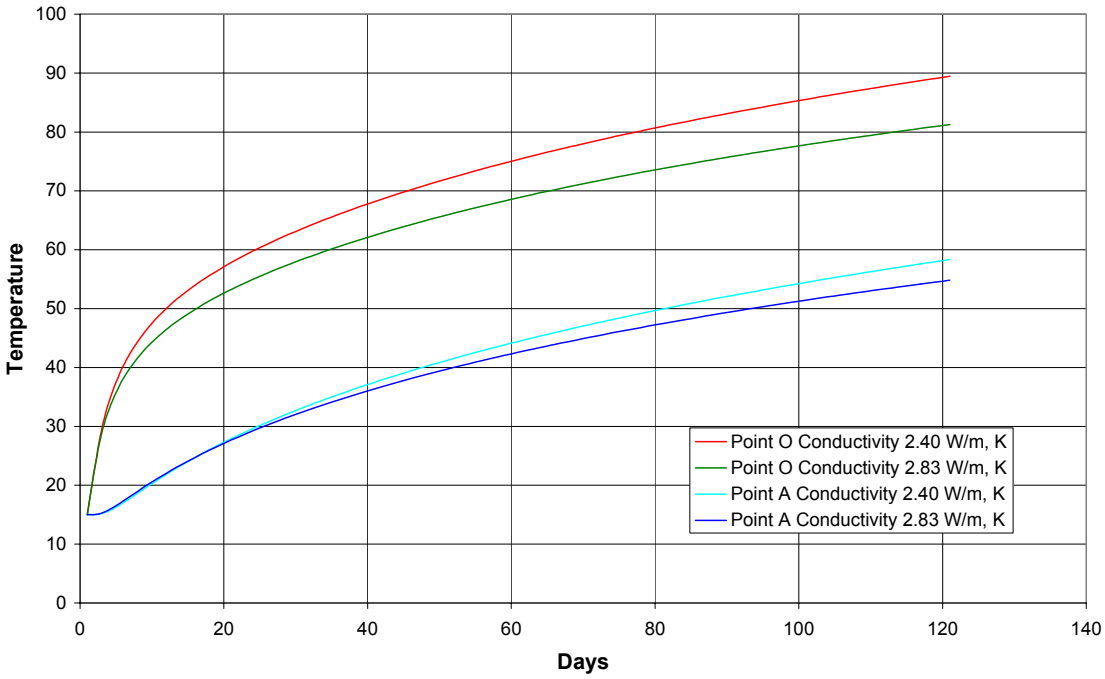

Figure 3-20. *Influence of thermal conductivity on the evolution with time of temperature in two monitoring points.*

Figure 3-20 illustrates that the temperature increases faster at a given point when the thermal conductivity is lower.

3.3.4 Analysis of the results

From the results presented in sections 3.3.2 and 3.3.3 the influence of variation of thermal conductivity and deformation modulus after 120 days of heating can be established, see Table 3-4.

Table 3-4. Temperature, total major stress and deviatoric stresses in the middle (x=0) and at the border of the pillar (x=-0.5) after 120 days of heating.

E, GPa	λ, W/m, K	Depth, m	T, °		σ_1, MPa		σ_1-σ_3, MPa	
			X=0	X=-0.5	X=0	X=-0.5	X=0	X=-0.5
68	2.4	1.5	59	58	125	173	95	166
68	2.83		56	55	120	167	92	160
47	2.4		59	58	111	153	84	147
47	2.83		56	55	109	149	82	143

The influence of increase of deformation modulus or thermal conductivity can be summarized as shown in Table 3-5.

Table 3-5. General influence of increasing deformation modulus or thermal conductivity on temperatures, total stresses and deviatoric stresses.

Effect of / on	T	σ_1	σ_1-σ_3
Increased E	→	↗	↗
Increased λ	↘	↘	↘

The combination of variation of thermal conductivity and deformation modulus can be summarized as followed:

- The factor of influence for high temperatures in the rock mass is thermal conductivity. Indeed deformation modulus does not have any influence on the temperature reached in the rock mass for a given thermal conductivity.
- Total and deviatoric stresses increase with the deformation modulus for different values of thermal conductivity.
- Whatever the value of the deformation modulus the temperatures and total stresses reached in the pillar decrease when the thermal conductivity increase.

Study of highest and lowest cases

By means of all simulations the influence of depth, in-situ stresses, and mechanical and thermal properties has been tested. On the basis of the analysis of simulation results, temperature and temperature induced stresses can be estimated for the highest and lowest case:

- Highest case: σ_1= 35 MPa; E=68 GPa; λ=2.4 W/m, K
- Lowest case: σ_1= 25 MPa; E=47 GPa; λ=2.83 W/m, K

The determination of the cases has been based on the combined influence of the different parameters, exclusive depth. Both cases are run considering the section located 1.5 m below the tunnel floor.

The raw results of simulations are presented in appendix F.

The increase of temperature, total major stress and deviatoric stresses during heating is illustrated for both cases in Figure 3-21 to Figure 3-23. Curves are presented for the evolution of parameters in the middle of the pillar and at the border of the unconfined hole.

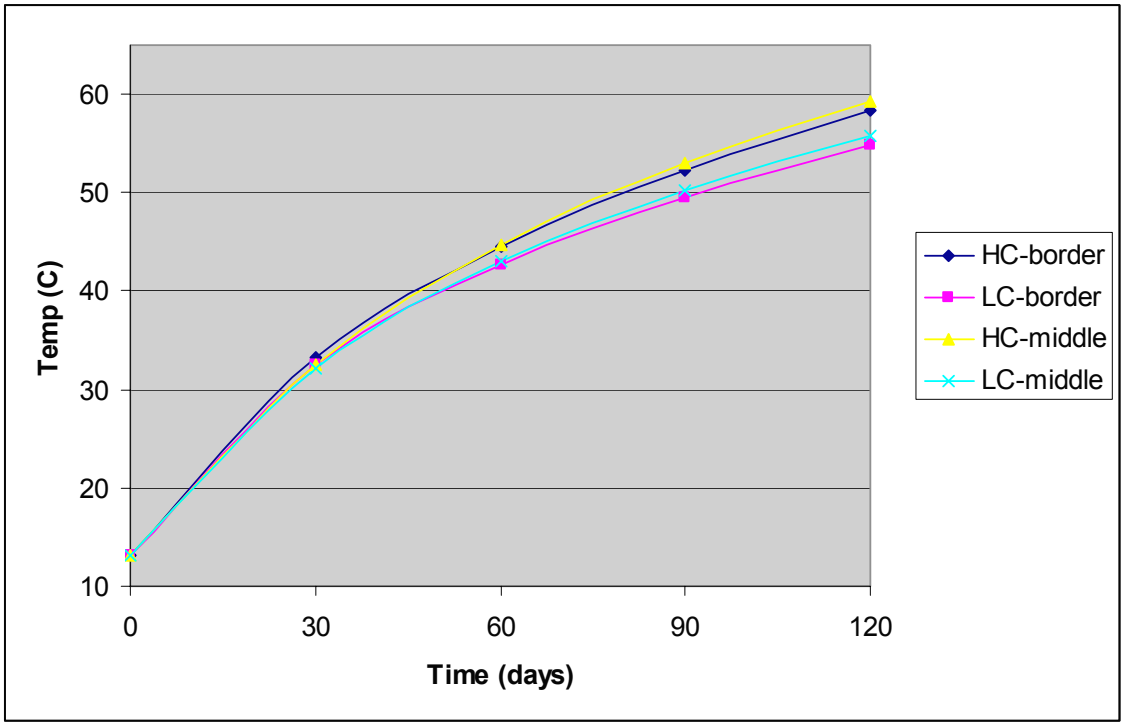

Figure 3-21. *Increase of temperature during heating at two different points in the pillar. LC: lowest case; HC: highest case.*

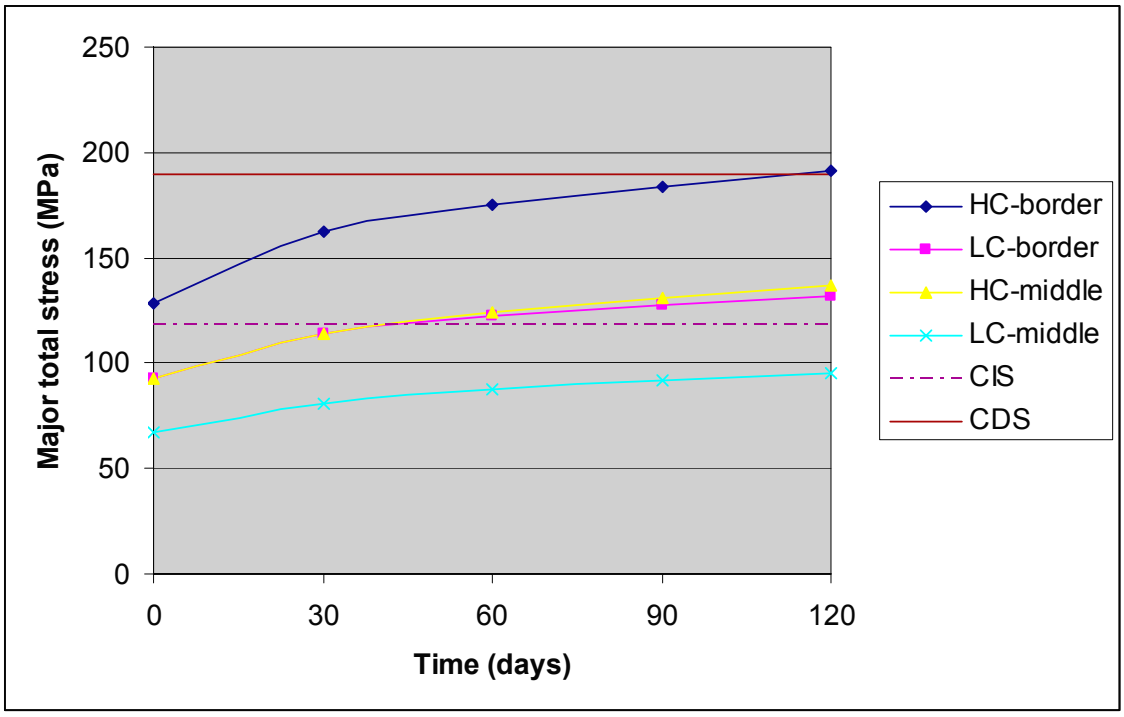

Figure 3-22. *Increase of major total stress during heating at two different points in the pillar. LC: lowest case; HC: highest case; CIS: crack-initiation stress; CDS: crack-damage stress..*

The level of stresses reached in the pillar can be analyzed with regards to the defined crack-initiation stress, σ_{ci}, and crack-damage stress, σ_{cd}, of the Diorite, which are evaluated by /Nordlund *et al.*, 1999/ to be respectively 118 MPa and 190 MPa /.

According to the modeling results illustrated in Figure 3-22, the crack-initiation stress might be reached after only a short heating time. The crack-damage stress will be exceeded only in case of the "highest case" combination.

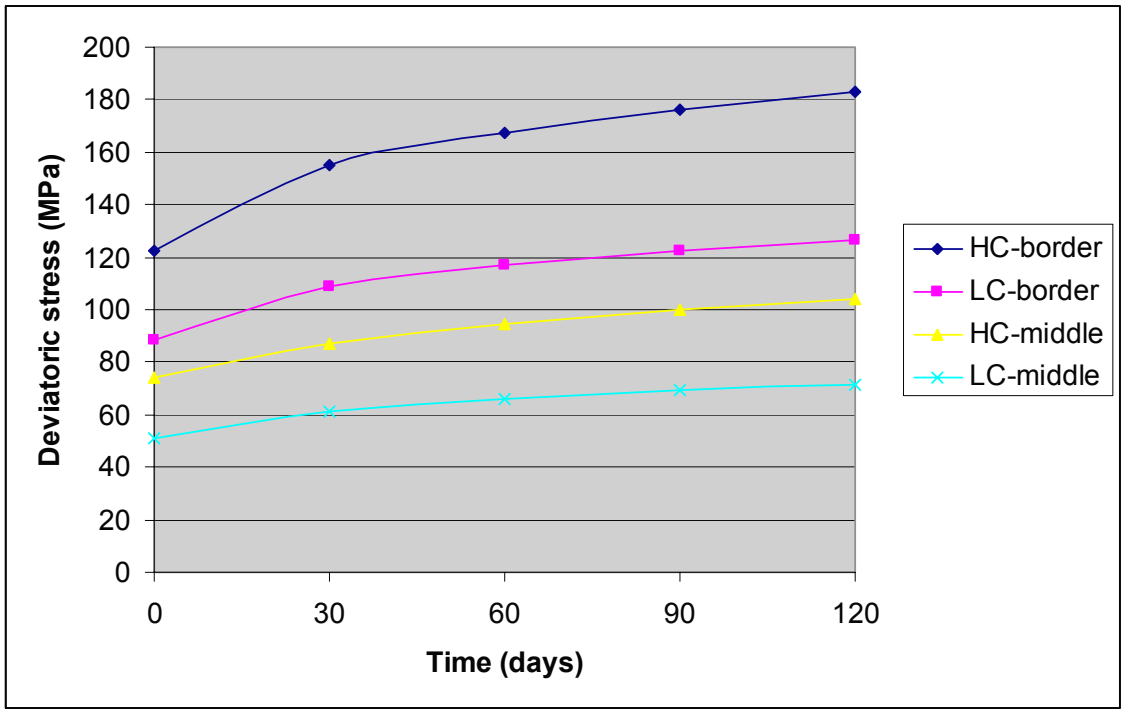

Figure 3-23. *Increase of deviatoric stresses during heating at two different points in the pillar. LC: lowest case; HC: highest case.*

Temperature, major total stresses and deviatoric stresses reached after 60 days of heating are summarized in Table 3-6.

Table 3-6. Outcome of the model for "extreme" values, given in the middle (x=0) and at the border of the pillar (x=-0.5) after 60 days of heating

σ_1, MPa	E, GPa	λ, W/m, K	Depth, m	T, °		σ_1, MPa		σ_1-σ_3, MPa	
				X=0	X=-0.5	X=0	X=-0.5	X=0	X=-0.5
25	47	2.83	1.5	42.9	42.6	87.26	122.1	65.9	167.6
35	68	2.4		44.67	44.4	124.2	175.07	94.5	116.8

Strain values at the border of the boreholes have been recorded during simulations of the lowest and highest cases.

/Stacey, 1981/ has shown that micro cracking starts when the extension strain is larger than a critical value. The critical value is a characteristic material property of the intact rock in the range of 70 – 170 micro strain (10^{-06}). For the highest and lowest cases, noted respectively HC and LC, the principal strains have been calculated. The procedure is the same as used for calculating the stress increase in the model, see section 3.1.2. The 2D simulations provided the thermo-induced strains. Strains related to the excavation of the holes are calculated from the difference between in situ stresses and the stresses simulated in Examine3D. The Poisson's ratio used for the determination of strain values from stress values is 0.2 (section 2.1), the deformation modulus is 47 GPa and 68 GPa respectively for the lowest and highest cases.

In Figure 3-24 the development of the major and minor principal strains with time is shown for the HC and LC cases. In Appendix G the results are presented as contour maps before start of heating, and then after 30, 60, 90 and 120 days of heating.

According to the modelling results illustrated in Figure 3-24 the development of strains for the two cases is almost identical. The maximum extension strain after excavation of the holes is approximately 1200 micro strain. According to Stacey´s criteria micro cracking has already started. After 120 days of heating the maximum extension strain has increased to approximately 1900 micro strain.

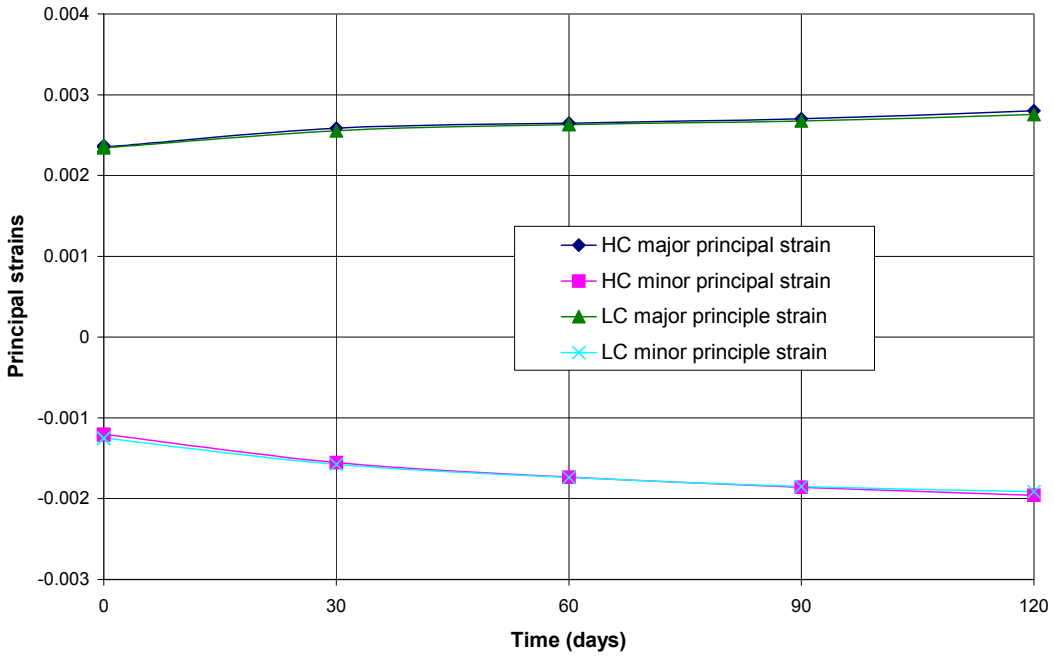

Figure 3-24 *Increase of major and minor strain during heating. 0.5 m below the tunnel floor (the largest values around the holes are plotted). Negative values: extension strain; positive values: compression strain*

The deformation vector related only to the 2D numerical simulations has also been studied. The results for both highest and lowest cases are illustrated in appendix H. In order to investigate the evolution of deformation with time the vector value has been extracted at 24 points, located every 15° at the border of the boreholes (Figure 3-25).

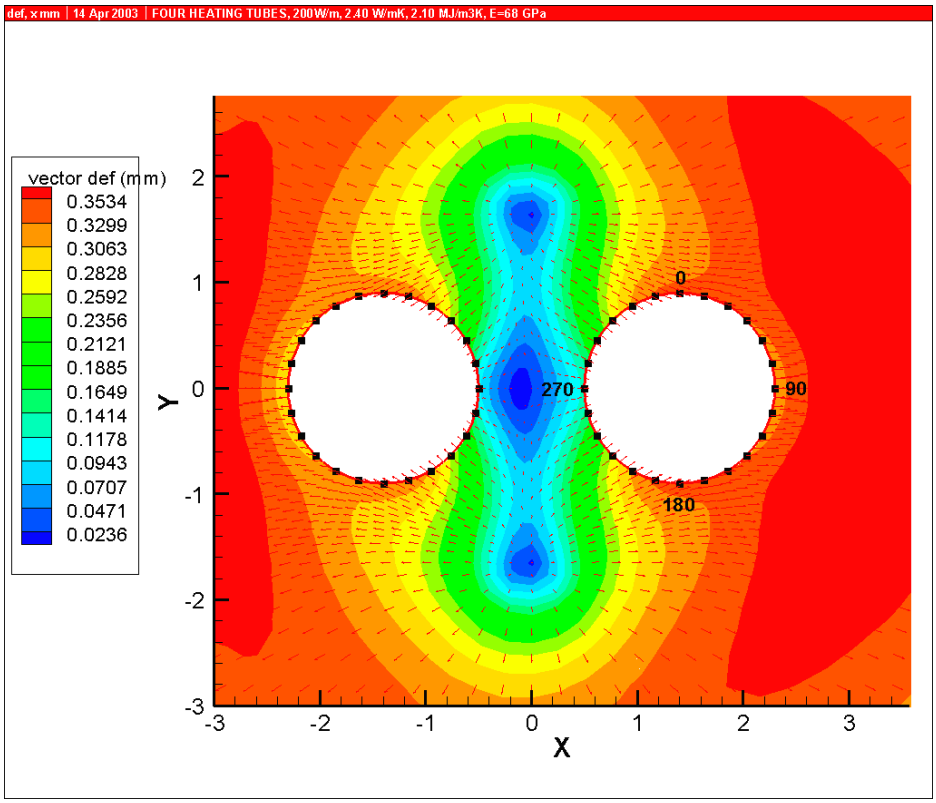

Figure 3-25 *Vector deformation. Localisation of the extraction points around the holes.*

The values of vector deformation have been extracted at the different stages of the experiment. The results are illustrated in Figure 3-26 for the highest case in the unconfined and confined holes, and in Figure 3-27 for the lowest case in the unconfined and confined holes.

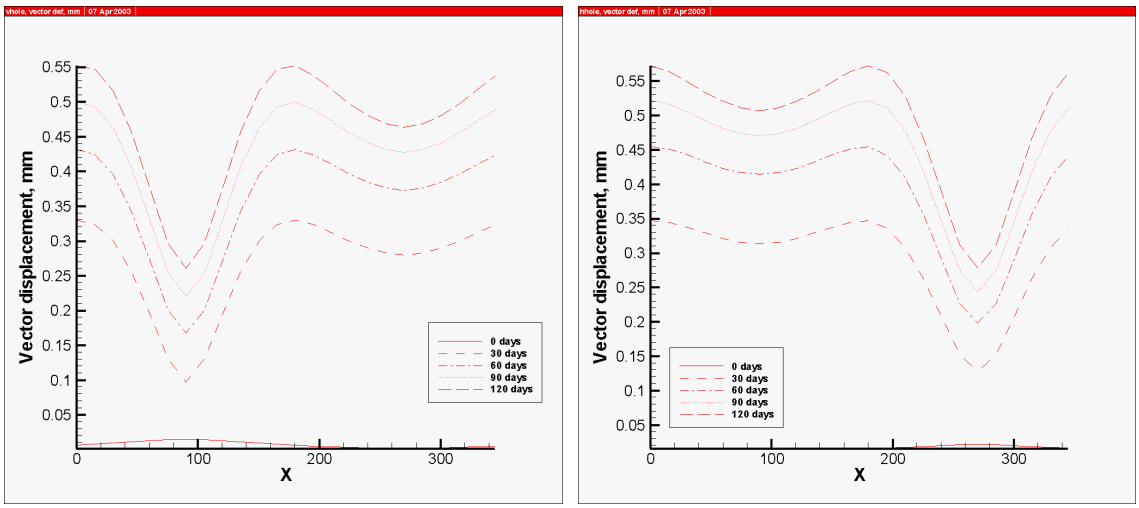

a) b)

Figure 3-26 *Vector deformation for the highest case. a) unconfined hole; b) confined hole*

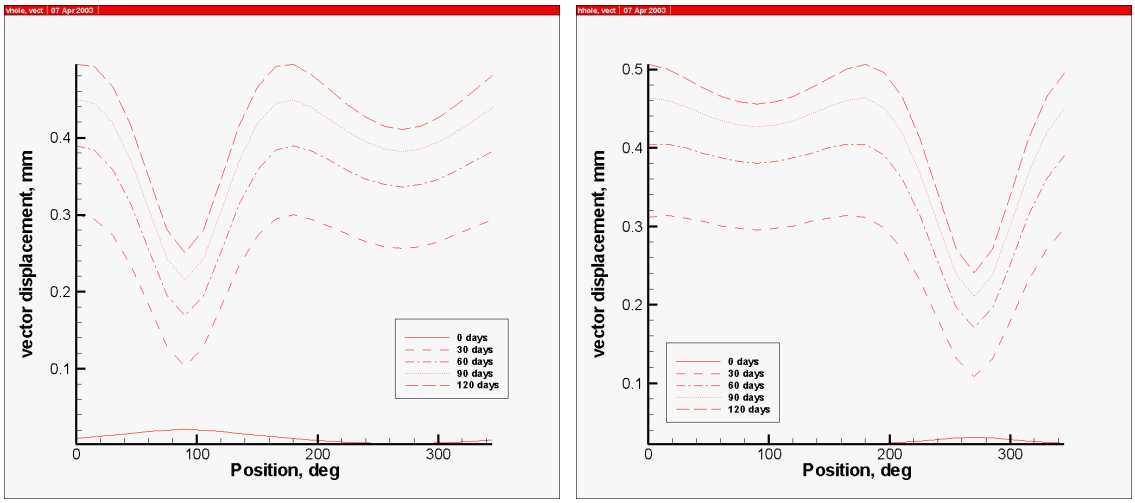

Figure 3-27 *Vector deformation for the lowest case. a) unconfined hole; b) confined hole*

The deformation is maximal on the outer boundary of the boreholes, and almost insignificant at the border of the pillar. The vector deformation is slightly higher in the confined hole for both cases. The maximal deformation at the border of the confined hole is 0.57 mm for the highest case and 0.51 mm for the lowest case.

3.4 Discussion

In consideration of the mechanical properties of the rock and fractures determined in the experiment volumes, and referring to the empirical relationship between vertical applied stress and uniaxial compressive strength /Hoek and Brown, 1980/, the stress levels that would lead to possible rockburst conditions might lay around 110 MPa, assuming a uniaxial compressive strength of around 210-220 MPa for the intact rock /Staub et al., 2003/.

The modeling results have been analyzed in order to check if such a stress level can be achieved with the given layout and input properties. According to the preliminary results the level of stress requires for spalling might be achieved after a period of 30-60 days of heating even without slots. The slots that had been designed to insure that the stress increase will be sufficient to initiate spalling appear to be unnecessary.

The sensitivity analysis on deformation modulus and thermal conductivity has then been conducted in order to determine the range of outcomes with regards to the potential range of mechanical and thermal properties of the rock mass. The range of values has been defined by considering the highest and lowest values these parameters might take in the experiment area. Nevertheless the modeling outcomes are quite sensitive to these parameters and these will be updated as core samples from the pilot boreholes are tested.

After 120 days of heating the level of total stresses lies between 150 and 173 MPa, all combinations presented in section 3.3 being considered.

4 Conclusions

Preliminary 2D coupled thermo-mechanical simulations grounded the determination of the optimal layout for the position of heaters around the experiment. The suggested heating system is composed of 4 heaters located 1.9 m away from the middle of the pillar, 2 on each side. The heaters are far enough from the AE system to avoid damages on the receivers and transmitters.

Further modeling has been conducted to estimate the response of the rock mass and the range of temperature, major total stress and deviatoric stresses reached in the pillar during heating. The evolution of these parameters has been analyzed as a function of depth, in-situ stresses, and thermal and mechanical properties.

The results point out that the level of stress required in the pillar to initiate spalling should be reached even if the properties tend to the “lowest case”. The Engineering of slots appears not to be necessary for the achievement of the experiment.

References

Andersson, C., 2003. Äspö Pillar Stability Experiment. Feasibility study. SKB, IPR-03-01.

Hoek, E., and Brown, E.T., 1980. Underground excavations in rock. The institution of mining and metallurgy, London. 527 p.

Nordlund,E., Chunlin, B. and Carlsson, B., 1999. Äspö Hard Rock Laboratory, Prototype repository. Mechanical properties of the diorite in the prototype repository at Äspö HRL – Laboratory tests. SKB, IPR-99-25.

Rehbinder, G., and Stille. H., 1985. Termoinducerade spänningar och förskjutningar – jämförelse mellan mätningar och beräkningar. Bergmekanikdag 1985, p. 93-101.

Stacey, T. R., 1981. A simple extension strain criterion for fracture of brittle rocl. Int. Jn. Rock Mech. Min. Sci., Vol. 18, page 469-474.

Staub, I., Janson, T., and Fredriksson, A., 2003. Äspö Pillar Stability Experiment. Geology and properties of the rock mass around the experiment volume. SKB, IPR-03-02.

Wanne, T., and Johansson, E., 2003. Äspö Pillar Stability Experiment. Coupled 3D thermo-mechanical modeling. SKB, IPR-03-04.

Appendix A. Results of heating, alternative 1, 2 heaters

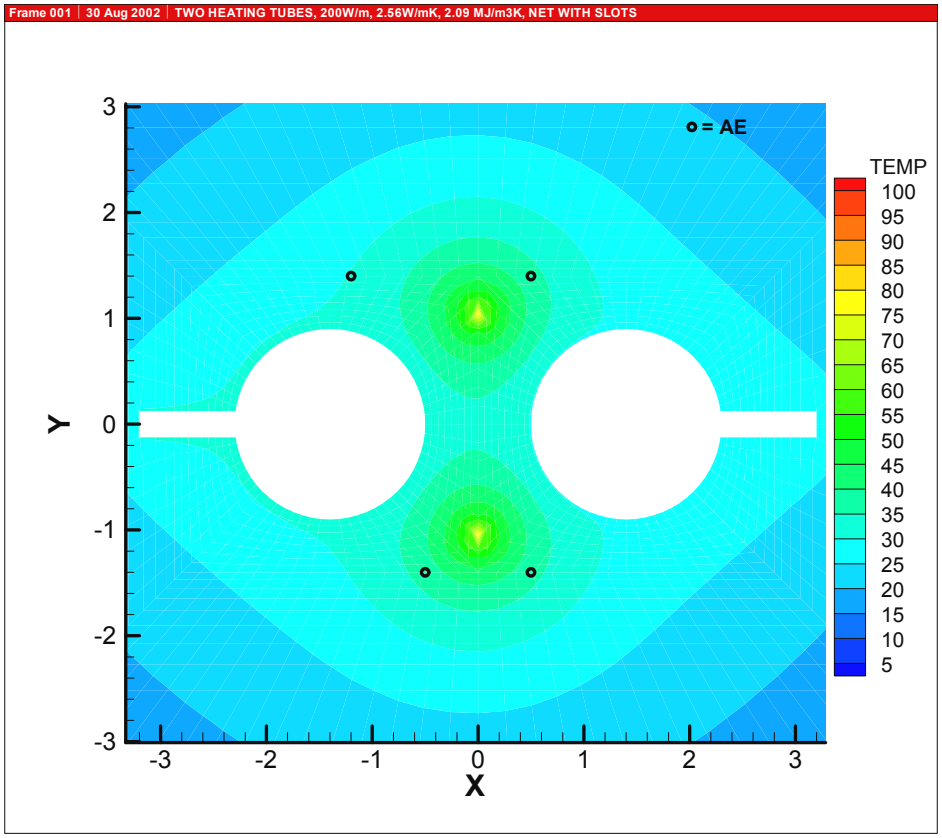

Figure A3. *Temperature distribution after 60 days, ^{o}C. Two heating tubes 200W/m.*

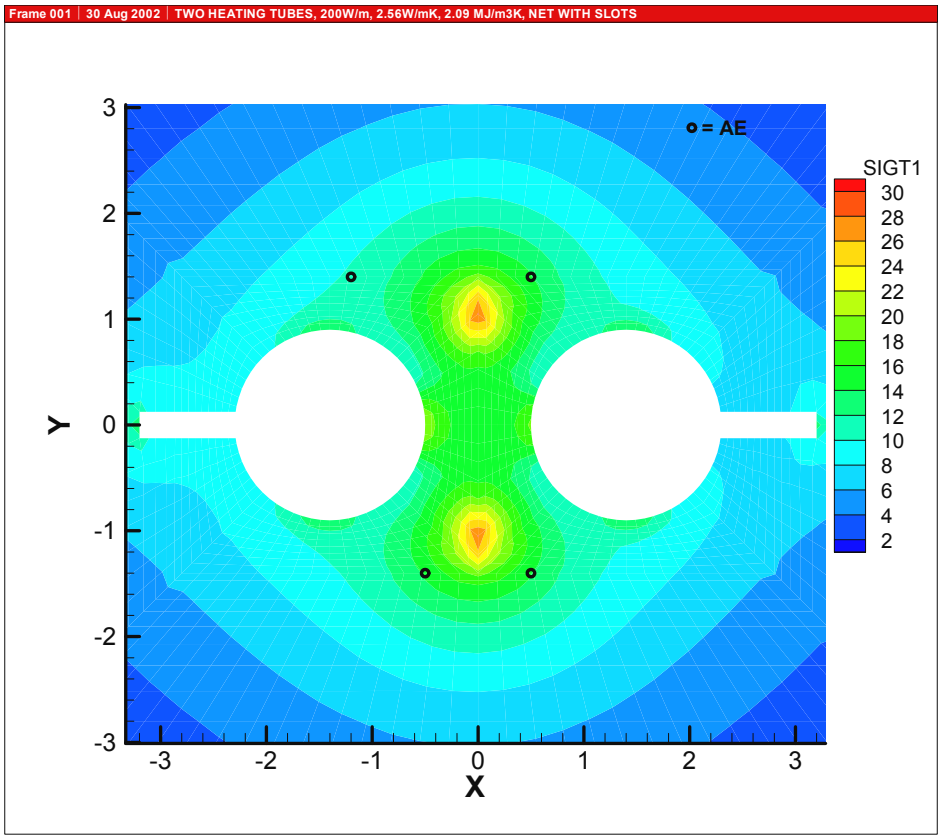

Figure A4. *Temperature induced stresses, MPa, after 60 days. Two heating tubes 200W/m.*

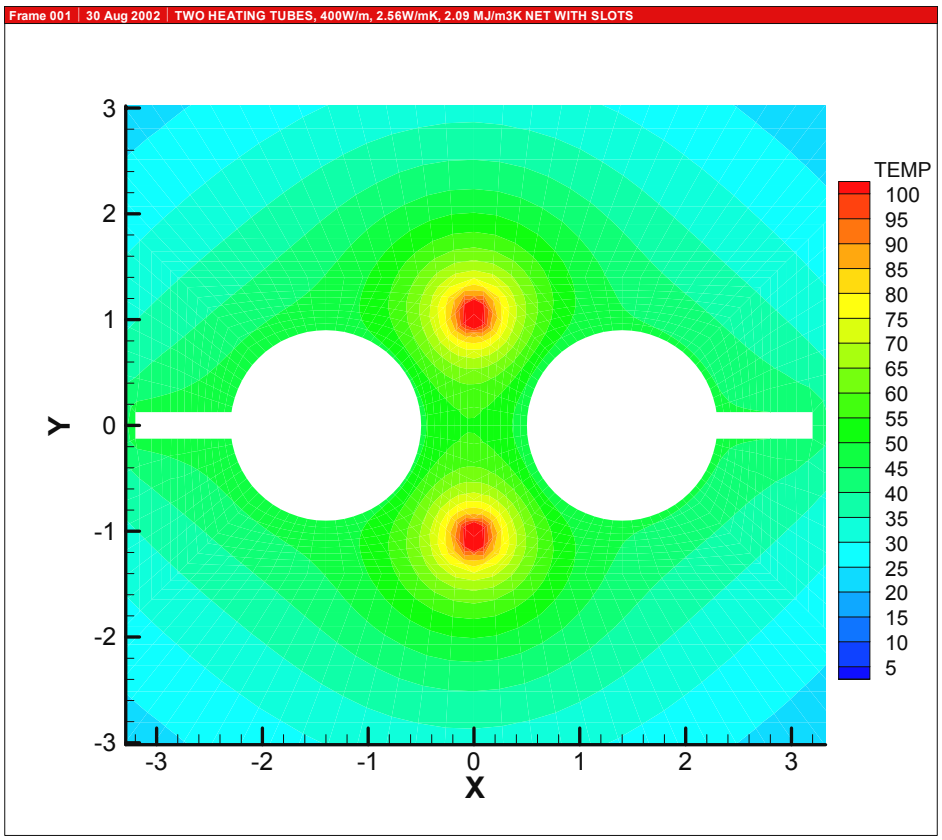

Figure A7. *Temperature distribution after 60 days, ^{o}C. Two heating tubes 400W/m.*

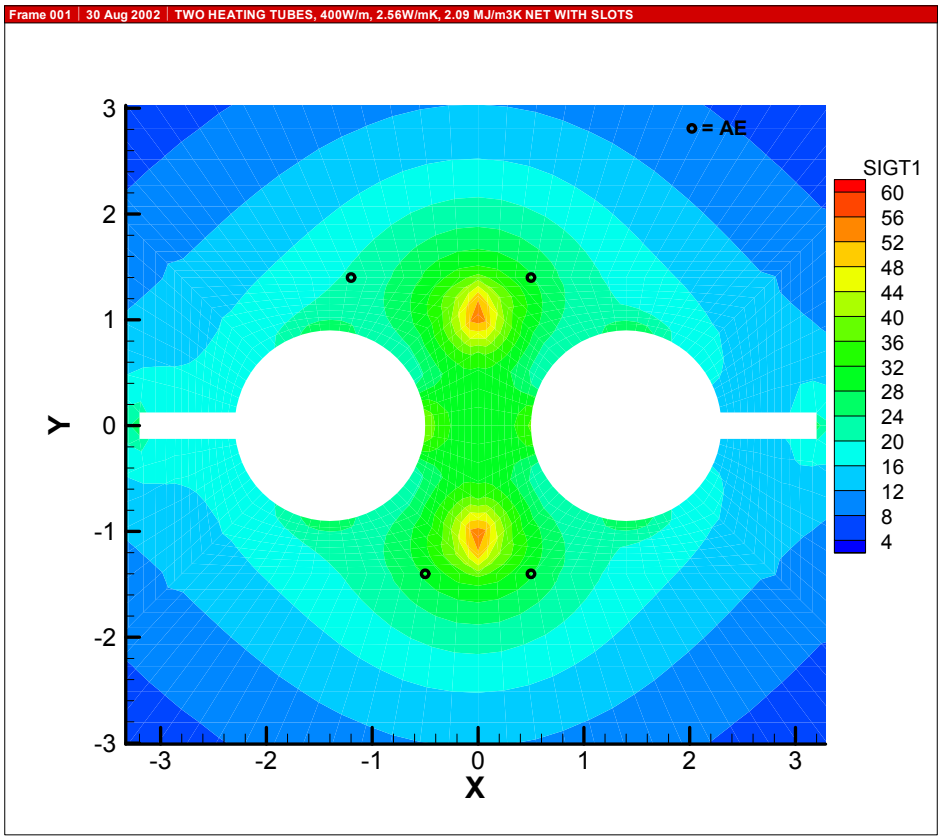

Figure A8. *Temperature induced stresses, MPa, after 60 days. Two heating tubes 400W/m.*

Appendix B. Results of heating, alternative 2, 4 heaters

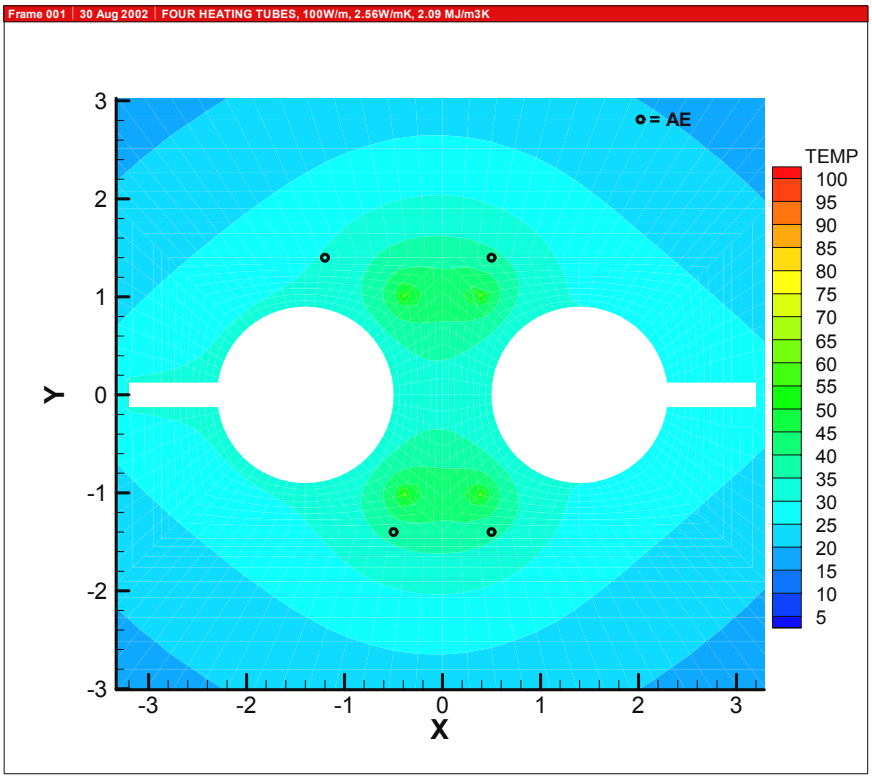

Figure B1. *Temperature distribution after 60 days, ^{o}C. Four heating tubes 100W/m.*

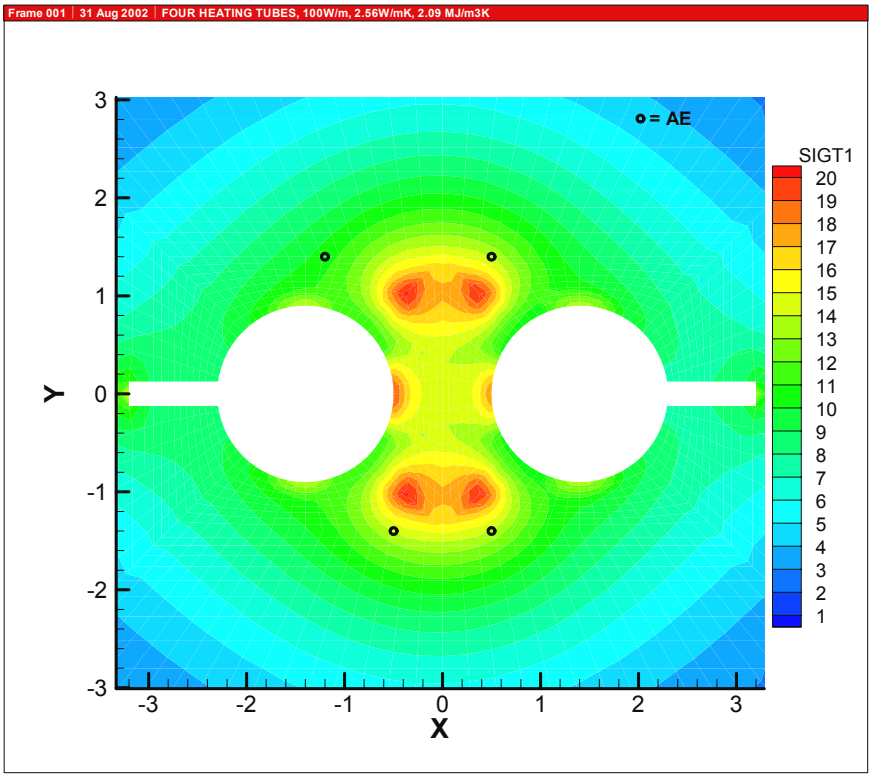

Figure B2. *Temperature induced stresses, MPa, after 60 days.*

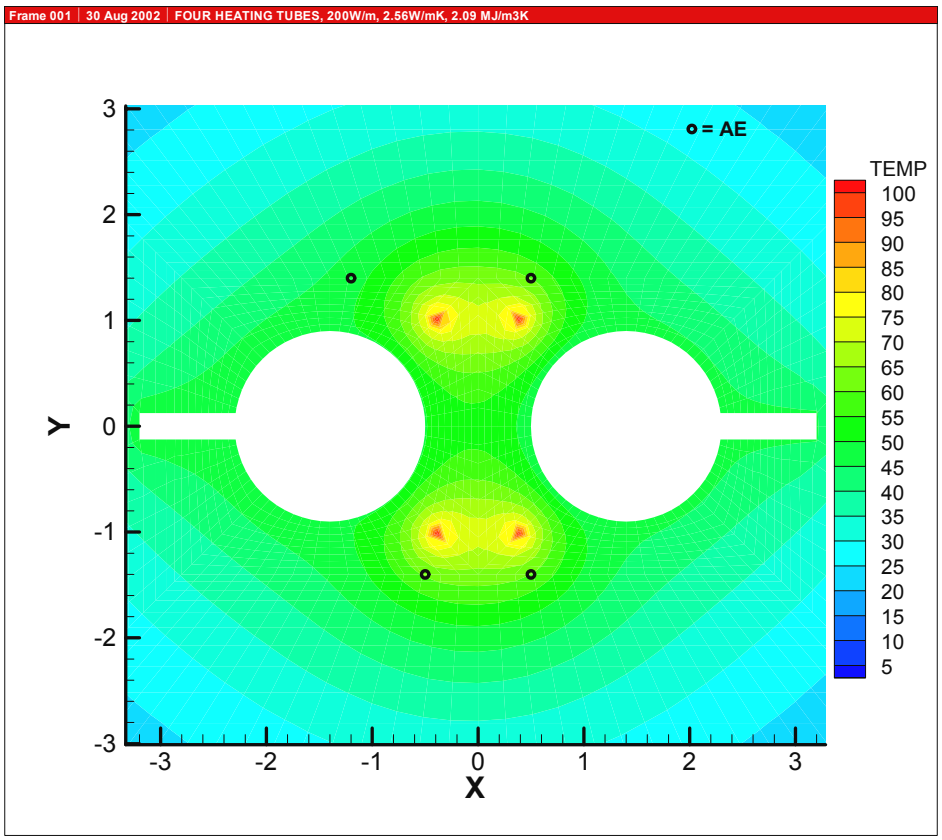

Figure B3. *Temperature distribution after 60 days, ^{o}C. Four heating tubes 200W/m.*

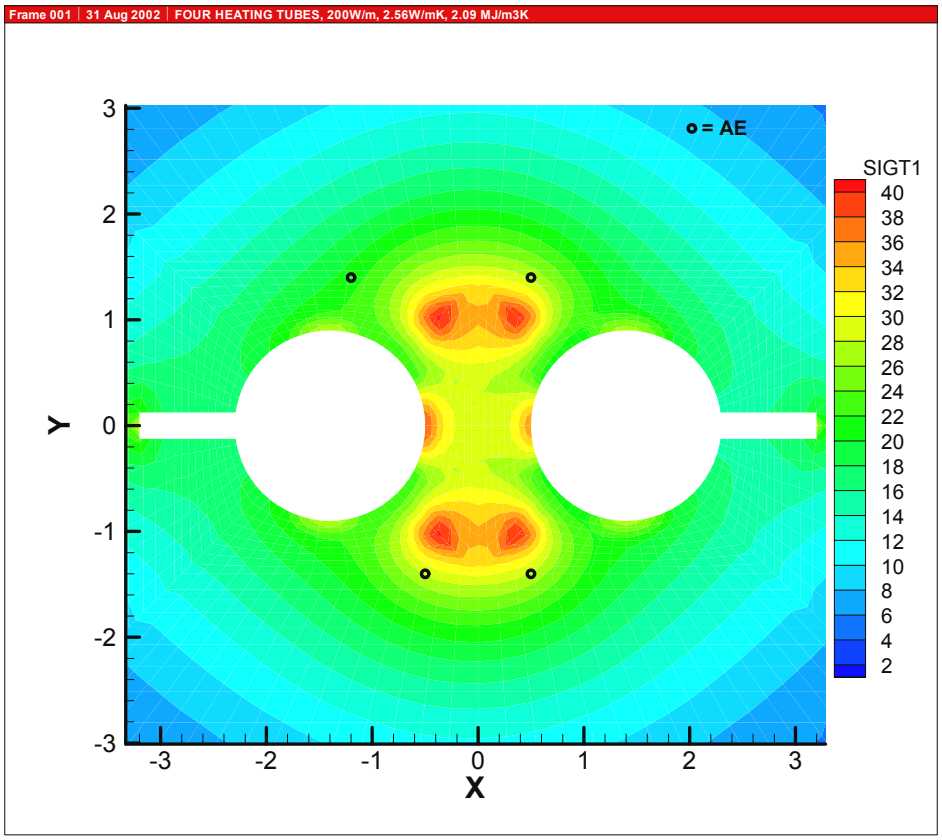

Figure B4. *Temperature induced stresses, MPa, after 60 days.*

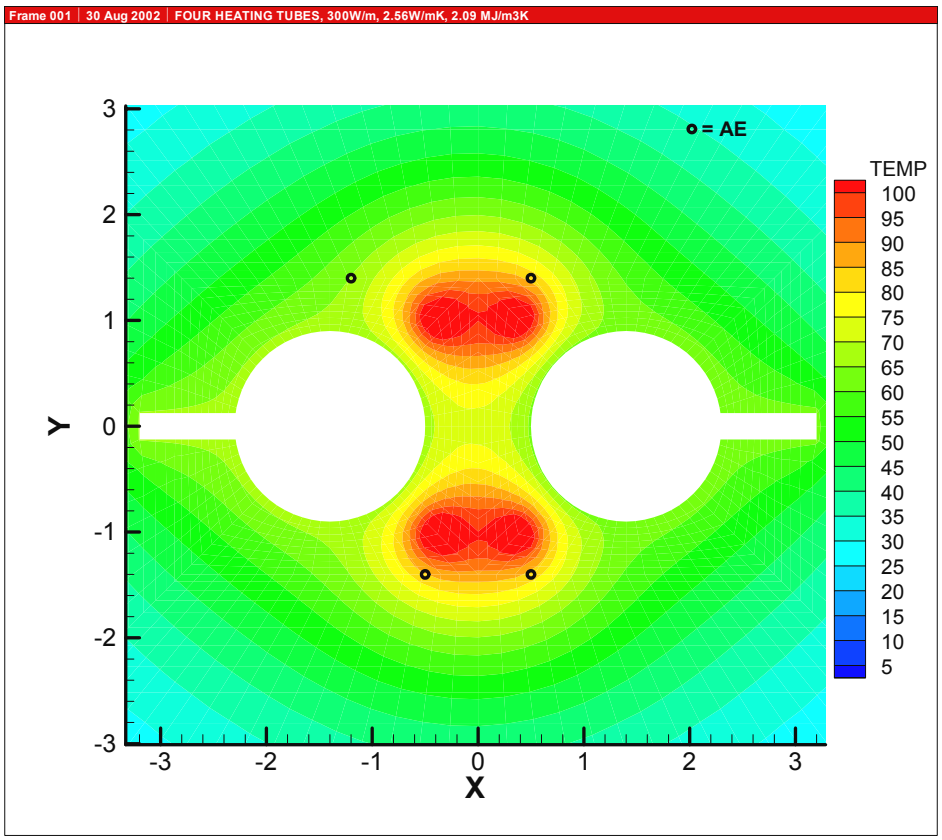

Figure B5. *Temperature distribution after 60 days, ^{o}C. Four heating tubes 300W/m.*

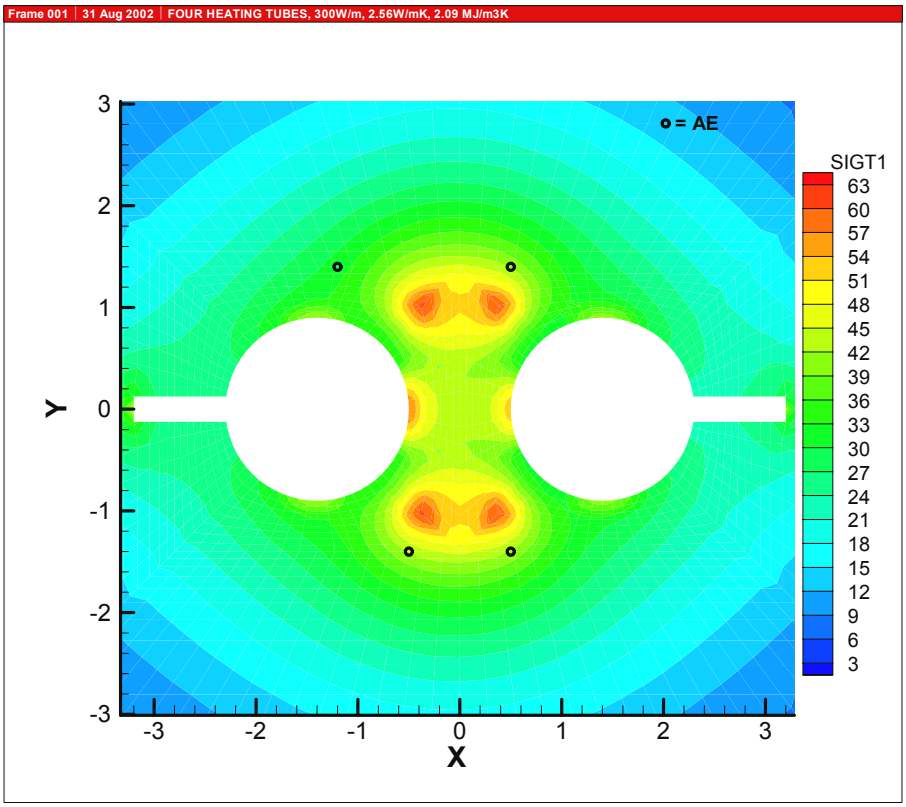

Figure B6. *Temperature induced stresses, MPa, after 60 days.*

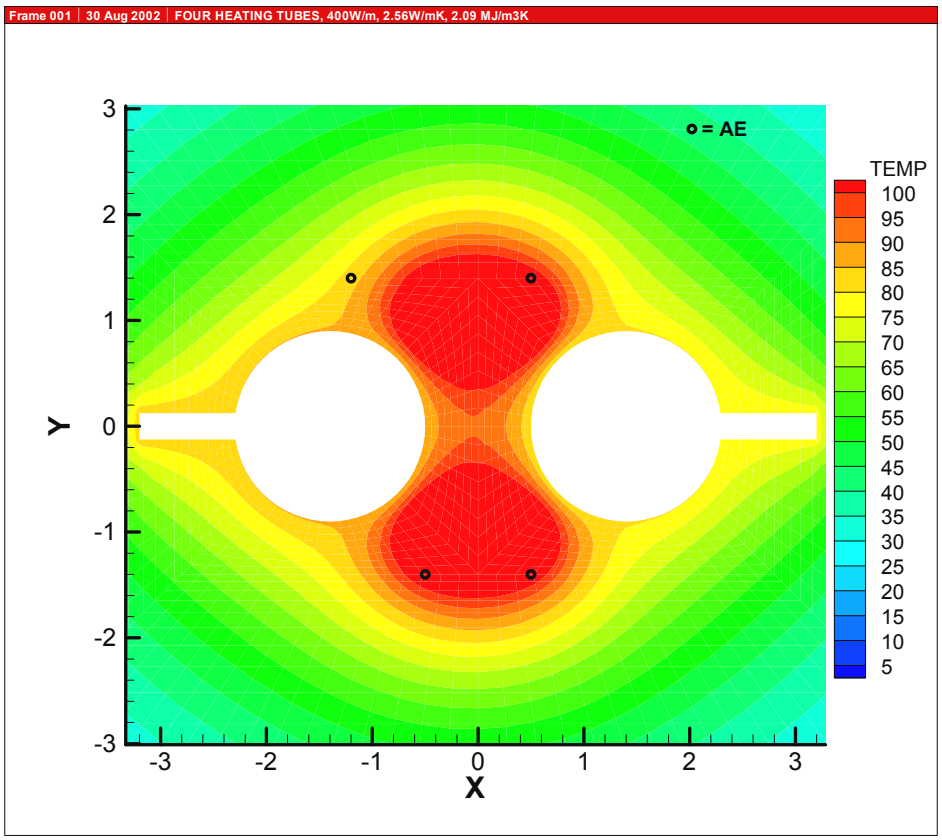

Figure B7. *Temperature distribution after 60 days, ^{o}C. Four heating tubes 400W/m.*

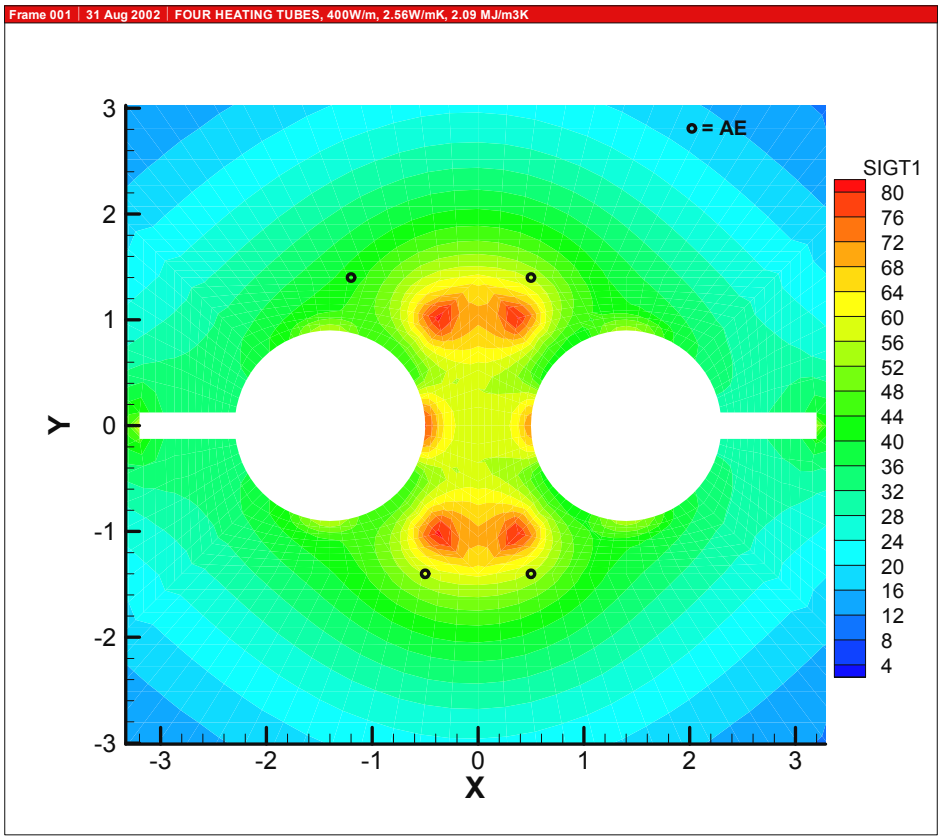

Figure B8. *Temperature induced stresses, MPa, after 60 days.*

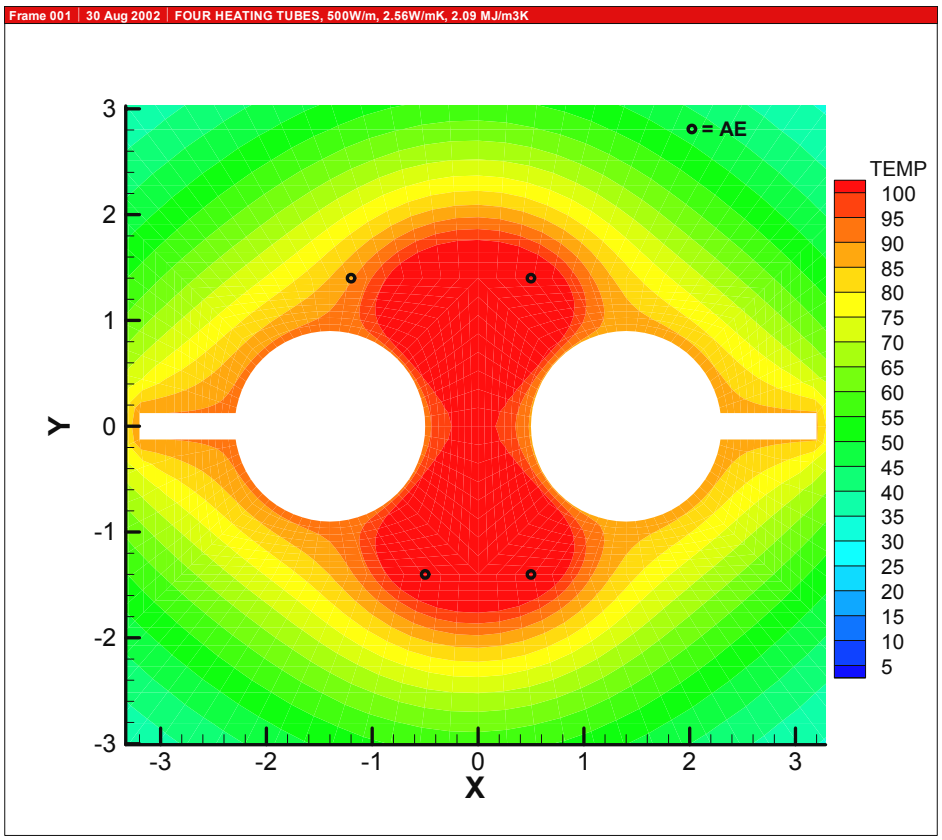

Figure B9. *Temperature distribution after 60 days, °C. Four heating tubes 500W/m.*

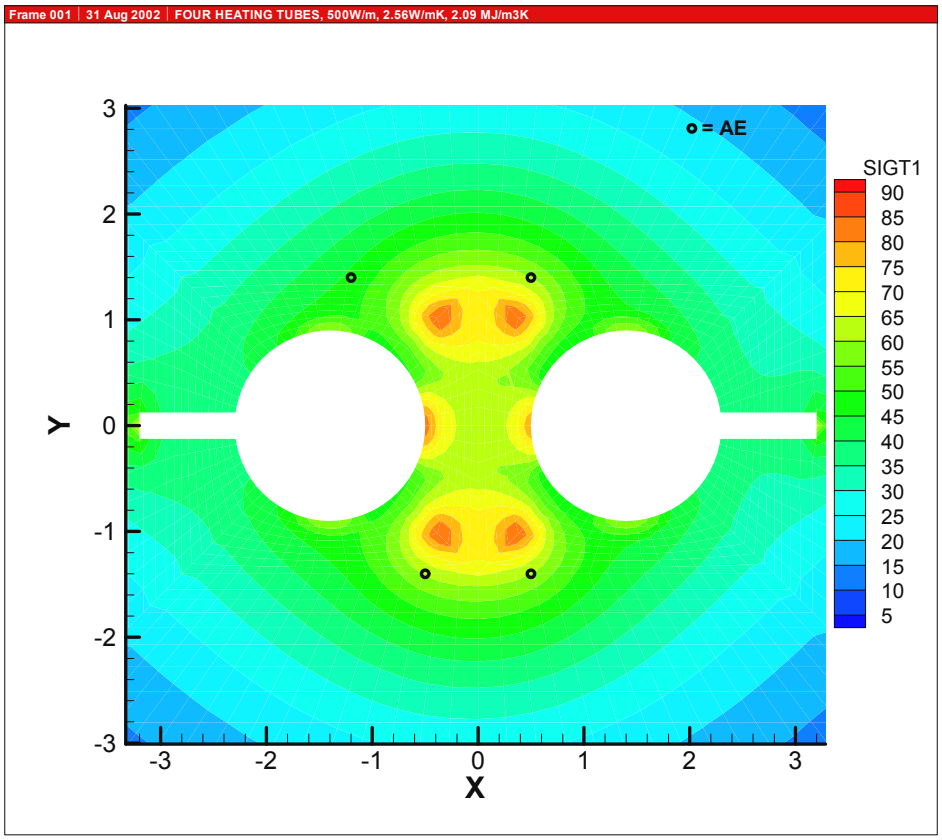

Figure B10. *Temperature induced stresses, MPa, after 60 days.*

Appendix C. Results of heating, alternative 3, 4 heaters

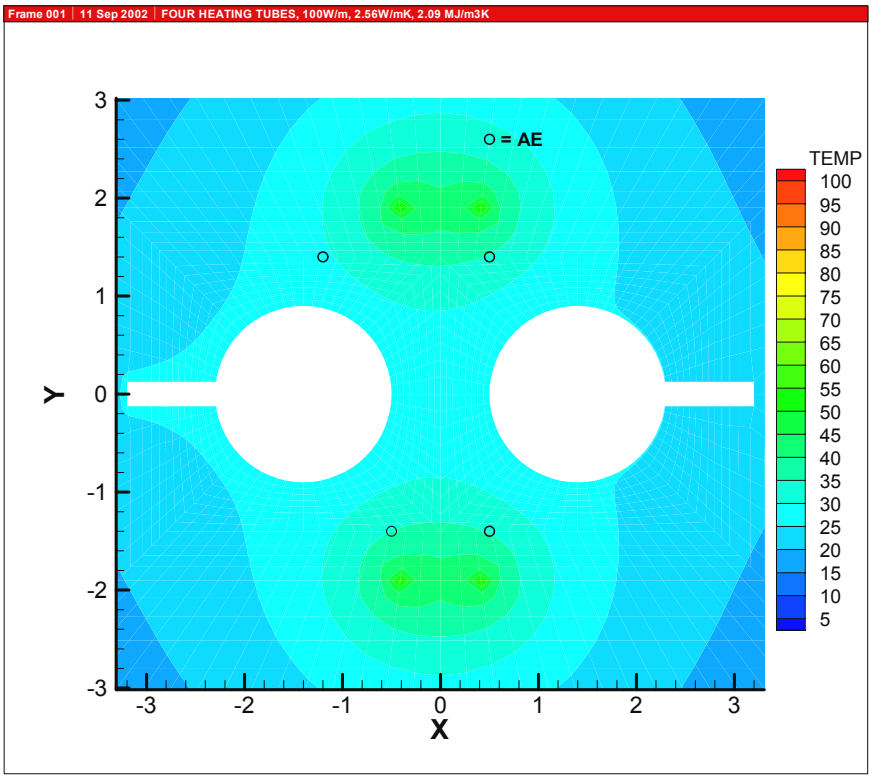

Figure C1. *Temperature distribution after 60 days, ^{o}C. Four heating tubes 100W/m.*

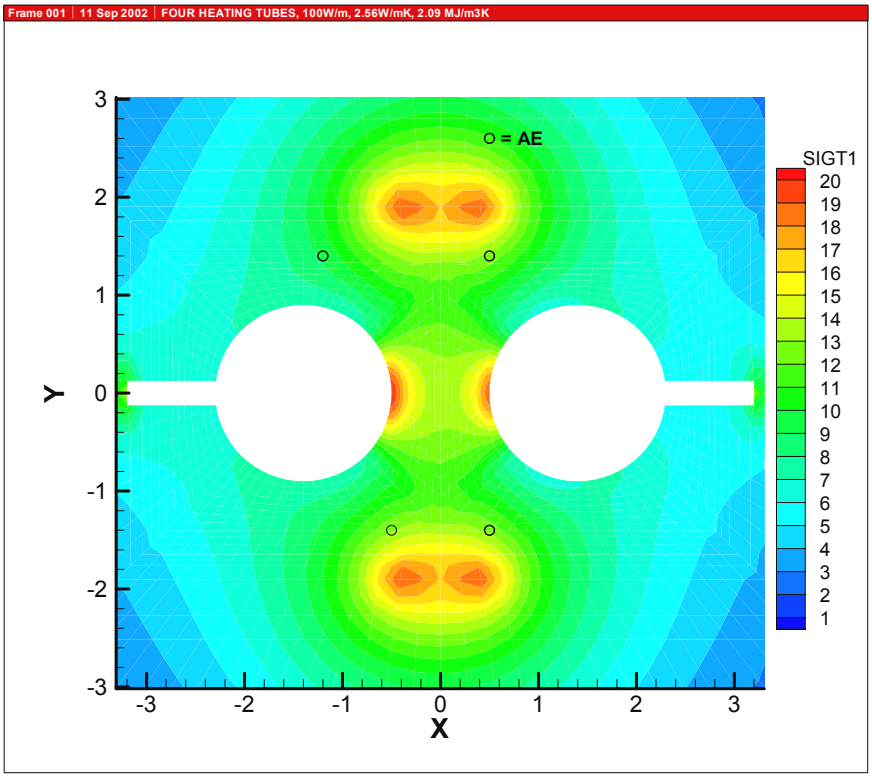

Figure C2*. Temperature induced stresses, MPa, after 60 days.*

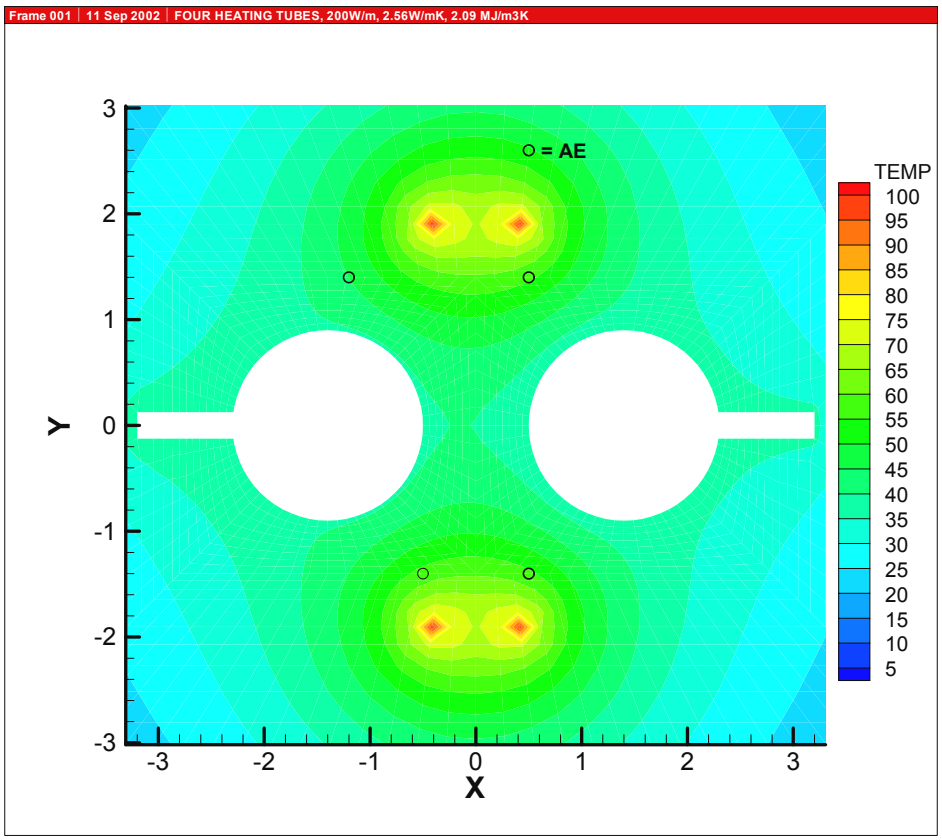

Figure C3. *Temperature distribution after 60 days, ^{o}C. Four heating tubes 200W/m.*

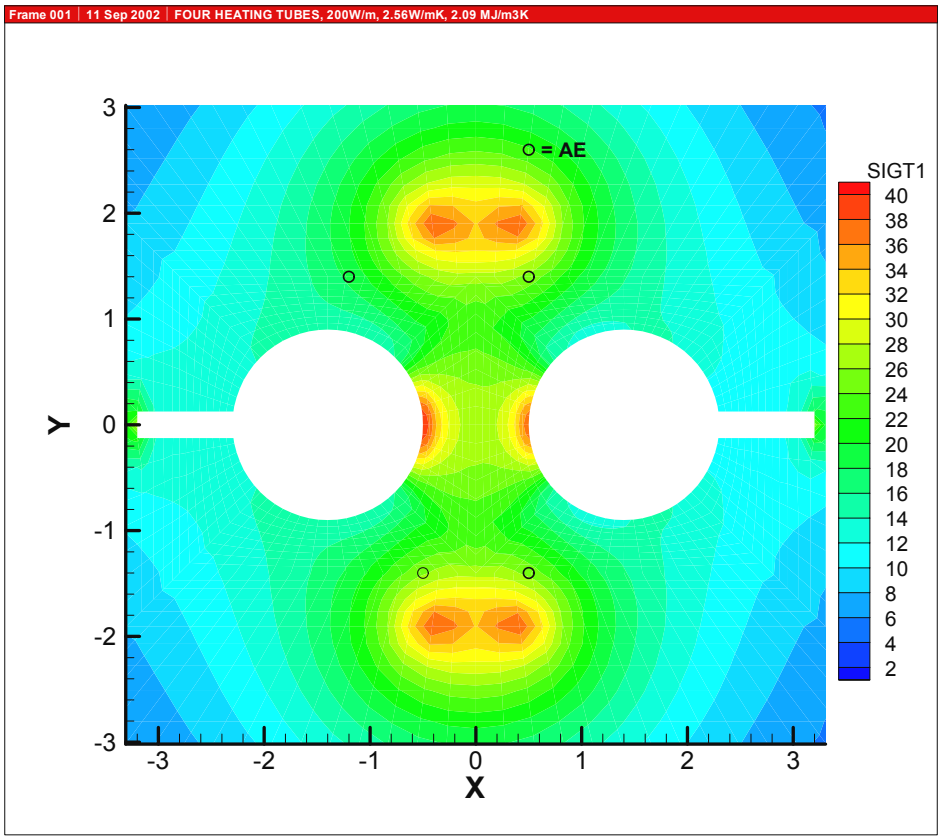

Figure C4. *Temperature induced stresses, MPa, after 60 days.*

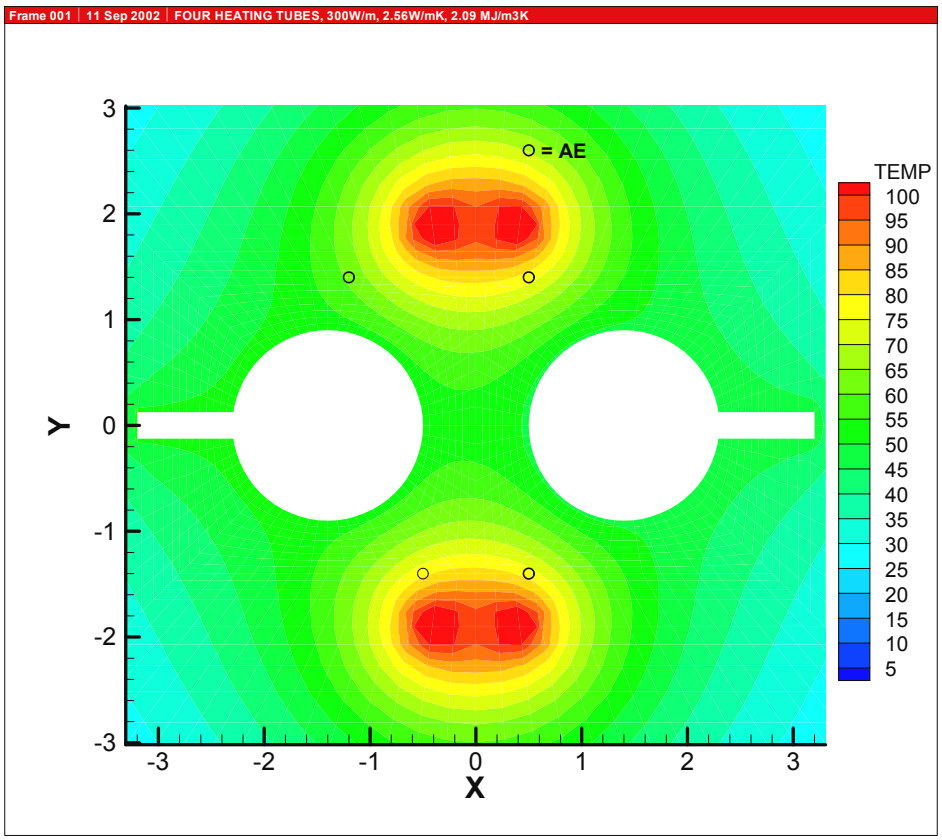

Figure C5. *Temperature distribution after 60 days, ^{o}C. Four heating tubes 300W/m.*

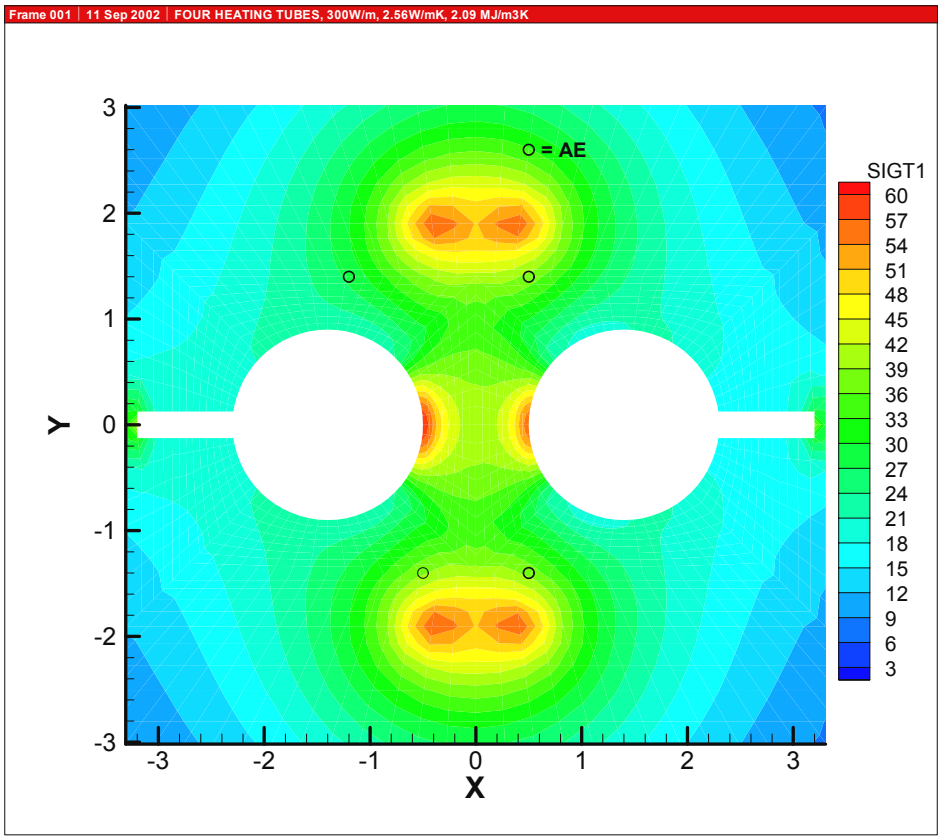

Figure C6. *Temperature induced stresses, MPa, after 60 days.*

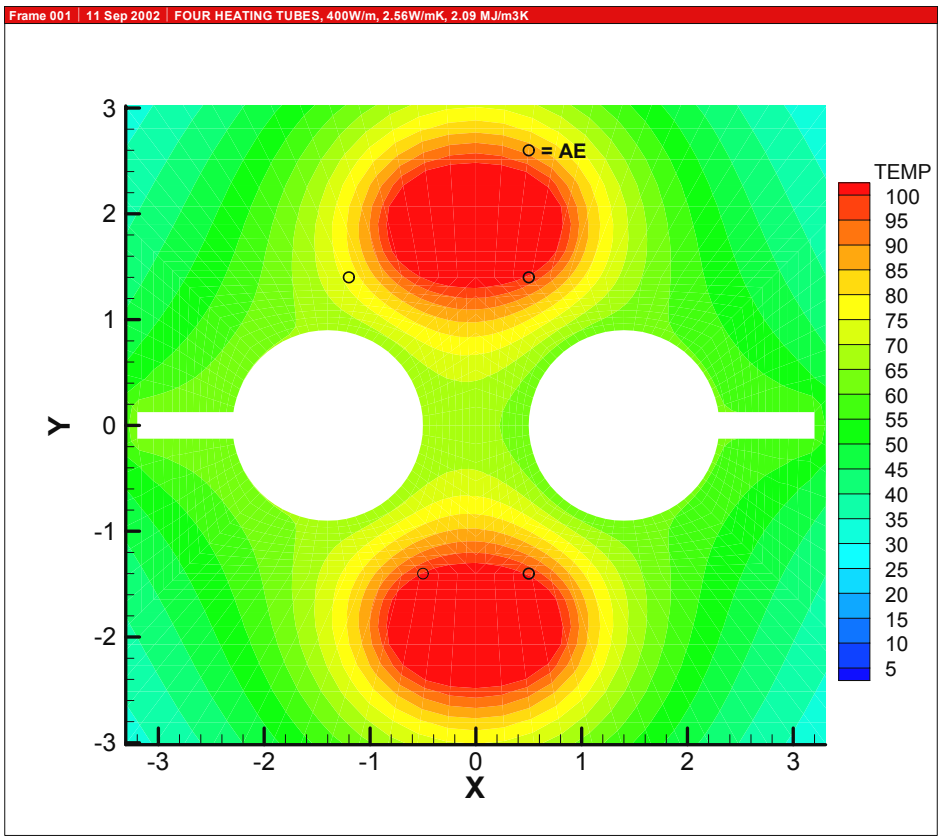

Figure C7. *Temperature distribution after 60 days, °C. Four heating tubes 400W/m.*

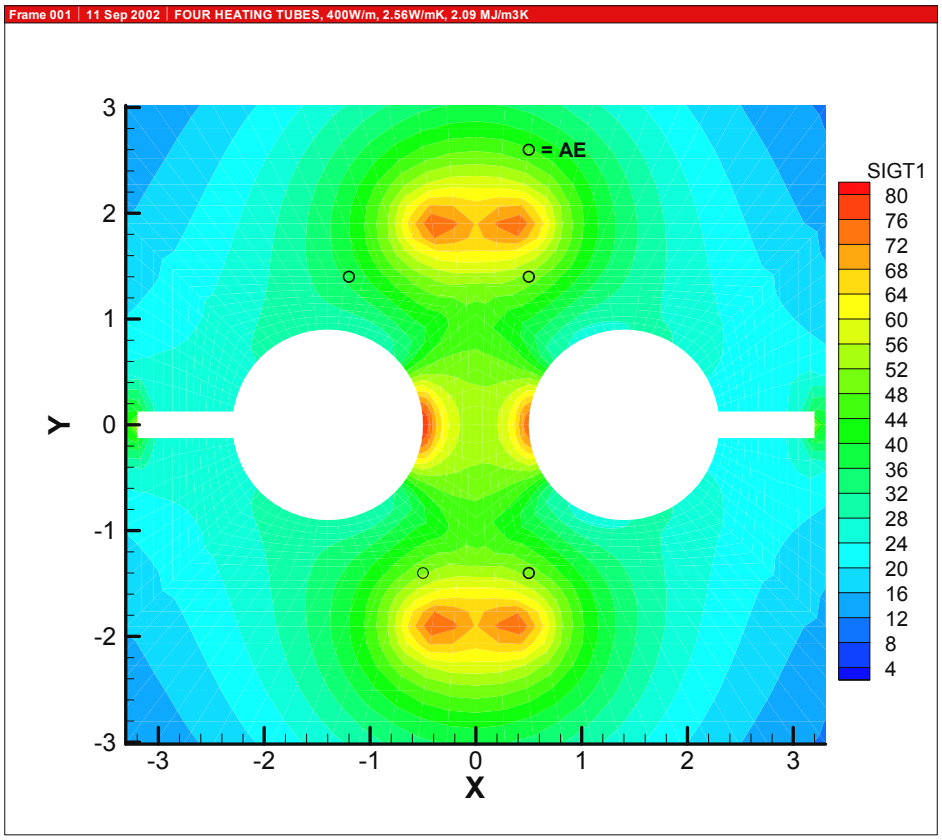

Figure C8. *Temperature induced stresses, MPa, after 60 days.*

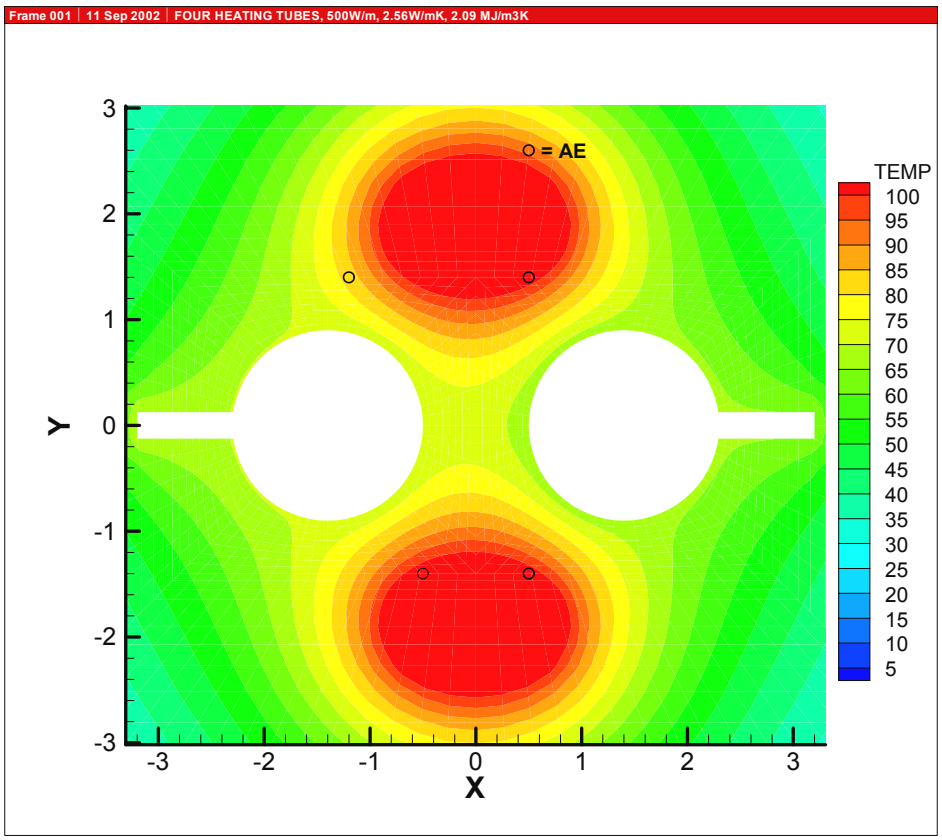

Figure C9. *Temperature distribution after 60 days, ^{o}C. Four heating tubes 500W/m.*

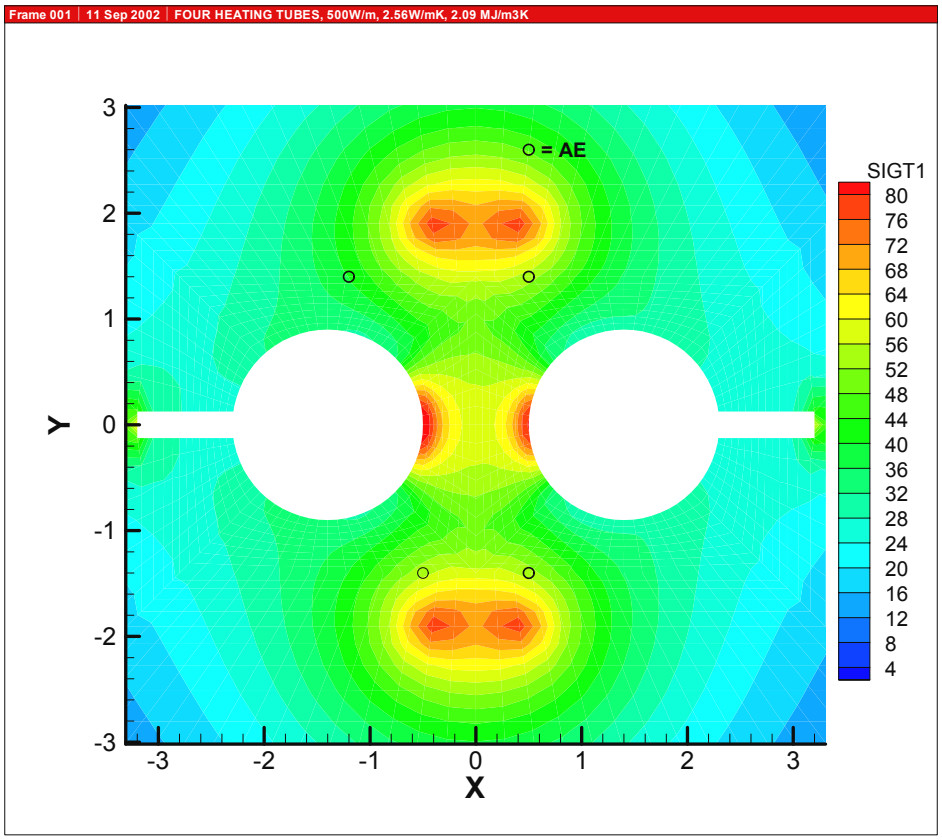

Figure C10. *Temperature induced stresses, MPa, after 60 days.*

Appendix D. Complementary test results for the proposed layout

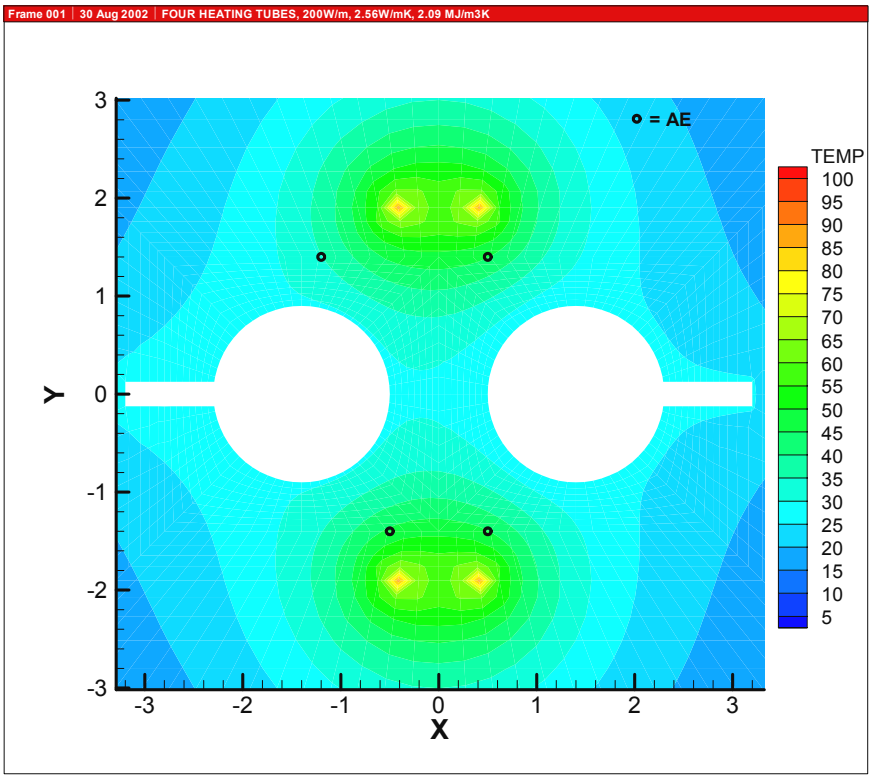

Figure D1. *Temperature distribution after 30 days, ^{o}C. Four heating tubes 200W/m.*

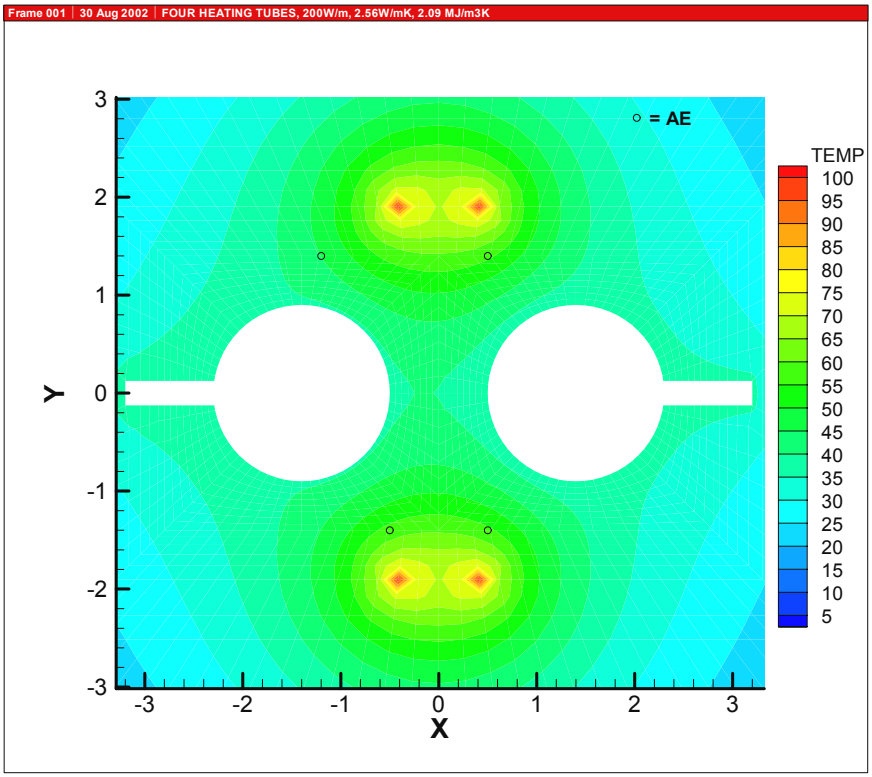

Figure D2. *Temperature distribution after 60 days, ^{o}C. Four heating tubes 200W/m.*

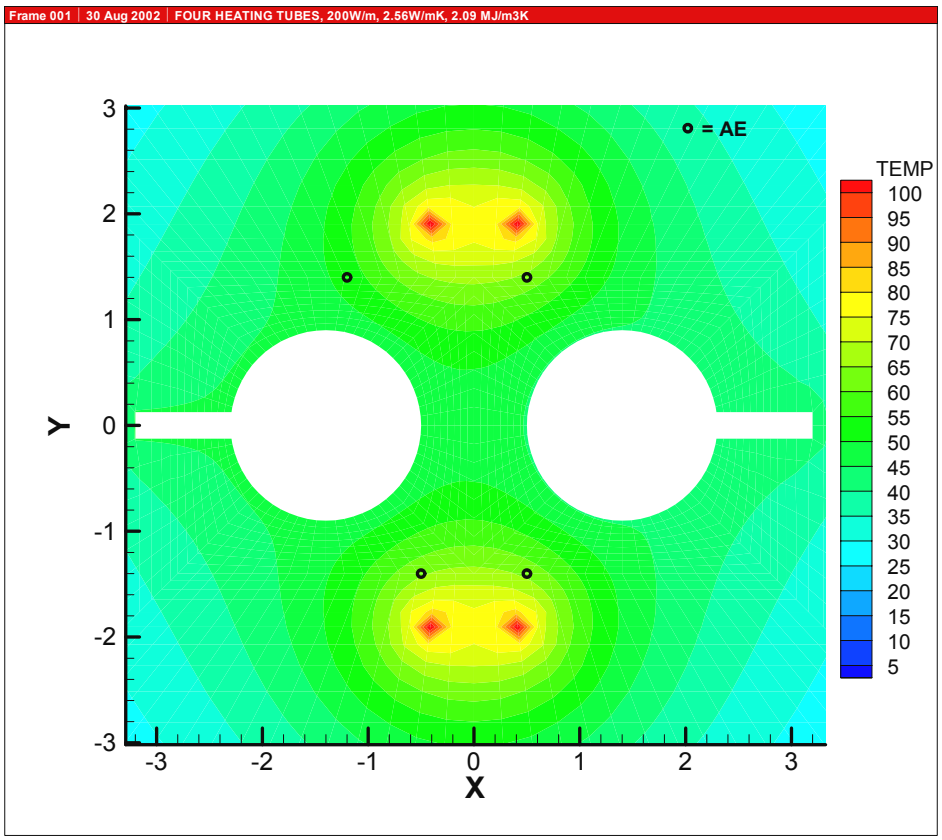

Figure D3. *Temperature distribution after 90 days, ^{o}C. Four heating tubes 200W/m.*

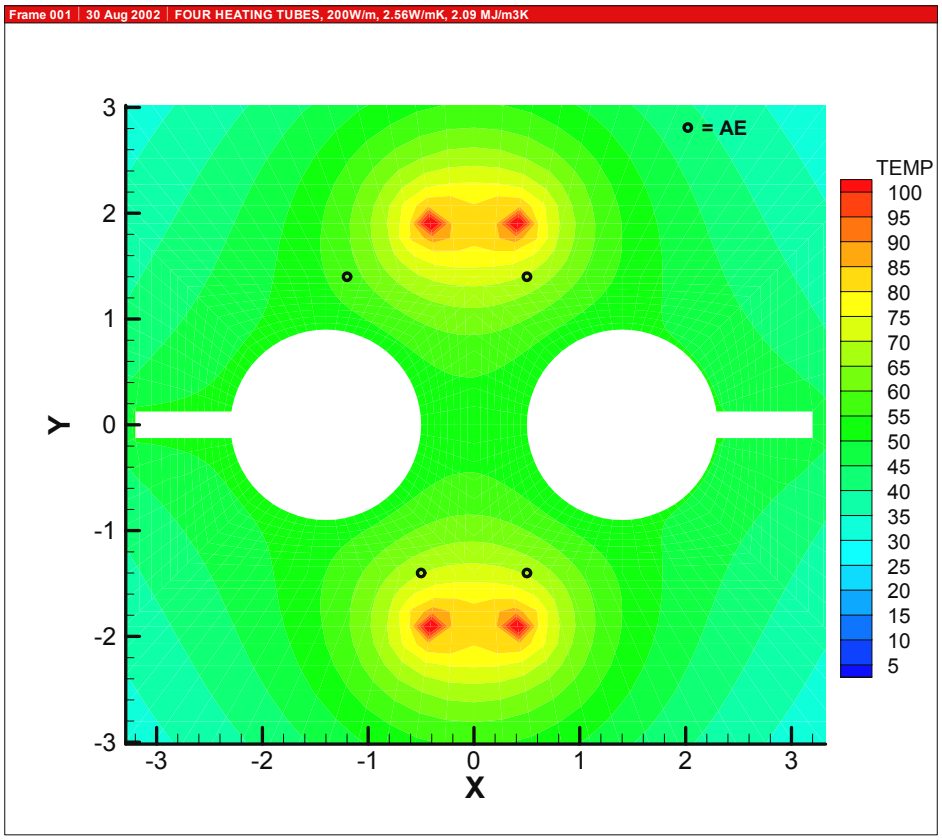

Figure D4. *Temperature distribution after 120 days, ^{o}C. Four heating tubes 200W/m.*

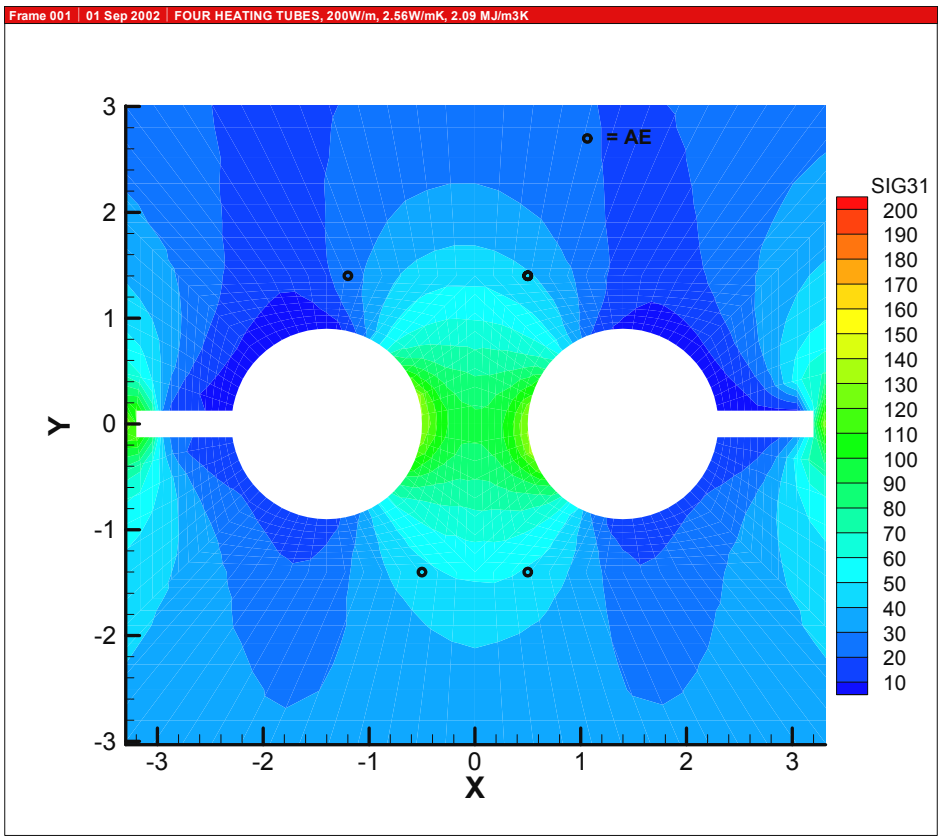

Figure D5. *Major stresses before start heating. 1.5 m below the tunnel floor.*

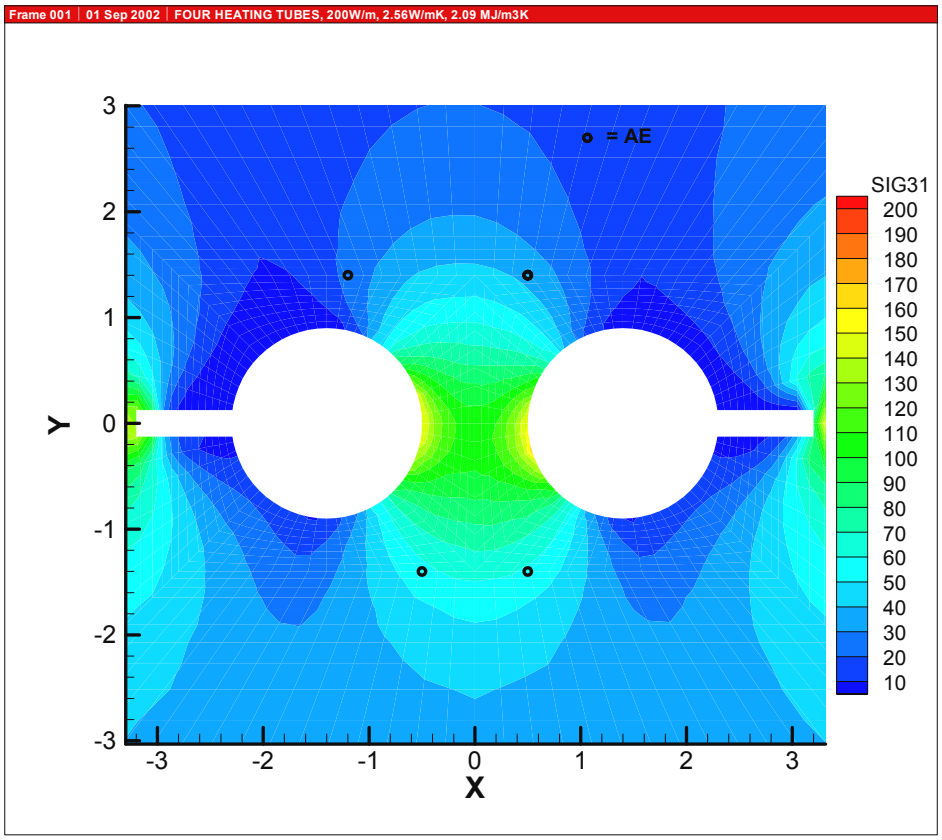

Figure D6. *Major stresses before start heating. 0.5 m below the tunnel floor.*

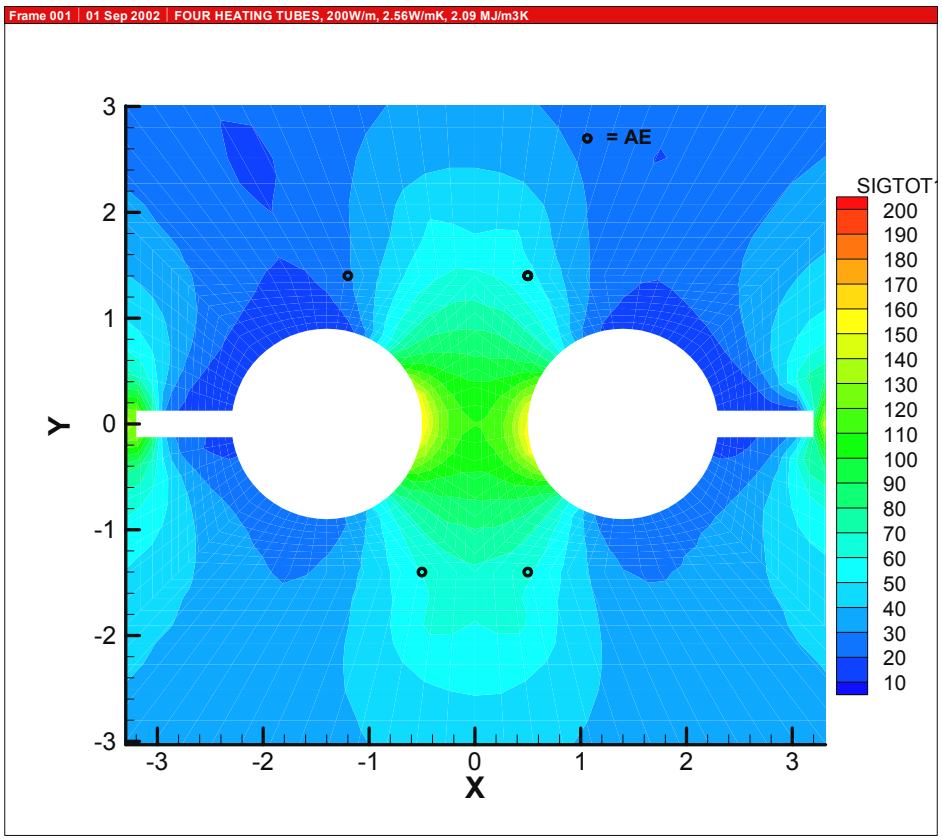

***Figure D7**. Major stresses after 30 days of heating, 200 W/m. 1.5 m below the tunnel floor.*

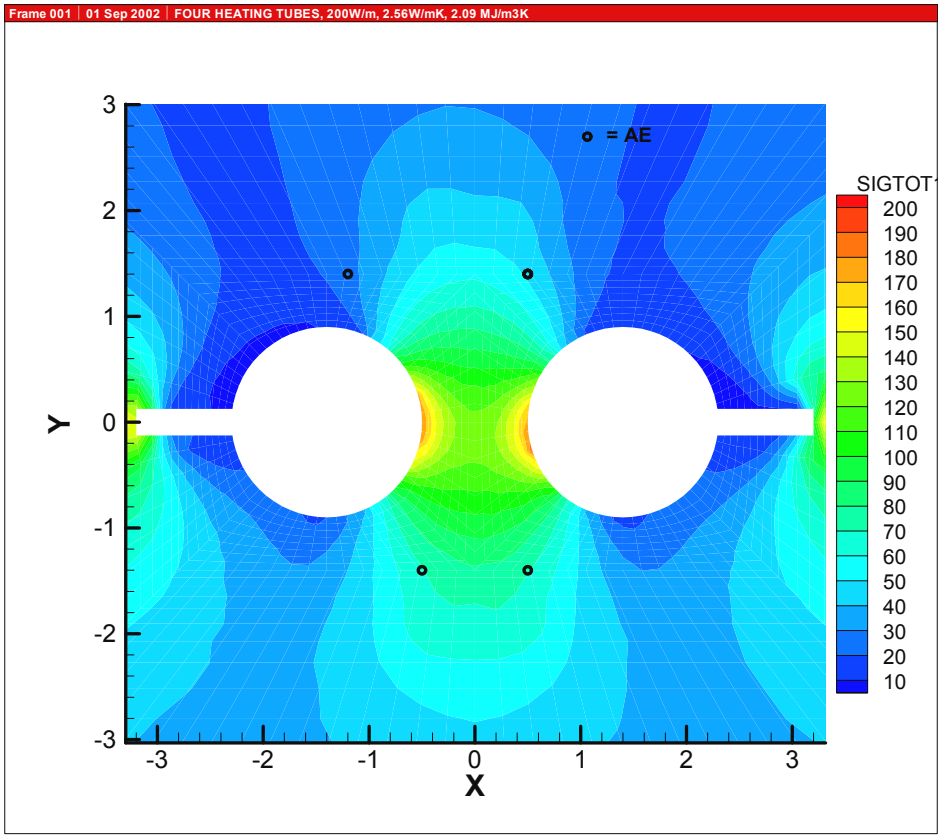

***Figure D8**. Major stresses after 30 days of heating, 200 W/m. 0.5 m below the tunnel floor.*

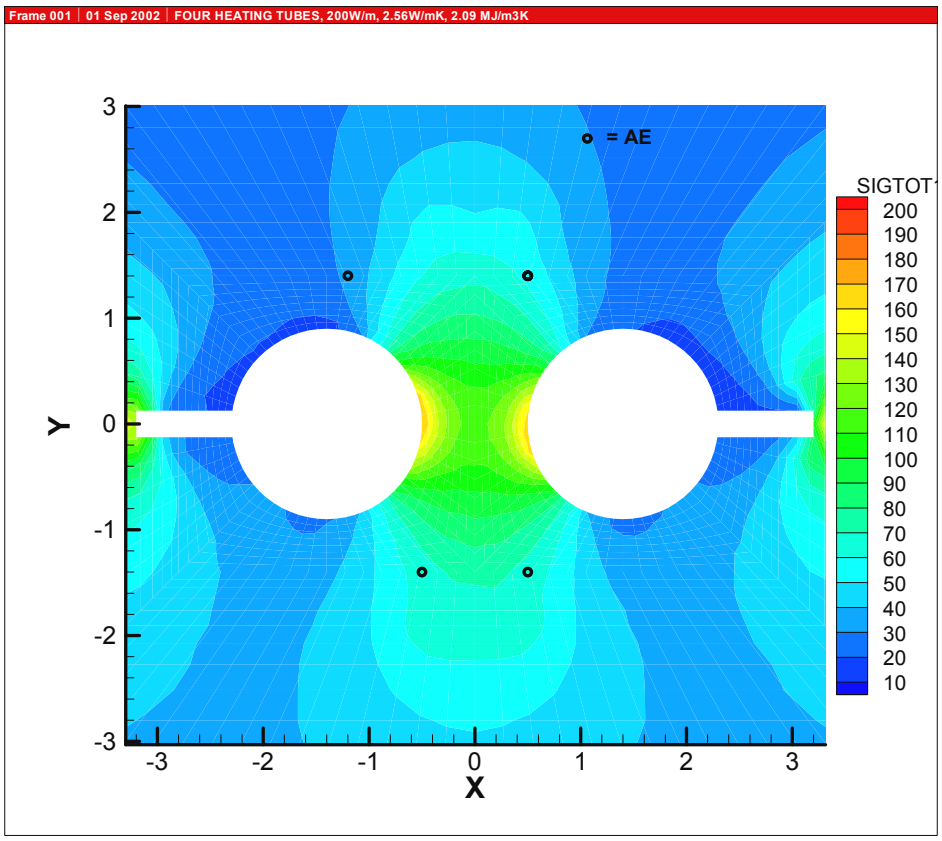

Figure D9. *Major stresses after 60 days of heating, 200 W/m. 1.5 m below the tunnel floor.*

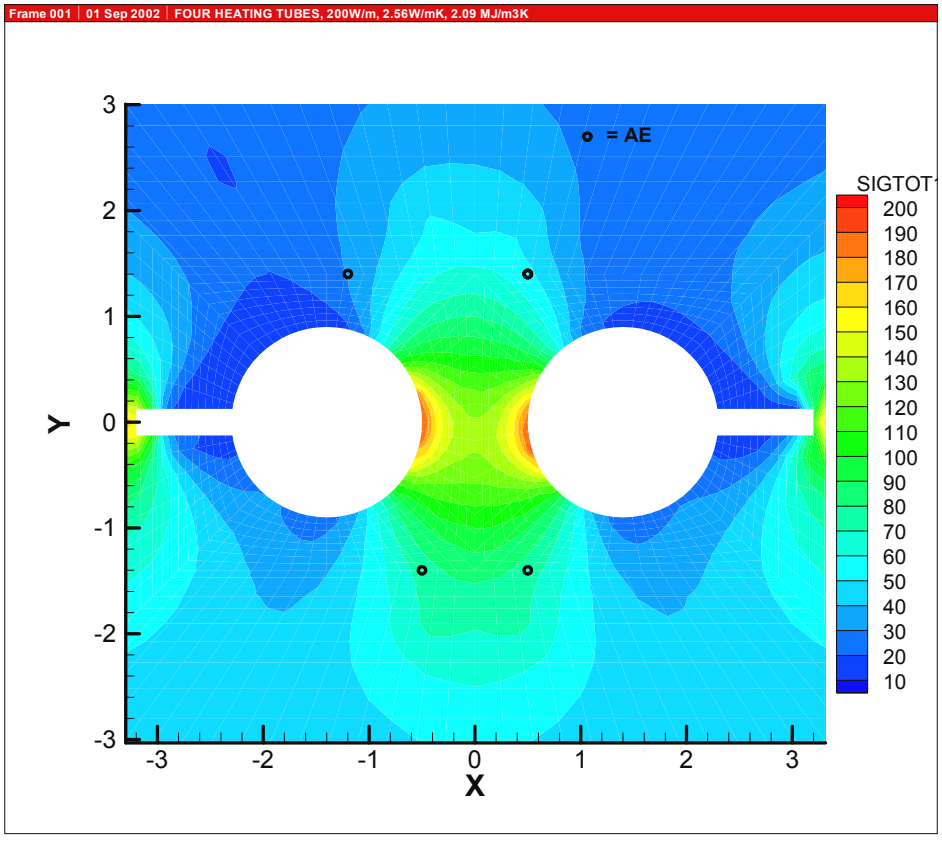

Figure D10. *Major stresses after 60 days of heating, 200 W/m. 0.5 m below the tunnel floor.*

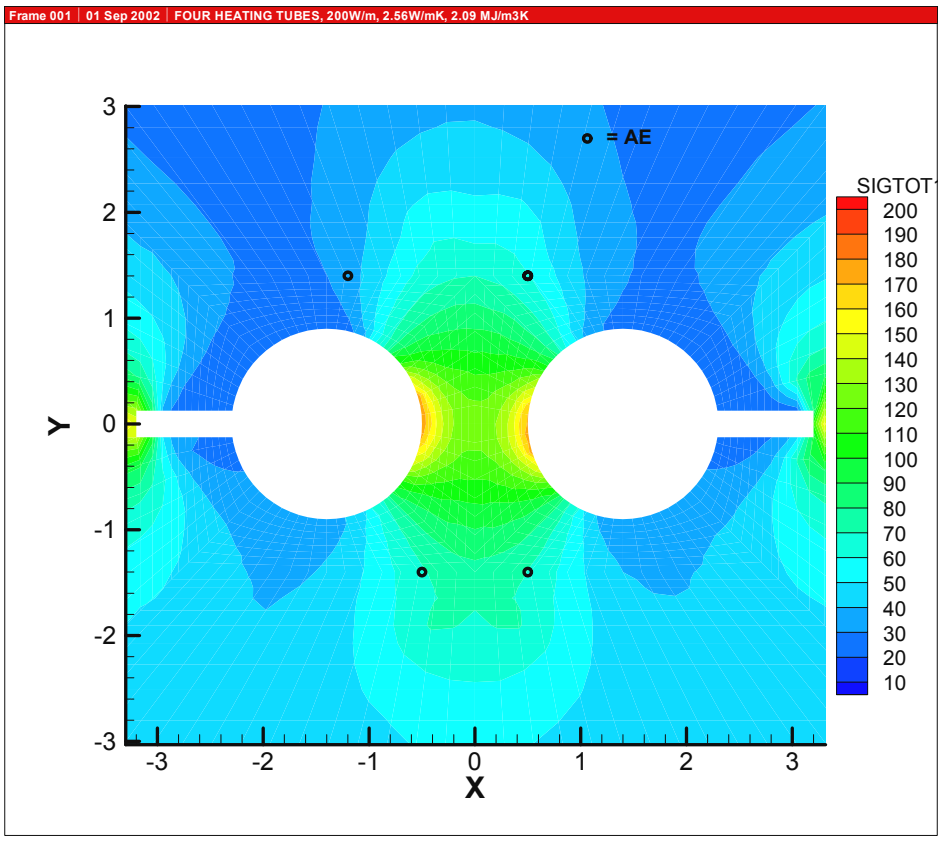

Figure D11. *Major stresses after 90 days of heating, 200 W/m. 1.5 m below the tunnel floor.*

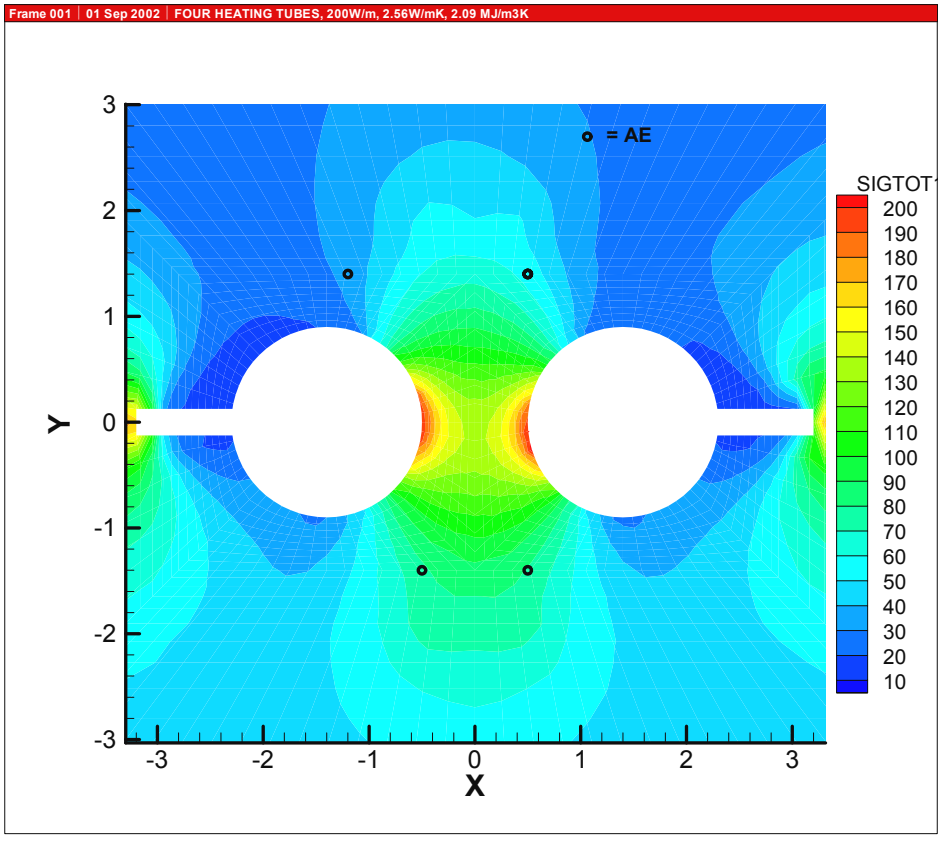

Figure D12. *Major stresses after 90 days of heating, 200 W/m. 0.5 m below the tunnel floor.*

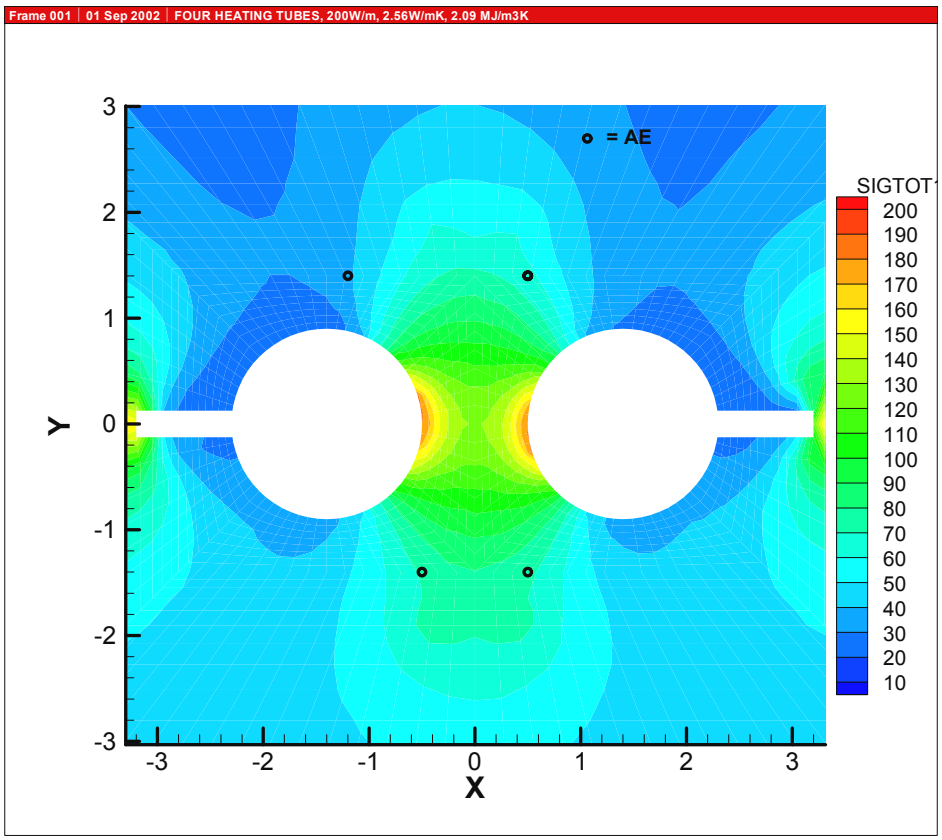

Figure D13. *Major stresses after 120 days of heating, 200 W/m. 1.5 m below the tunnel floor.*

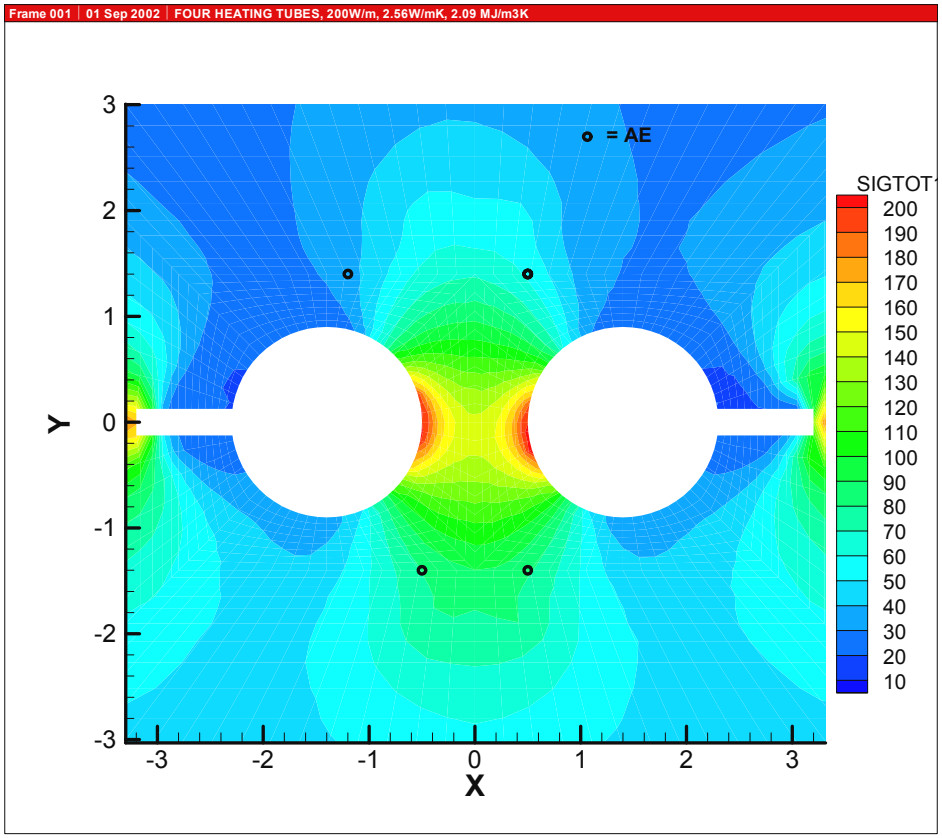

Figure D14. *Major stresses after 120 days of heating, 200 W/m. 0.5 m below the tunnel floor.*

Appendix E. Modeling results for the experiment

The Y-axis represent respectively: total stresses (σ_{TOT1}), deviatoric stresses (σ_{TOT1}-σ_{TOT3}) and temperatures (T).

Explanation of the legend:

xxMPa: value of σ_1 for the given simulation.

hole / 1 MPa / 30d / 60d / 90d / 120d: stage of the modelling. Hole means values taken after excavation of both holes, 1 MPa values monitored after applying the confining pressure of 1 MPa in one hole, 30d to 120d values monitored after 30/60/90/120 days of heating.

a / b refers to the depth level, a is the section located 1.5m below the tunnel floor, b the section located 0.5m below the tunnel floor.

Slots, σ_1=30 MPa, E=68GPa, λ=2.83 W/m, K.

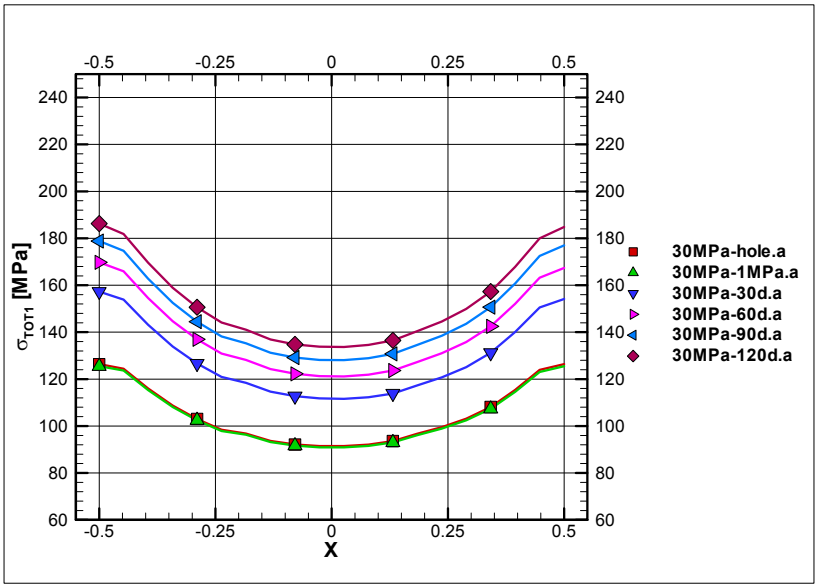

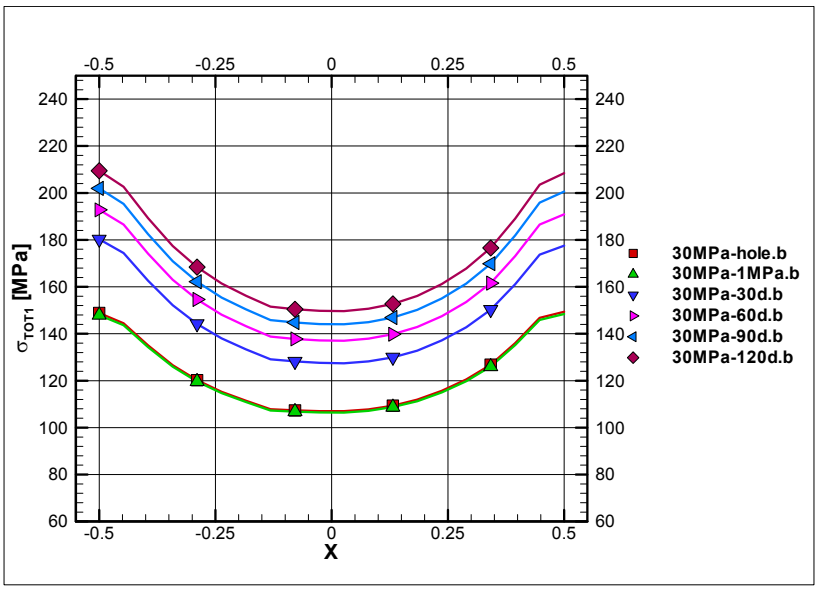
-0.5
-0.25
0
0.25
0.5
240
220
200
180
160
140
120
100
80
60
σTOT1 [MPa]
X
30MPa-hole.b
30MPa-1MPa.b
30MPa-30d.b
30MPa-60d.b
30MPa-90d.b
30MPa-120d.b

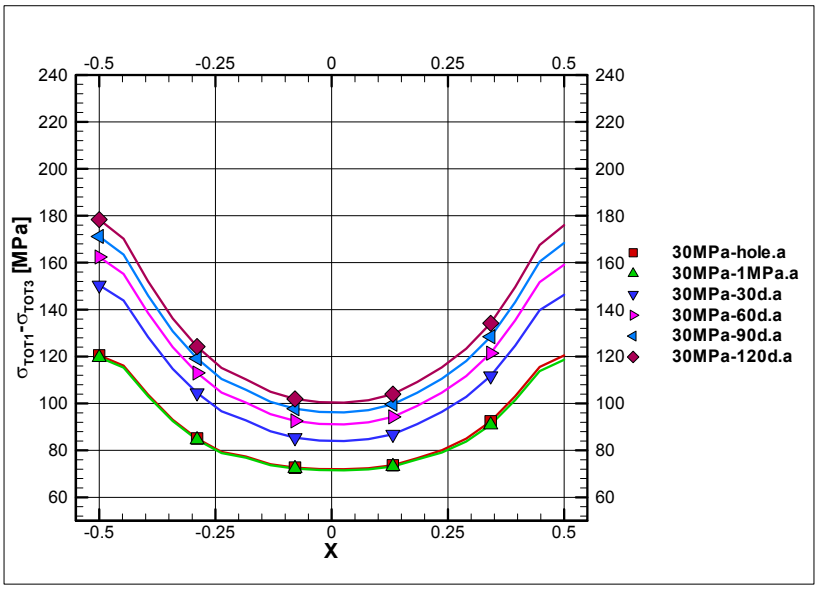
-0.5
-0.25
0
0.25
0.5
240
220
200
180
160
140
120
100
80
60
σTOT1-σTOT3 [MPa]
X
30MPa-hole.a
30MPa-1MPa.a
30MPa-30d.a
30MPa-60d.a
30MPa-90d.a
30MPa-120d.a

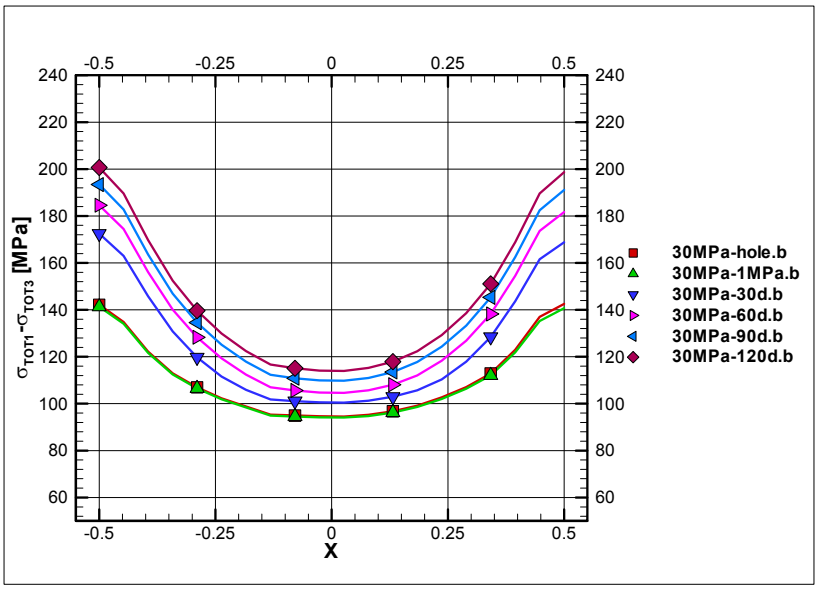
-0.5
-0.25
0
0.25
0.5
240
220
200
180
160
140
120
100
80
60
σTOT1-σTOT3 [MPa]
X
30MPa-hole.b
30MPa-1MPa.b
30MPa-30d.b
30MPa-60d.b
30MPa-90d.b
30MPa-120d.b

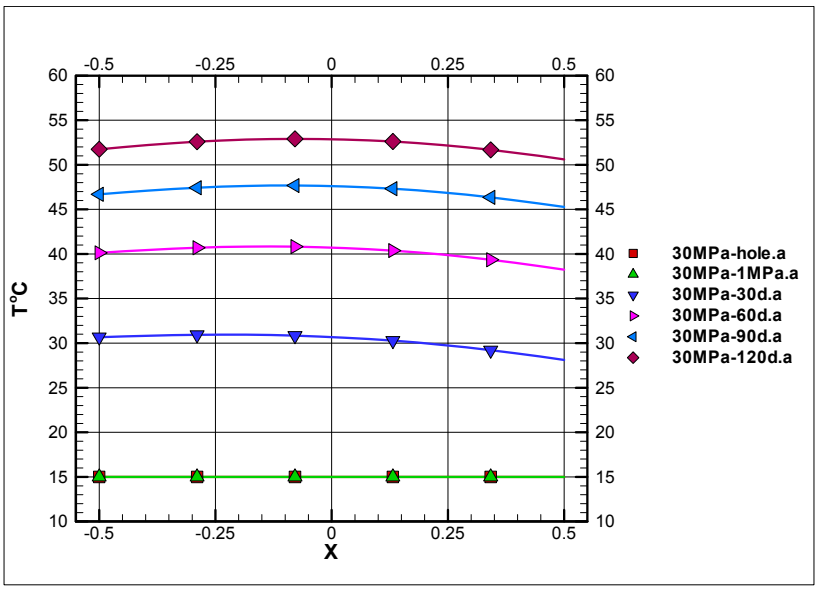
T°C
X
30MPa-hole.a
30MPa-1MPa.a
30MPa-30d.a
30MPa-60d.a
30MPa-90d.a
30MPa-120d.a

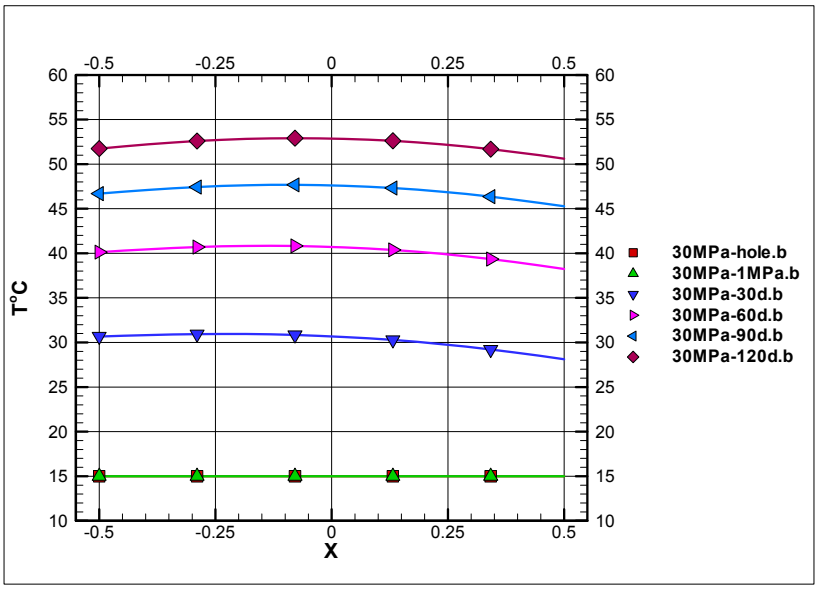
T°C
X
30MPa-hole.b
30MPa-1MPa.b
30MPa-30d.b
30MPa-60d.b
30MPa-90d.b
30MPa-120d.b

No slots, σ_1=30 MPa, E=68GPa, λ=2.83 W/m, K.

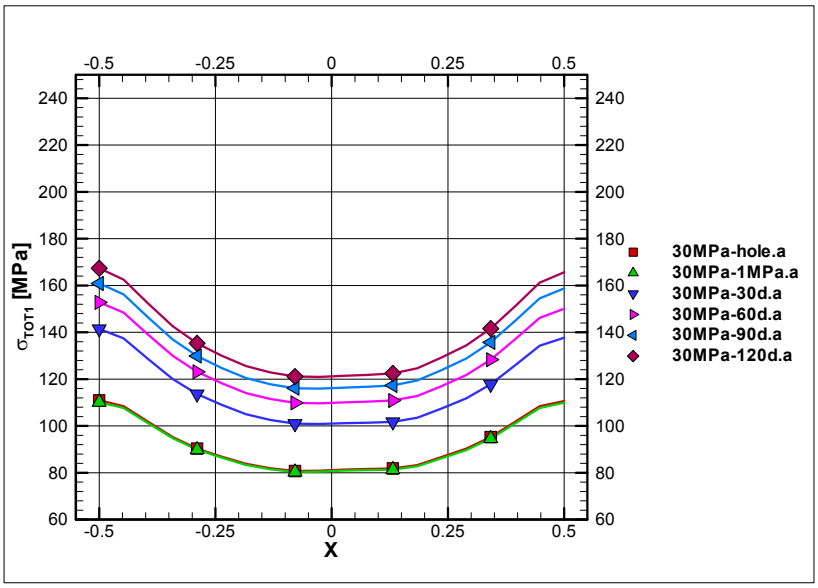

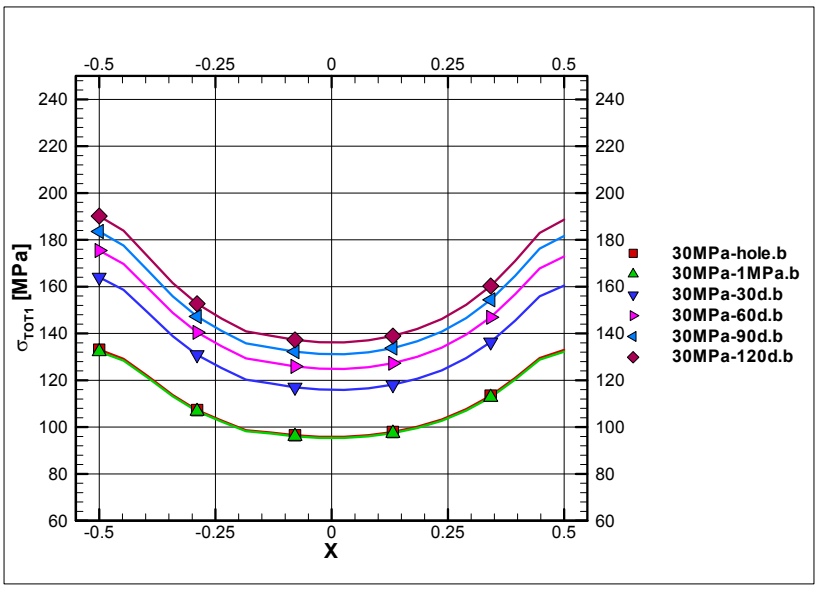

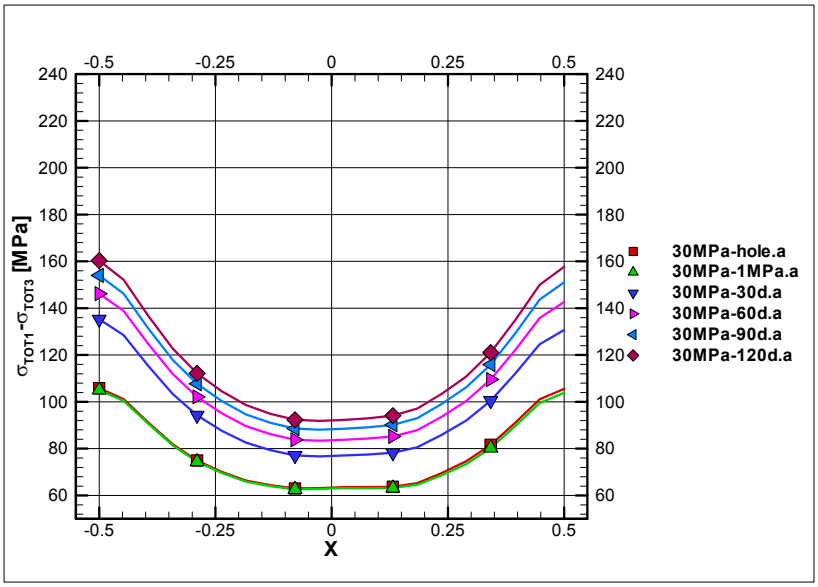

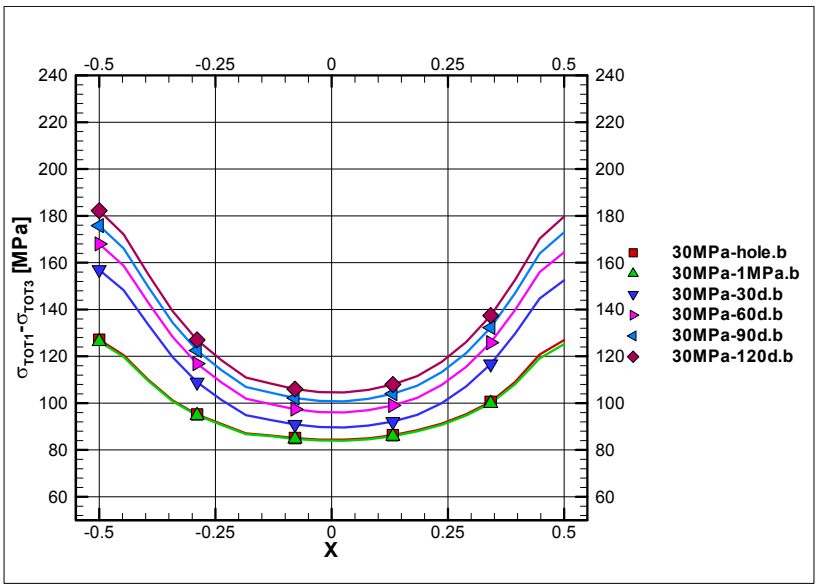
σTOT1-σTOT3 [MPa]
X
30MPa-hole.b
30MPa-1MPa.b
30MPa-30d.b
30MPa-60d.b
30MPa-90d.b
30MPa-120d.b

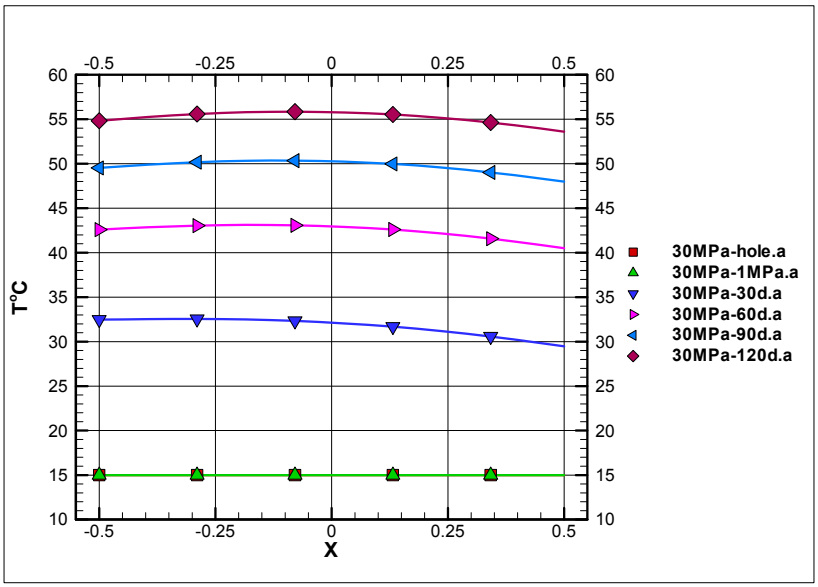
T°C
X
30MPa-hole.a
30MPa-1MPa.a
30MPa-30d.a
30MPa-60d.a
30MPa-90d.a
30MPa-120d.a

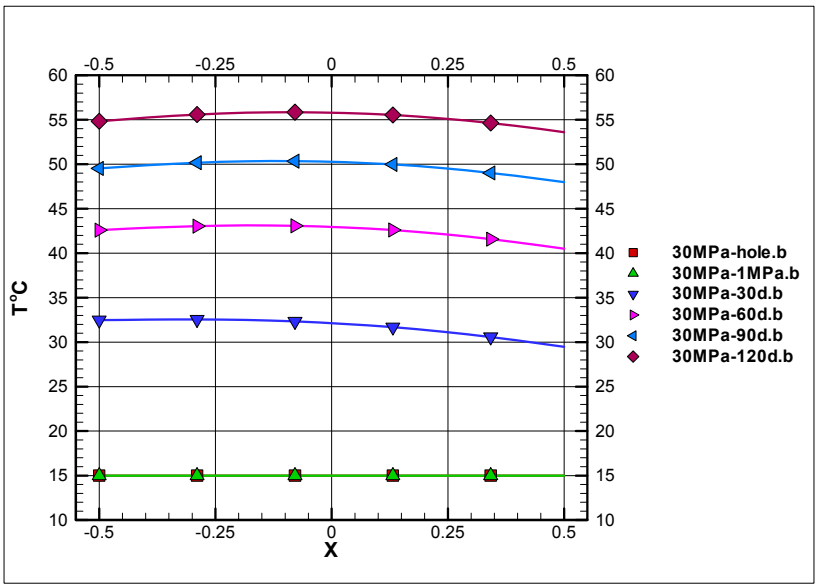
T°C
X
30MPa-hole.b
30MPa-1MPa.b
30MPa-30d.b
30MPa-60d.b
30MPa-90d.b
30MPa-120d.b

No slots, σ_1=25 MPa, E=68GPa, λ=2.83 W/m, K.

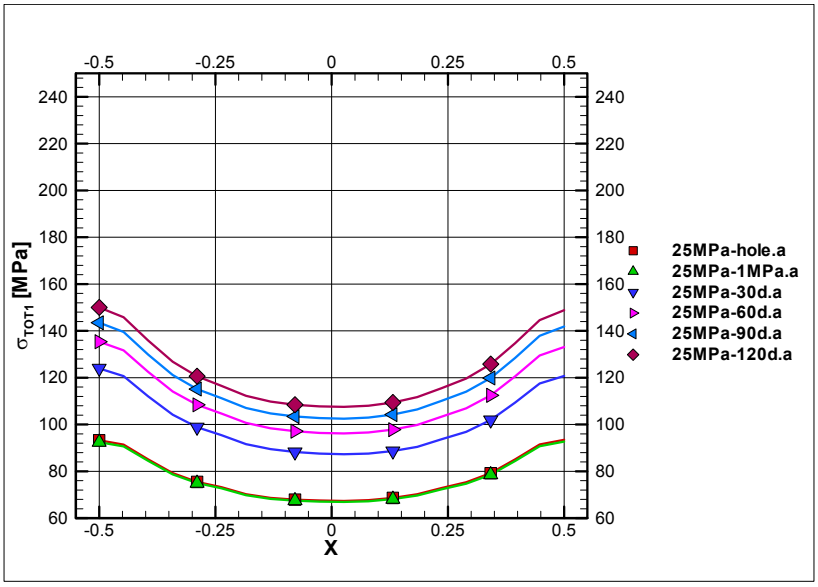

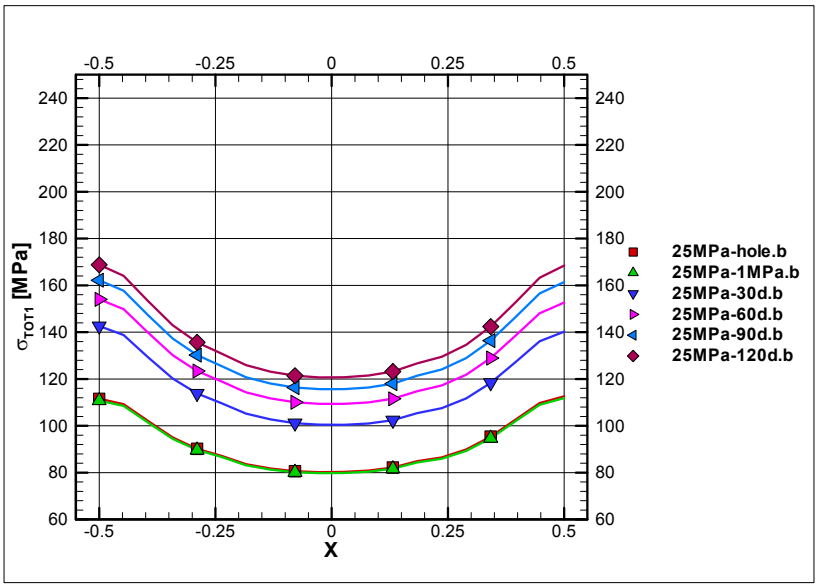

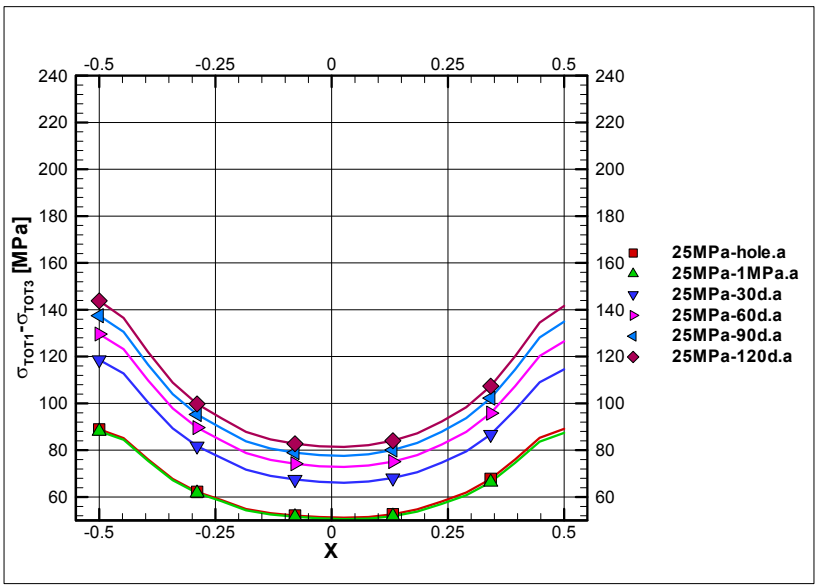

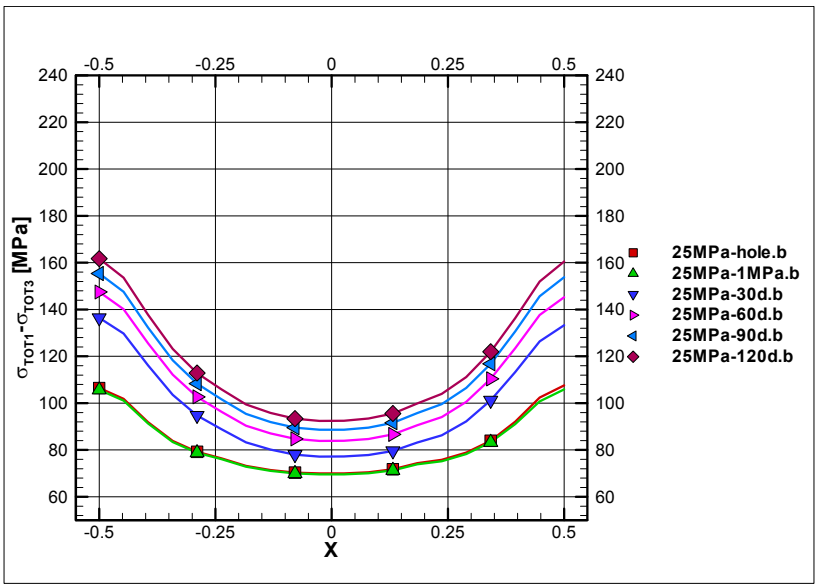
σ_{TOT1}-σ_{TOT3} [MPa]
X
25MPa-hole.b
25MPa-1MPa.b
25MPa-30d.b
25MPa-60d.b
25MPa-90d.b
25MPa-120d.b

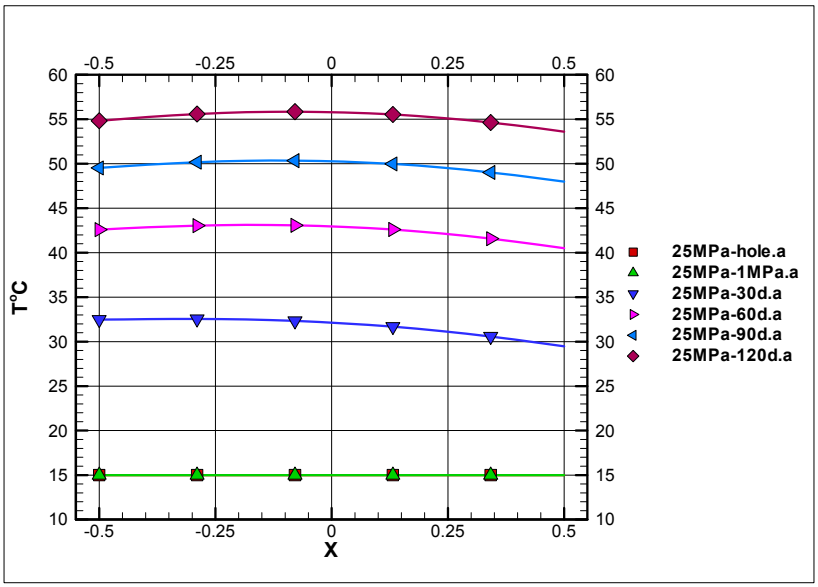
T°C
X
25MPa-hole.a
25MPa-1MPa.a
25MPa-30d.a
25MPa-60d.a
25MPa-90d.a
25MPa-120d.a

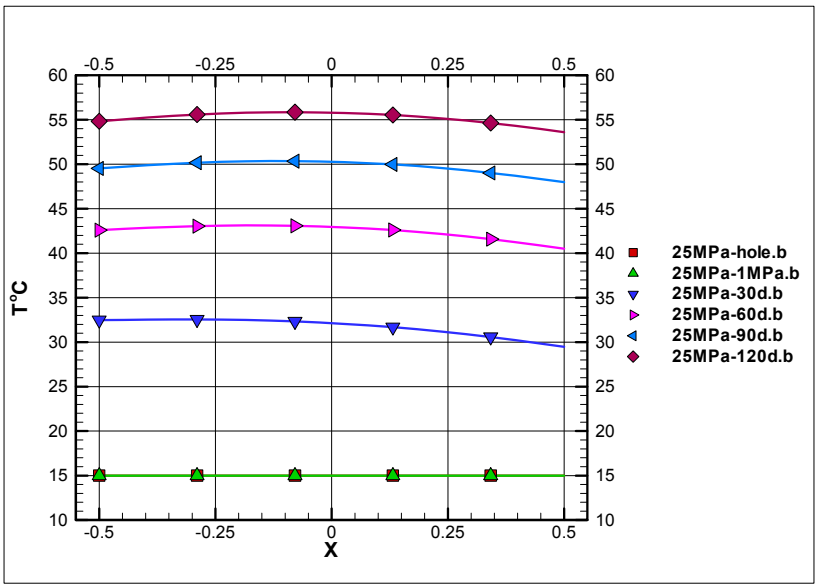
T°C
X
25MPa-hole.b
25MPa-1MPa.b
25MPa-30d.b
25MPa-60d.b
25MPa-90d.b
25MPa-120d.b

No slots, σ_1=35 MPa, E=68GPa, λ=2.83 W/m, K.

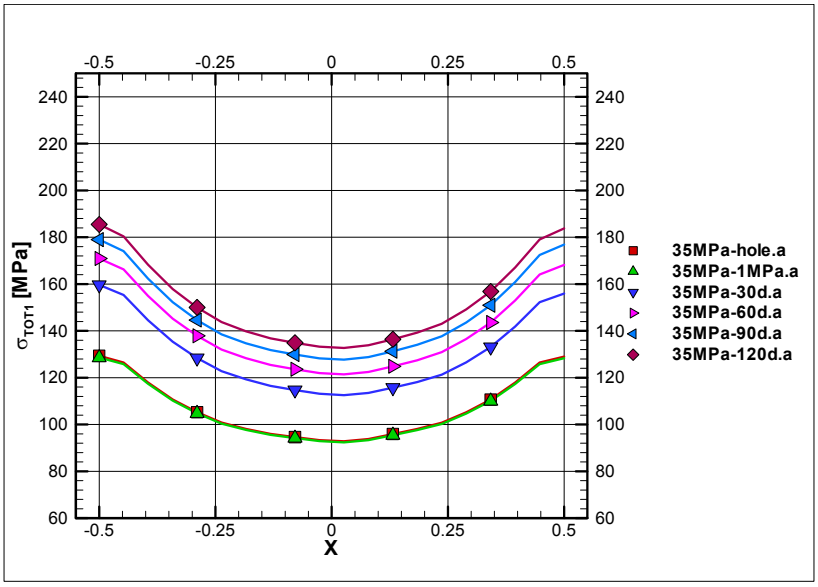

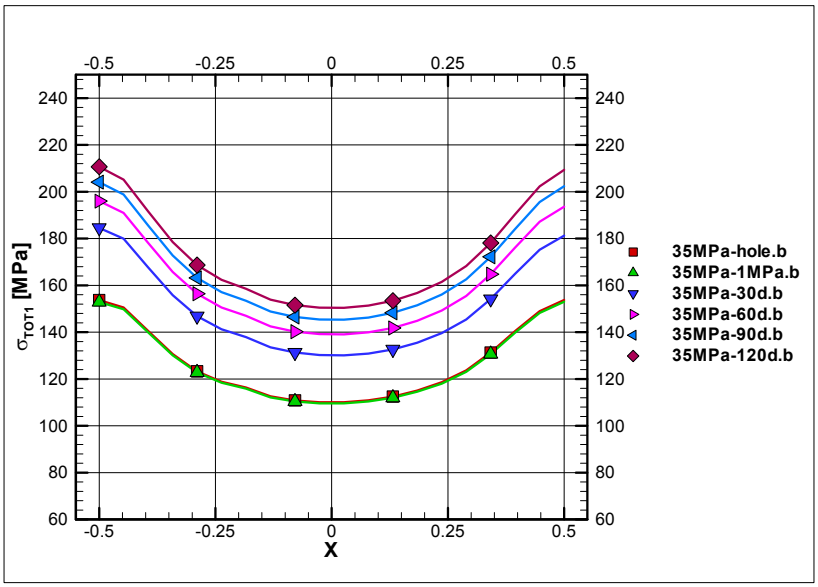

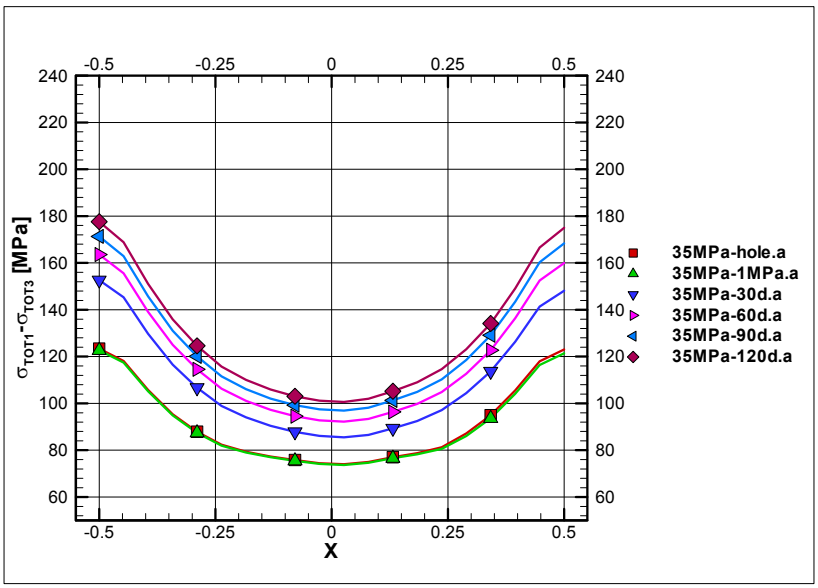

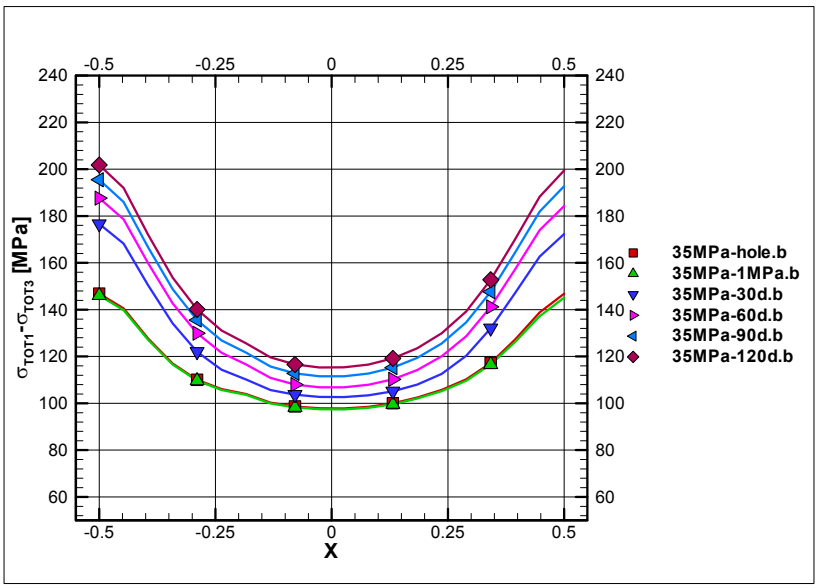
σ_{TOT1}-σ_{TOT3} [MPa]
X
35MPa-hole.b
35MPa-1MPa.b
35MPa-30d.b
35MPa-60d.b
35MPa-90d.b
35MPa-120d.b

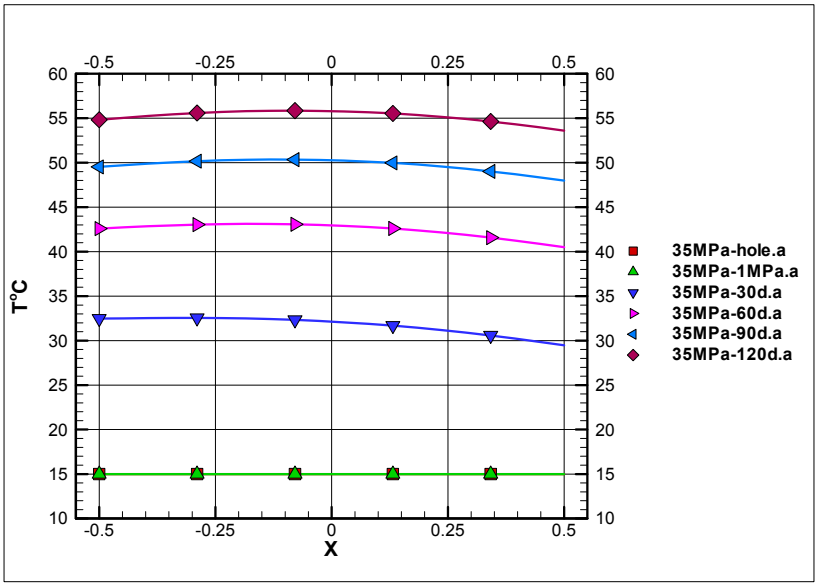
T°C
X
35MPa-hole.a
35MPa-1MPa.a
35MPa-30d.a
35MPa-60d.a
35MPa-90d.a
35MPa-120d.a

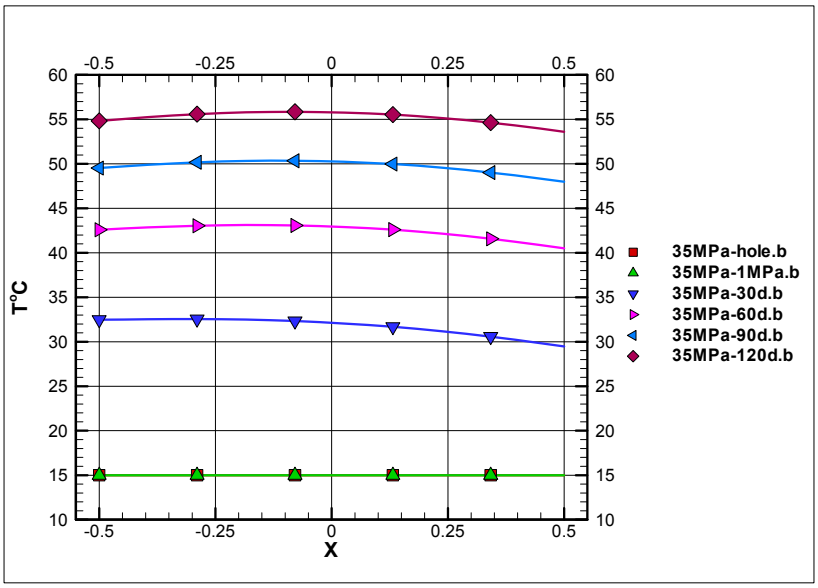
T°C
X
35MPa-hole.b
35MPa-1MPa.b
35MPa-30d.b
35MPa-60d.b
35MPa-90d.b
35MPa-120d.b

No slots, σ_1=30 MPa, E=68GPa, λ=2.4 W/m, K.

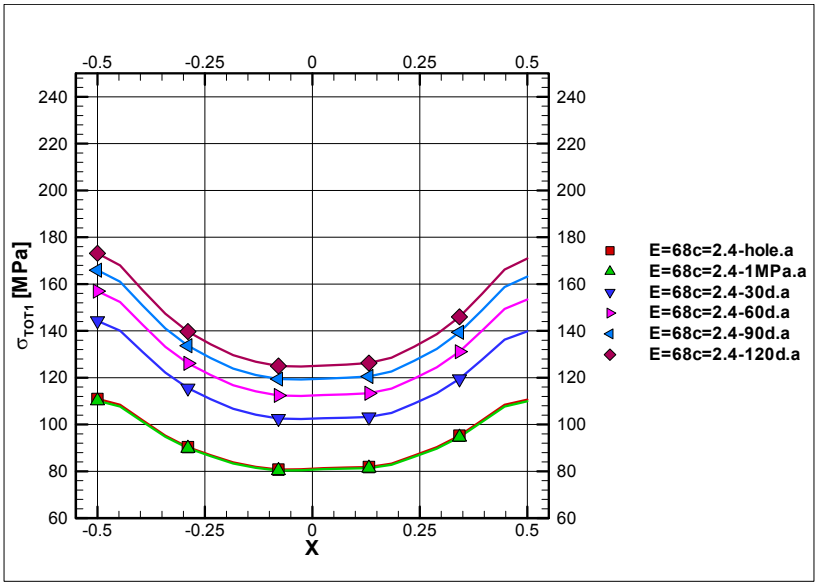

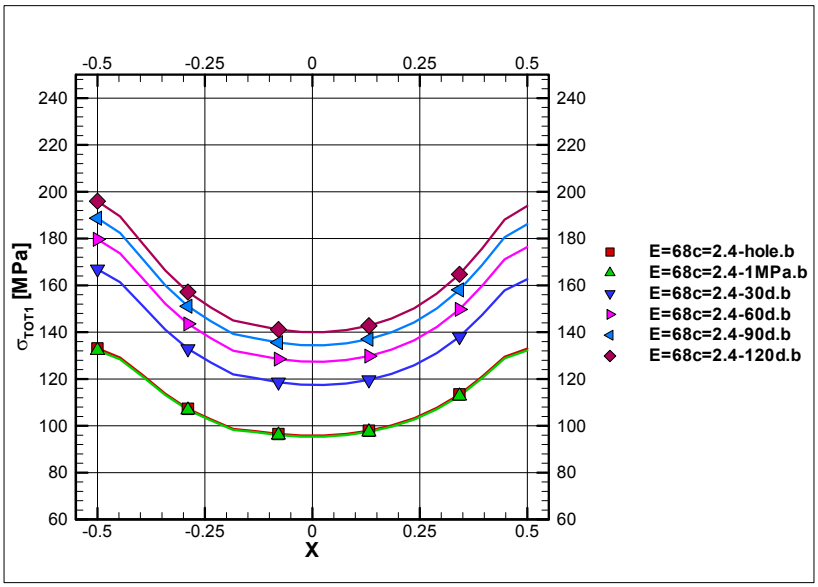

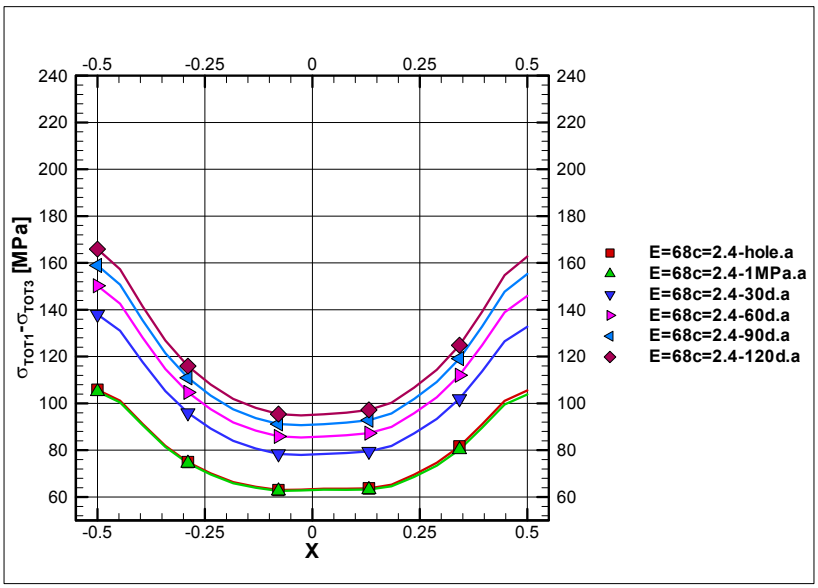

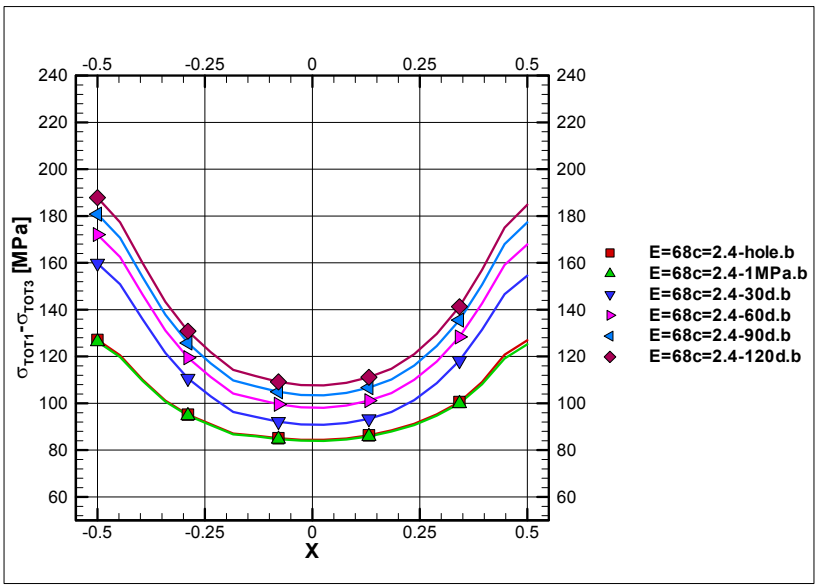
σTOT1-σTOT3 [MPa]
X
E=68c=2.4-hole.b
E=68c=2.4-1MPa.b
E=68c=2.4-30d.b
E=68c=2.4-60d.b
E=68c=2.4-90d.b
E=68c=2.4-120d.b

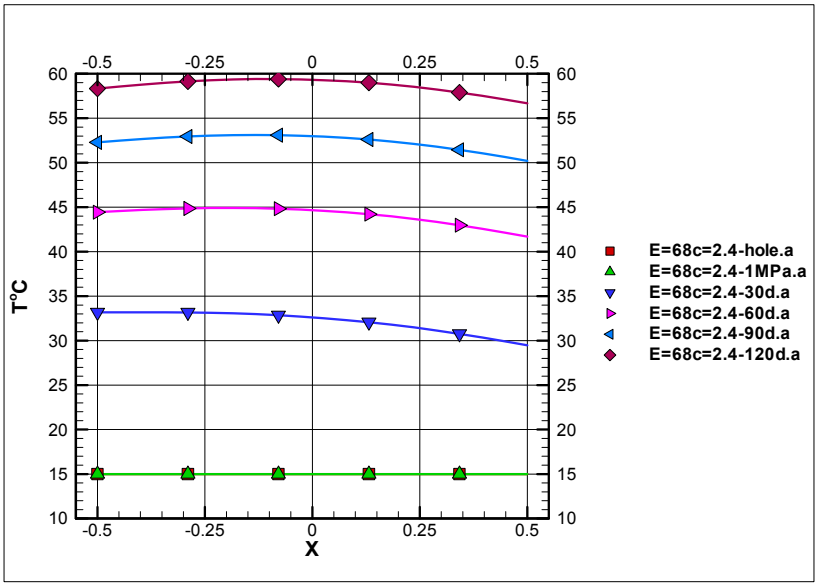
T°C
X
E=68c=2.4-hole.a
E=68c=2.4-1MPa.a
E=68c=2.4-30d.a
E=68c=2.4-60d.a
E=68c=2.4-90d.a
E=68c=2.4-120d.a

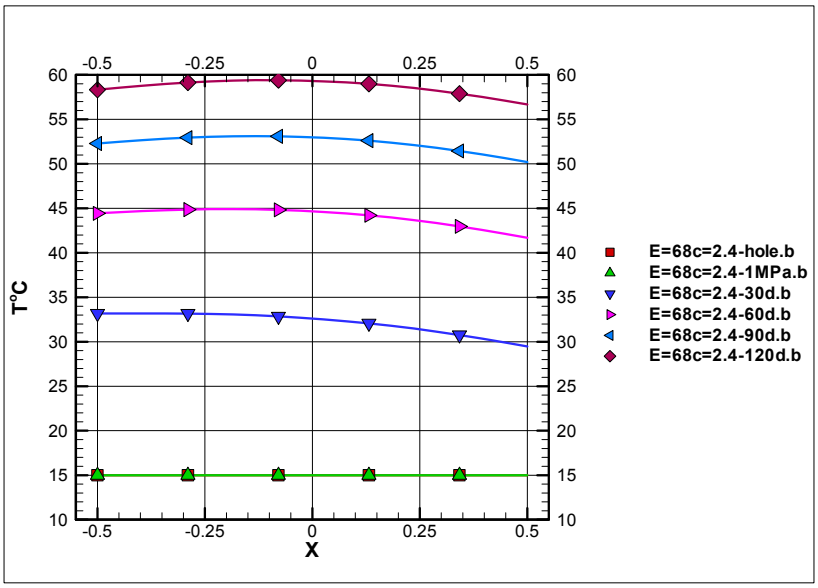
T°C
X
E=68c=2.4-hole.b
E=68c=2.4-1MPa.b
E=68c=2.4-30d.b
E=68c=2.4-60d.b
E=68c=2.4-90d.b
E=68c=2.4-120d.b

No slots, σ_1=30 MPa, E=47GPa, λ=2.4 W/m, K.

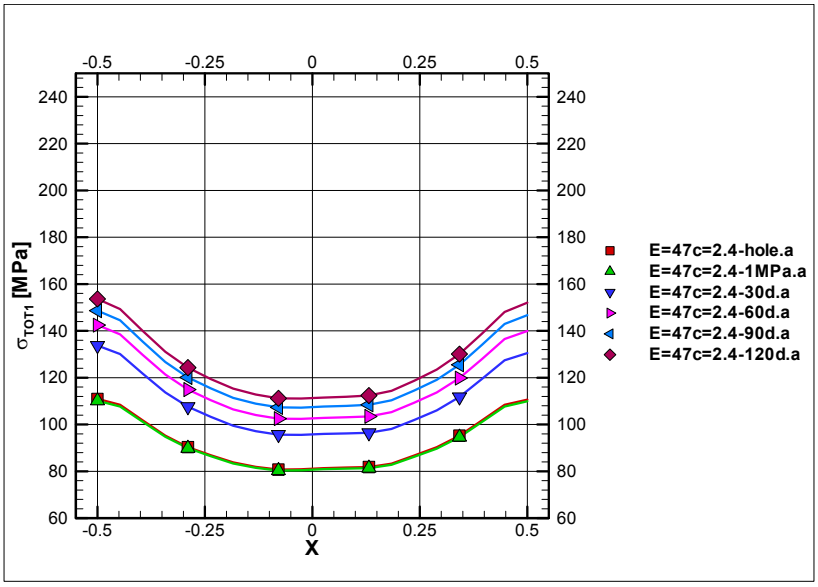

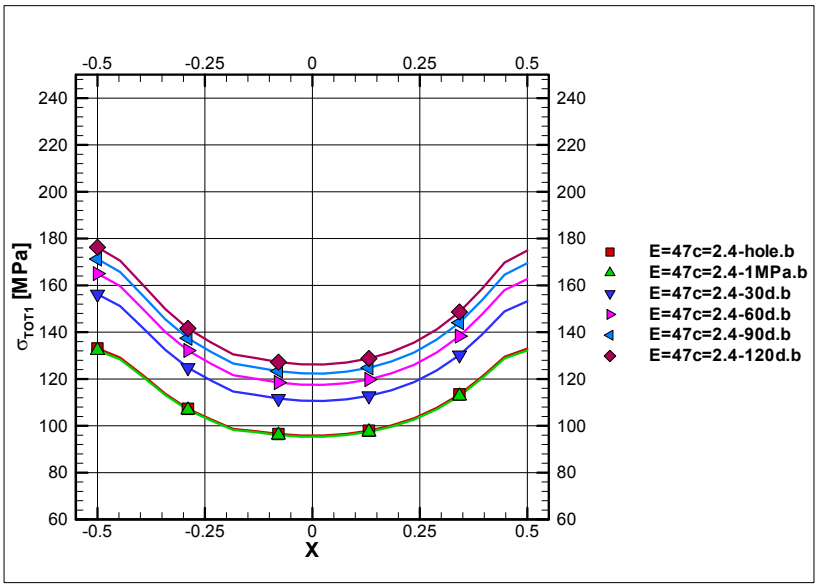

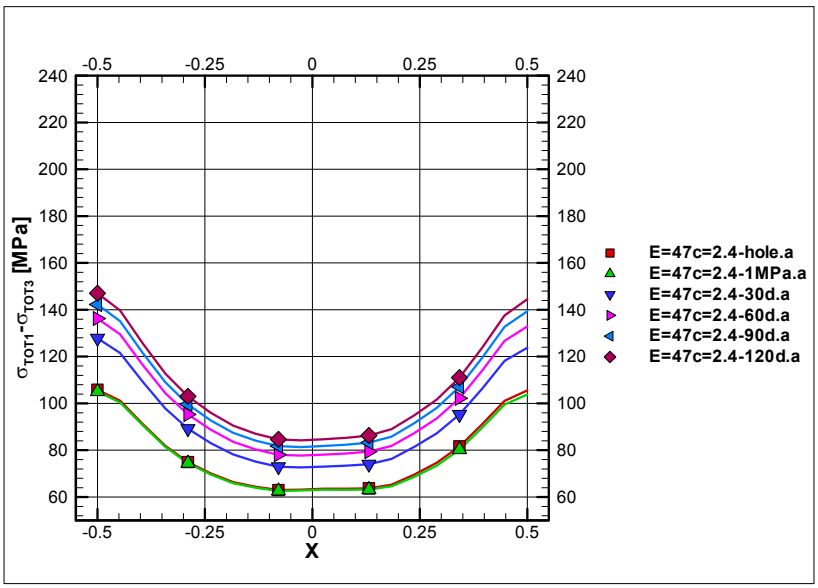

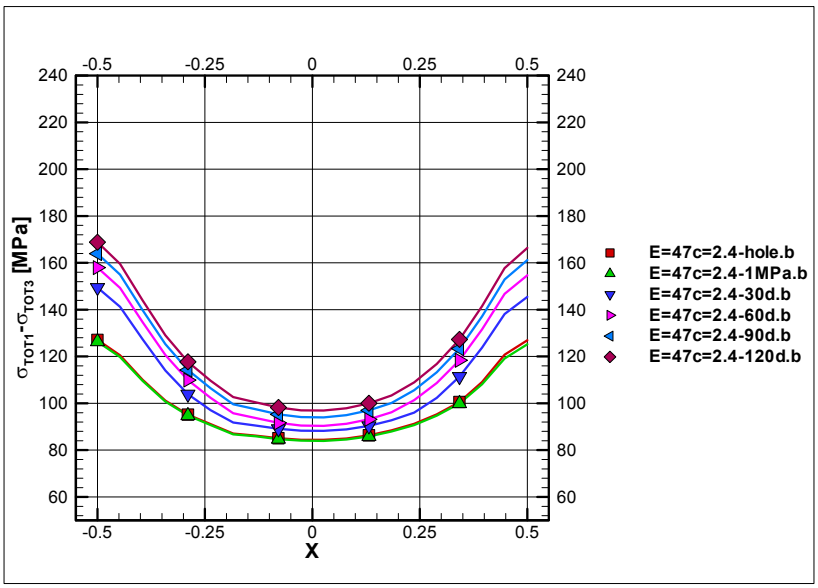
σTOT1-σTOT3 [MPa]
X
E=47c=2.4-hole.b
E=47c=2.4-1MPa.b
E=47c=2.4-30d.b
E=47c=2.4-60d.b
E=47c=2.4-90d.b
E=47c=2.4-120d.b

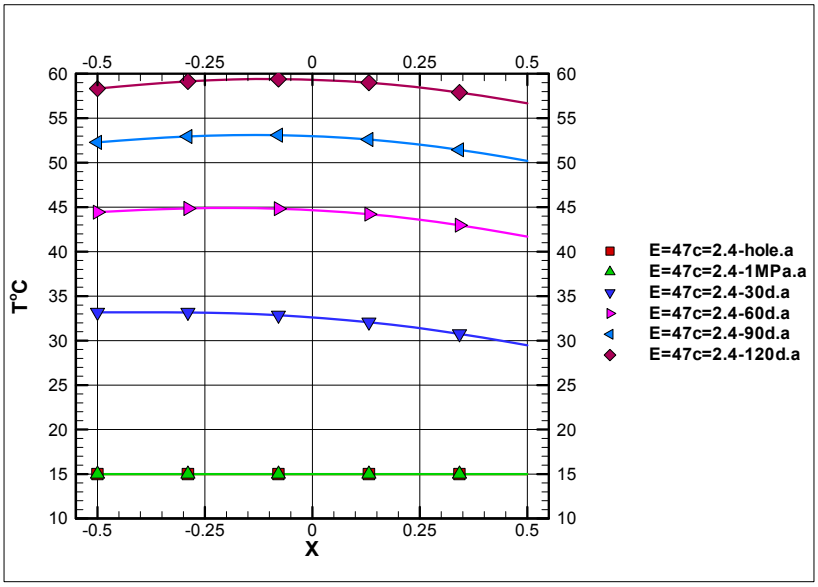
T°C
X
E=47c=2.4-hole.a
E=47c=2.4-1MPa.a
E=47c=2.4-30d.a
E=47c=2.4-60d.a
E=47c=2.4-90d.a
E=47c=2.4-120d.a

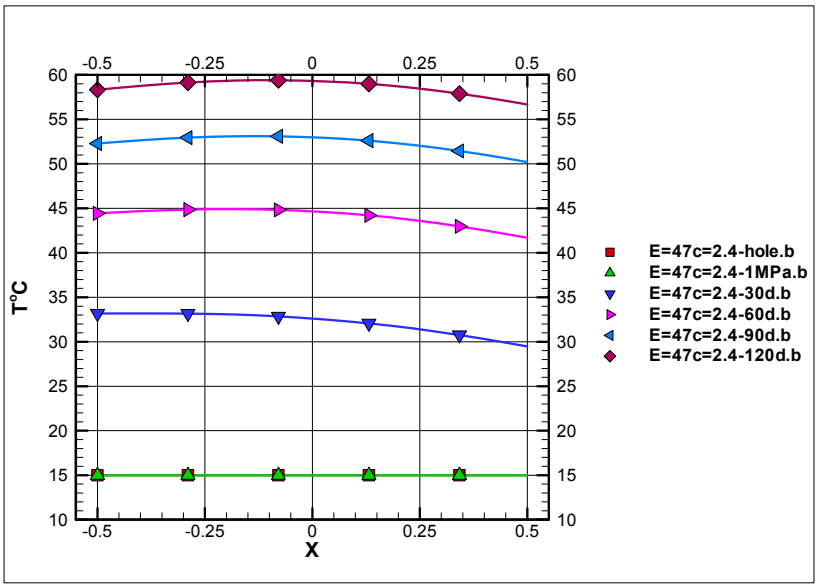
T°C
X
E=47c=2.4-hole.b
E=47c=2.4-1MPa.b
E=47c=2.4-30d.b
E=47c=2.4-60d.b
E=47c=2.4-90d.b
E=47c=2.4-120d.b

No slots, σ_1=30 MPa, E=47GPa, λ=2.83 W/m, K.

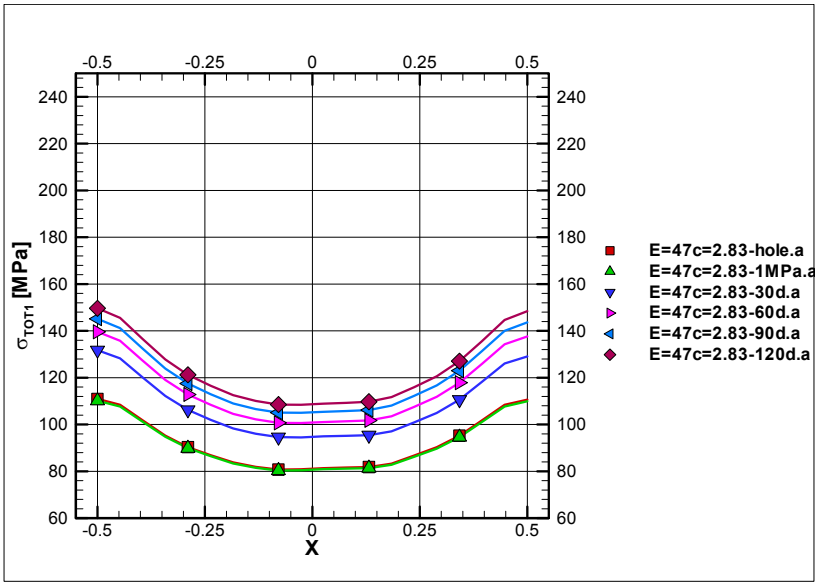

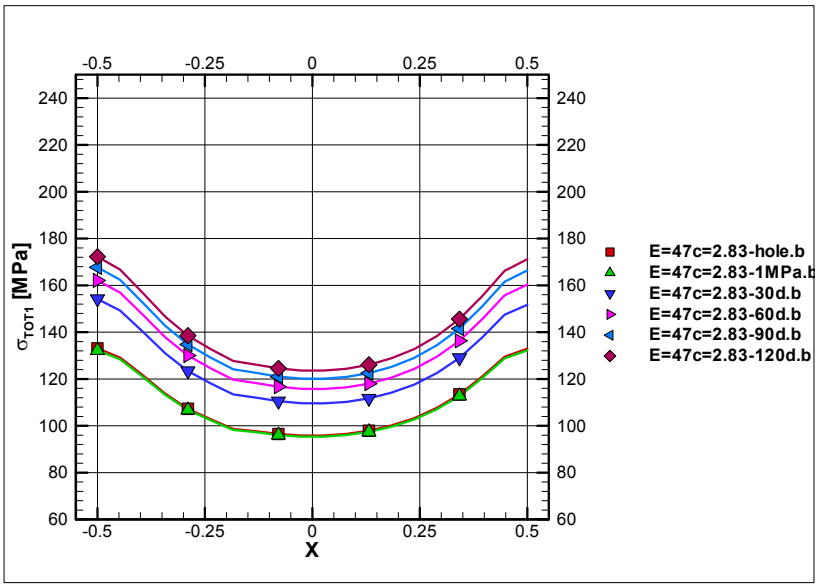

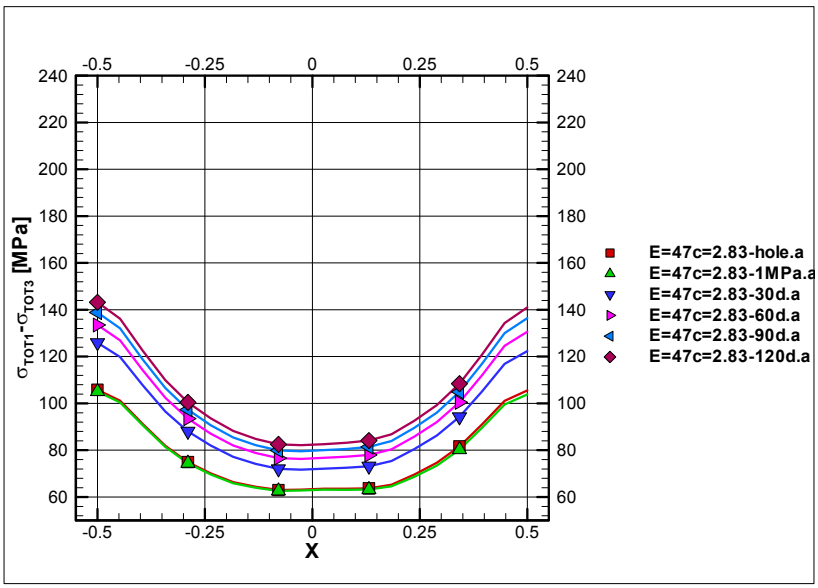

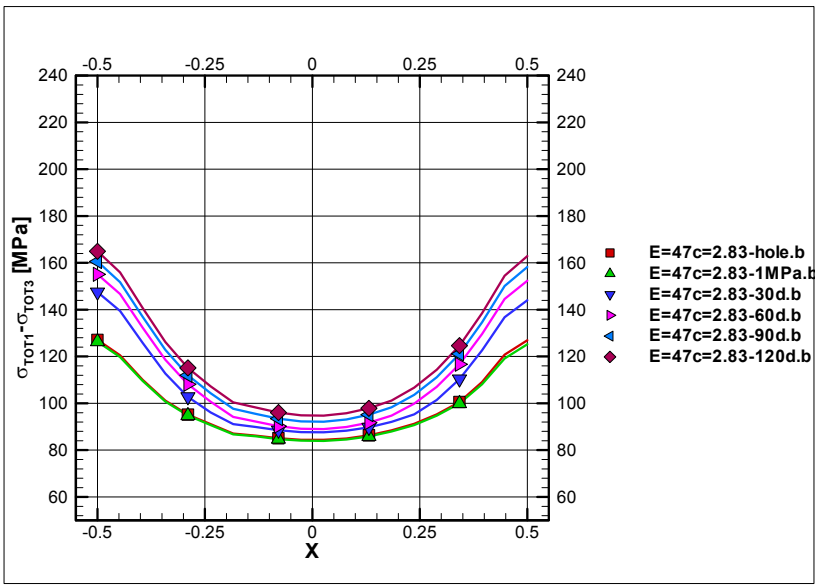
-0.5
-0.25
0
0.25
0.5
240
220
200
180
160
140
120
100
80
60
σTOT1-σTOT3 [MPa]
X
E=47c=2.83-hole.b
E=47c=2.83-1MPa.b
E=47c=2.83-30d.b
E=47c=2.83-60d.b
E=47c=2.83-90d.b
E=47c=2.83-120d.b

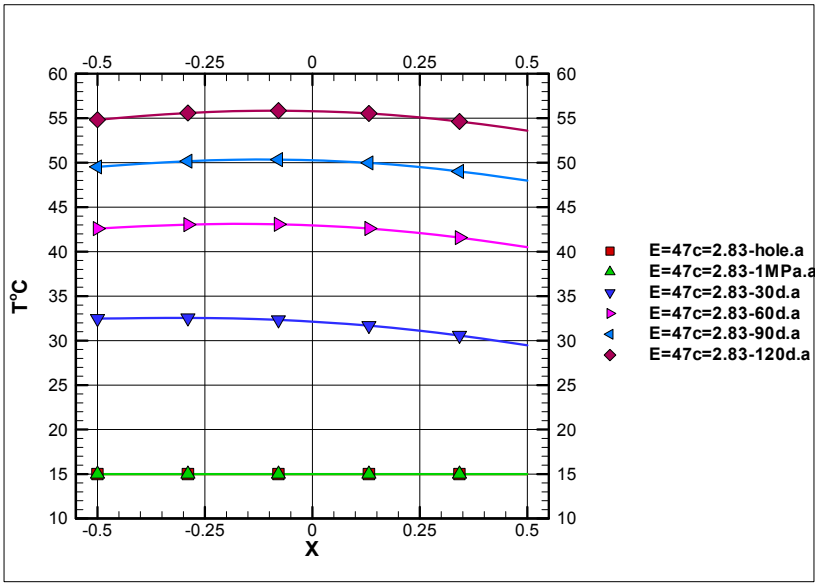
-0.5
-0.25
0
0.25
0.5
60
55
50
45
40
35
30
25
20
15
10
T°C
X
E=47c=2.83-hole.a
E=47c=2.83-1MPa.a
E=47c=2.83-30d.a
E=47c=2.83-60d.a
E=47c=2.83-90d.a
E=47c=2.83-120d.a

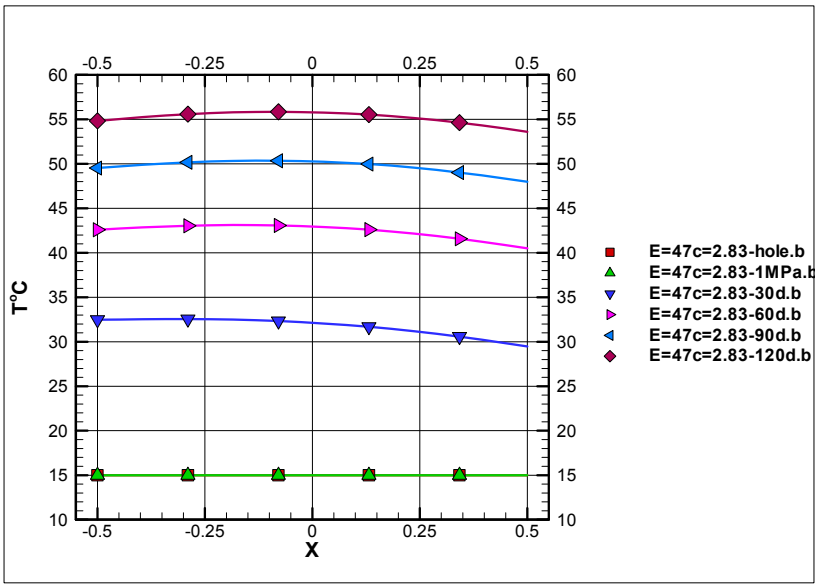
-0.5
-0.25
0
0.25
0.5
60
55
50
45
40
35
30
25
20
15
10
T°C
X
E=47c=2.83-hole.b
E=47c=2.83-1MPa.b
E=47c=2.83-30d.b
E=47c=2.83-60d.b
E=47c=2.83-90d.b
E=47c=2.83-120d.b

Appendix F. Modeling results, lowest and highest cases

The Y-axis represent respectively: total stresses (σ_{TOT1}), deviatoric stresses (σ_{TOT1}-σ_{TOT3}) and temperatures (T).

Explanation of the legend:

xxMPa: value of σ_1 for the given simulation.

hole / 1 MPa / 30d / 60d / 90d / 120d: stage of the modelling. Hole means values taken after excavation of both holes, 1 MPa values monitored after applying the confining pressure of 1 MPa in one hole, 30d to 120d values monitored after 30/60/90/120 days of heating.

a / b refers to the depth level, a is the section located 1.5m below the tunnel floor, b the section located 0.5m below the tunnel floor.

No slots, σ_1=25 MPa, E=47GPa, λ=2.83 W/m, K, level a.

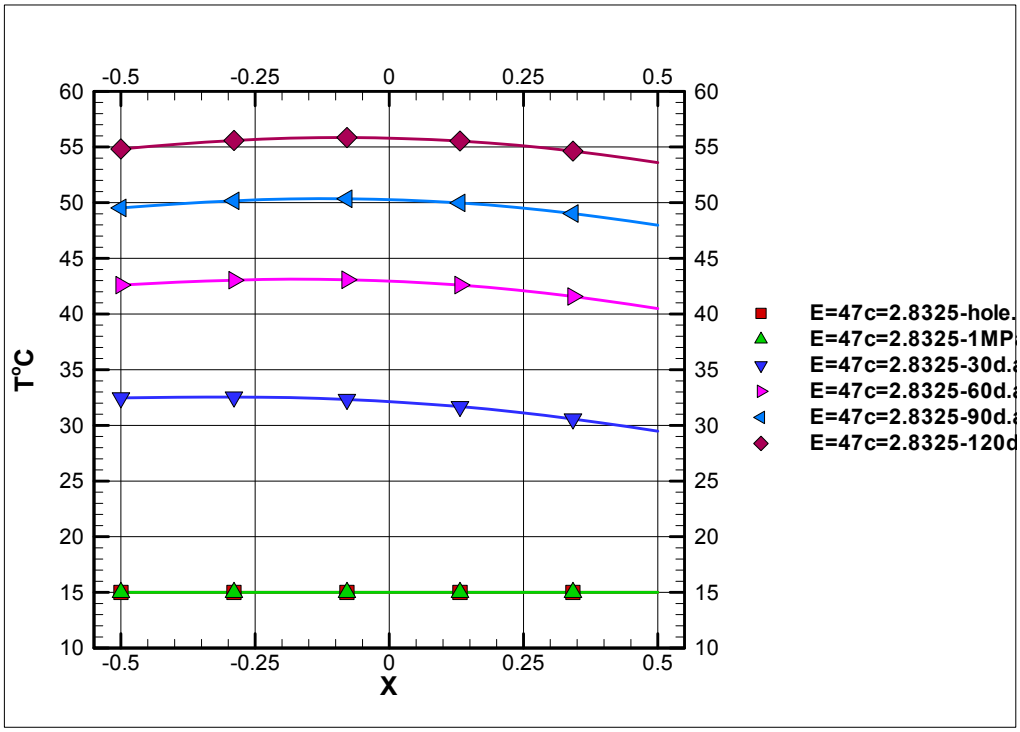

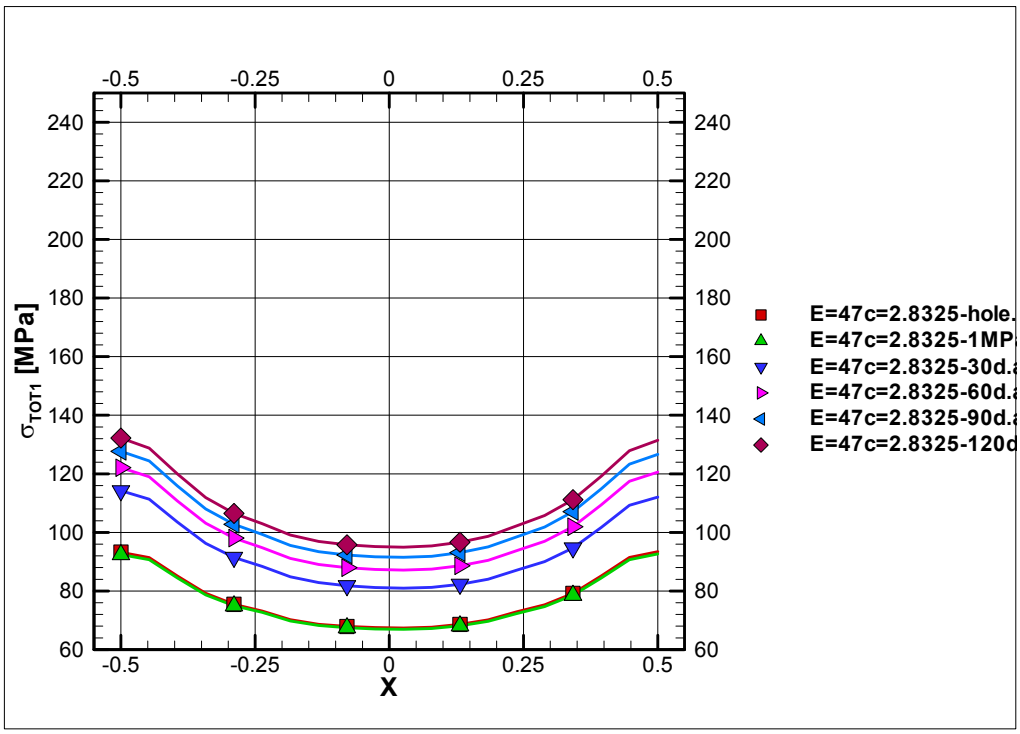
-0.5
-0.25
0
0.25
0.5
240
220
200
180
160
140
120
100
80
60
σTOT1 [MPa]
X
E=47c=2.8325-hole.
E=47c=2.8325-1MP
E=47c=2.8325-30d.
E=47c=2.8325-60d.
E=47c=2.8325-90d.
E=47c=2.8325-120d

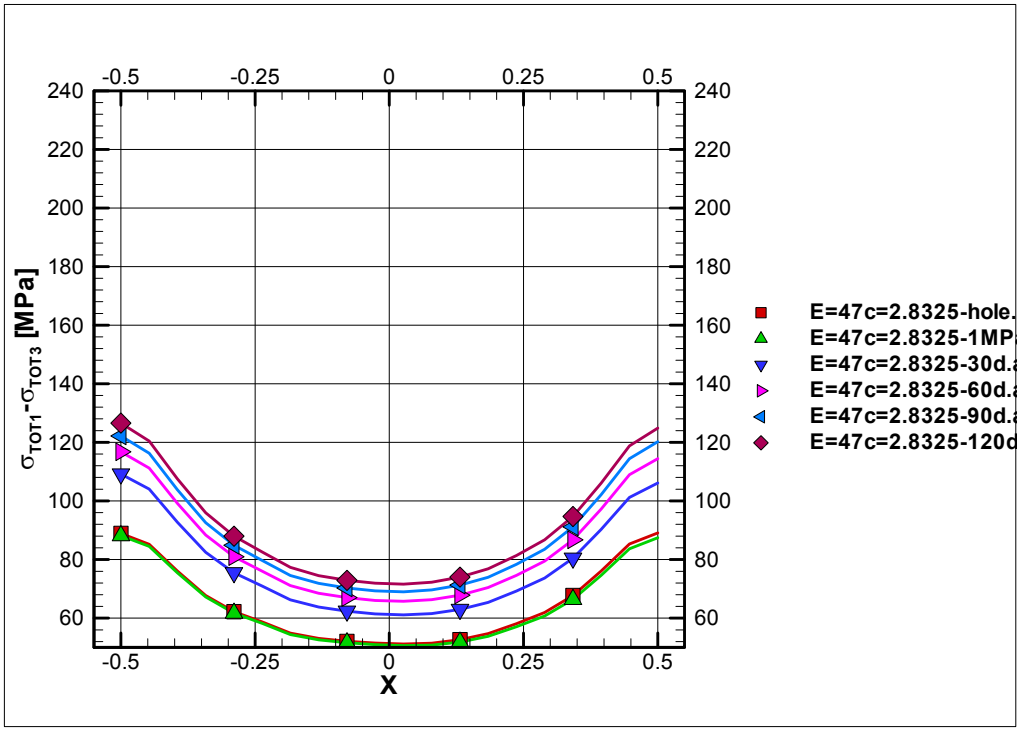
-0.5
-0.25
0
0.25
0.5
240
220
200
180
160
140
120
100
80
60
σTOT1-σTOT3 [MPa]
X
E=47c=2.8325-hole.
E=47c=2.8325-1MP
E=47c=2.8325-30d.
E=47c=2.8325-60d.
E=47c=2.8325-90d.
E=47c=2.8325-120d

No slots, σ_1=35 MPa, E=68GPa, λ=2.4 W/m, K, level a.

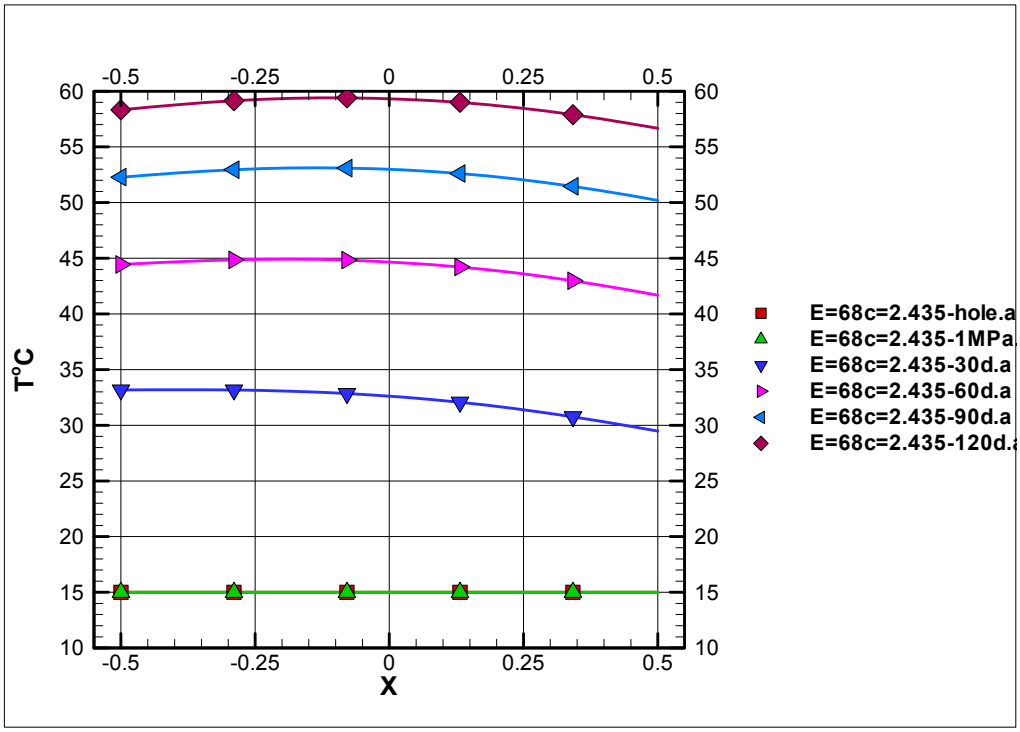

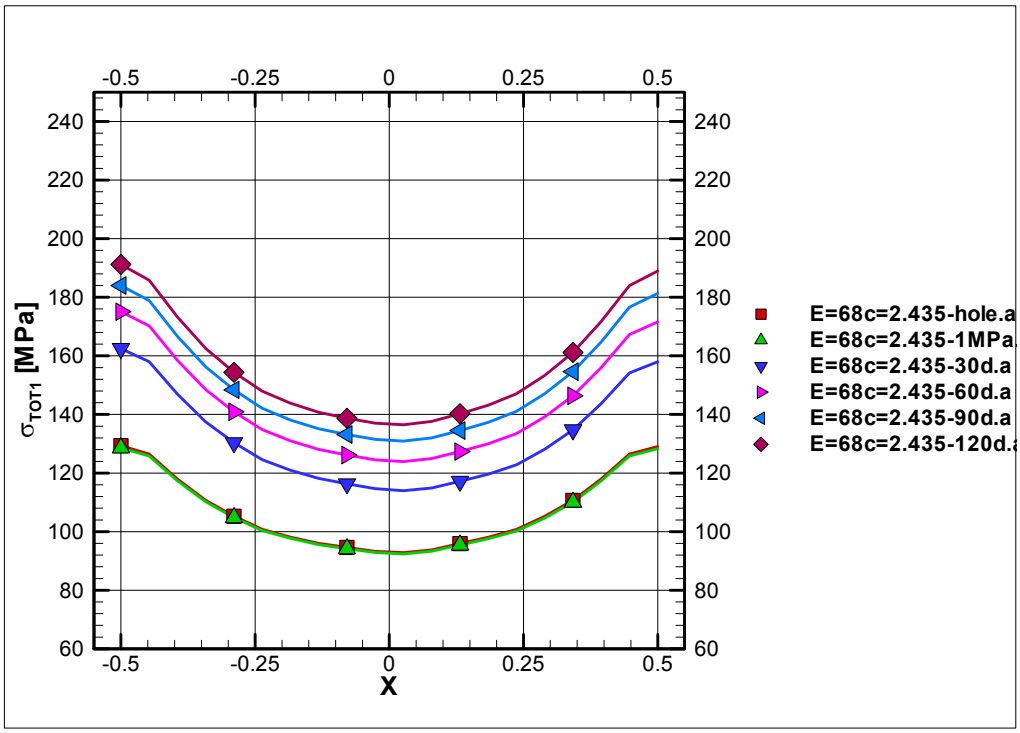

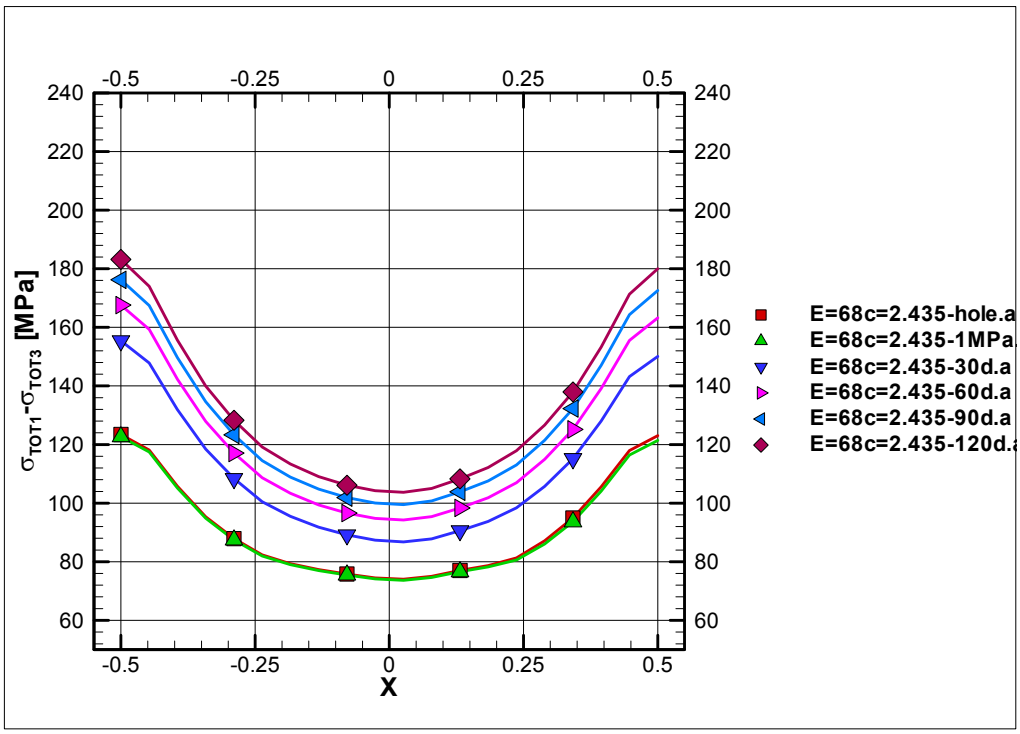
-0.5
-0.25
0
0.25
0.5
240
220
200
180
160
140
120
100
80
60
σTOT1-σTOT3 [MPa]
X
E=68c=2.435-hole.a
E=68c=2.435-1MPa
E=68c=2.435-30d.a
E=68c=2.435-60d.a
E=68c=2.435-90d.a
E=68c=2.435-120d.

No slots, σ_1=25 MPa, E=47GPa, λ=2.83 W/m, K, level b.

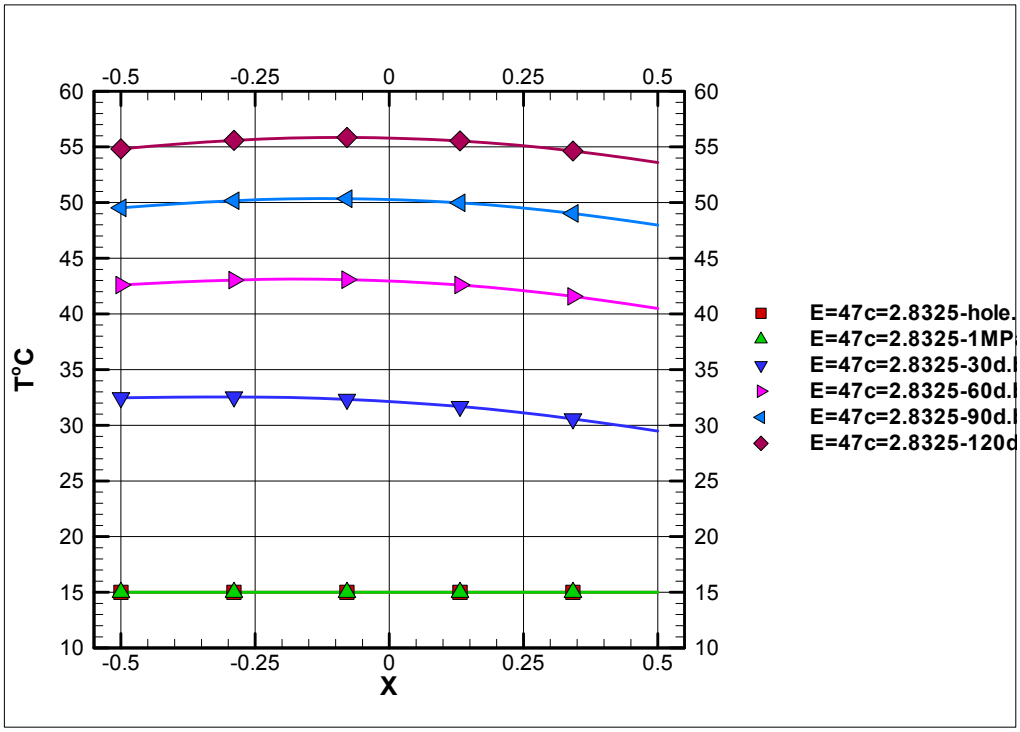

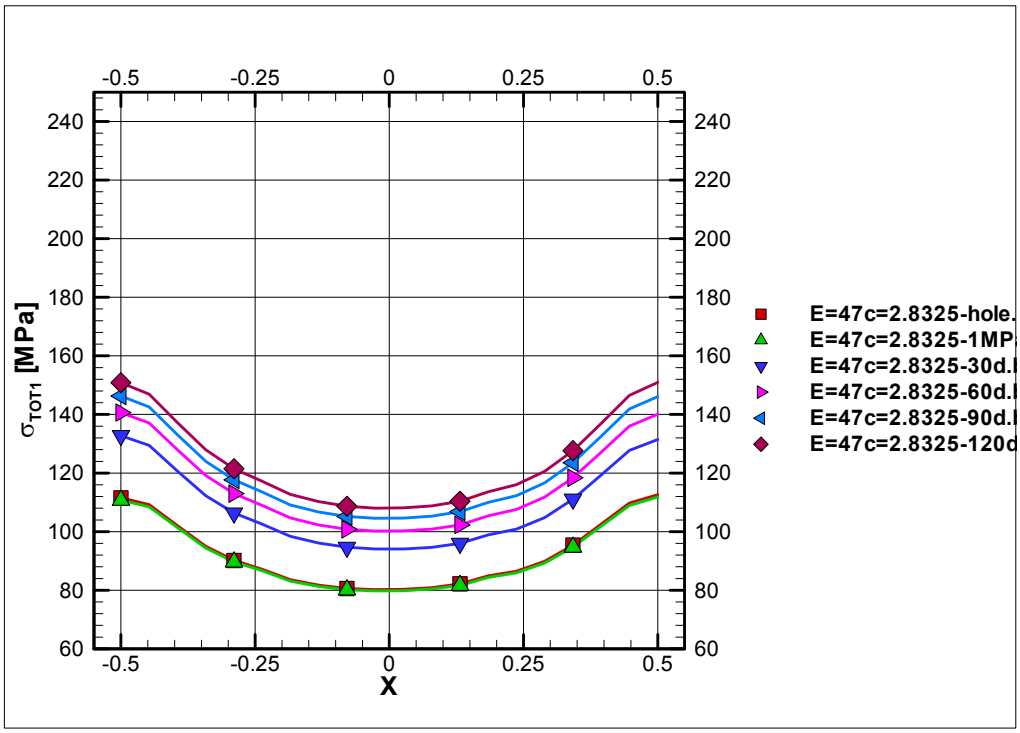

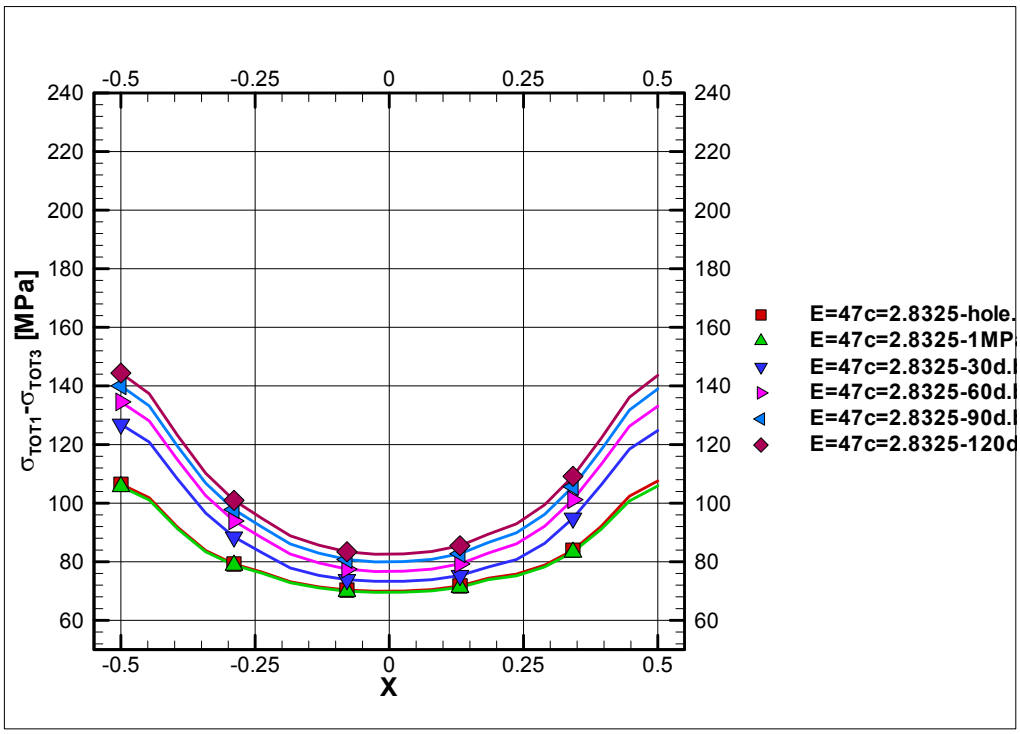
-0.5
-0.25
0
0.25
0.5
240
220
200
180
160
140
120
100
80
60
σTOT1-σTOT3 [MPa]
X
E=47c=2.8325-hole.
E=47c=2.8325-1MP
E=47c=2.8325-30d.
E=47c=2.8325-60d.
E=47c=2.8325-90d.
E=47c=2.8325-120d

No slots, σ_1=35 MPa, E=68GPa, λ=2.4 W/m, K, level b.

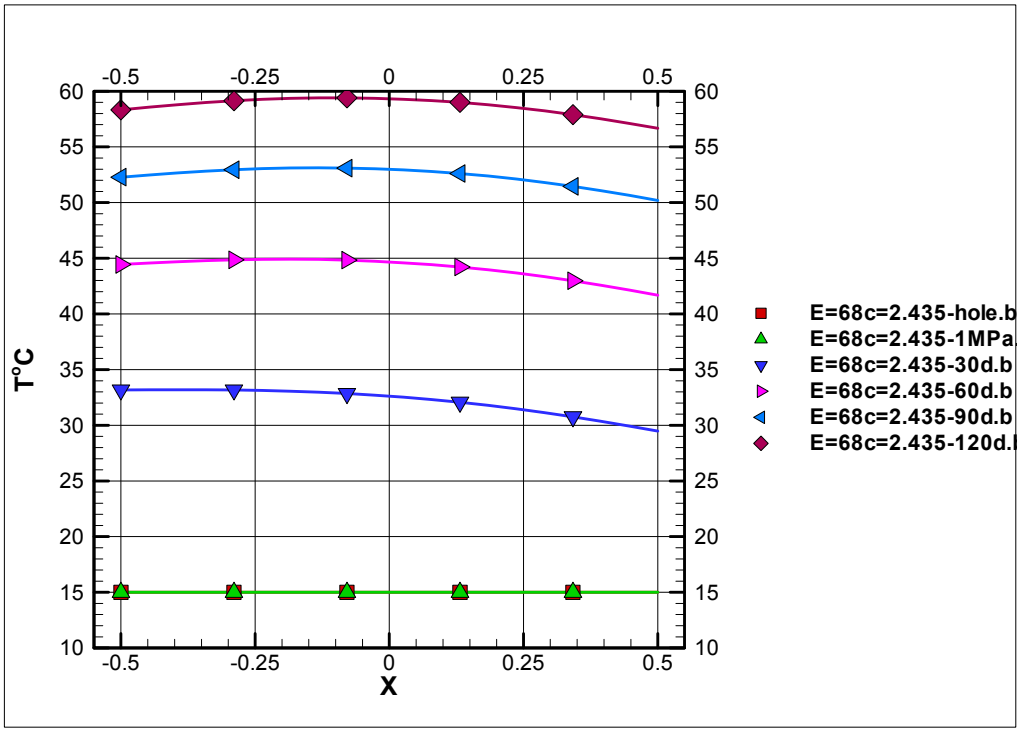

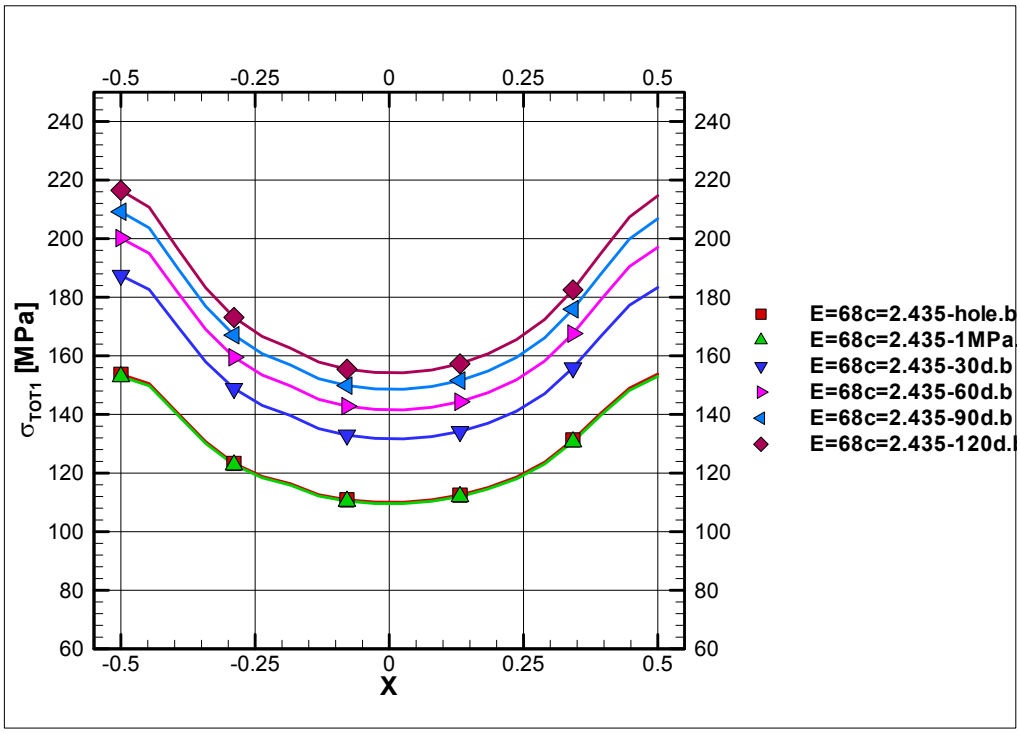

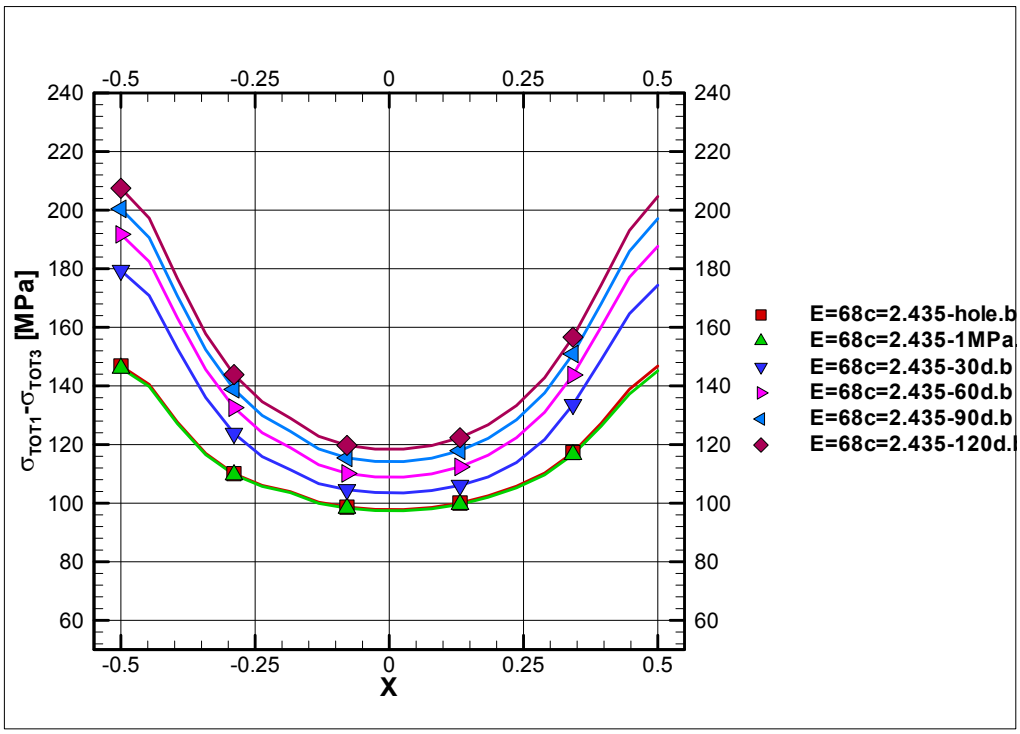
-0.5
-0.25
0
0.25
0.5
240
220
200
180
160
140
120
100
80
60
σTOT1-σTOT3 [MPa]
X
E=68c=2.435-hole.b
E=68c=2.435-1MPa
E=68c=2.435-30d.b
E=68c=2.435-60d.b
E=68c=2.435-90d.b
E=68c=2.435-120d.

Appendix G. Strain values contour maps

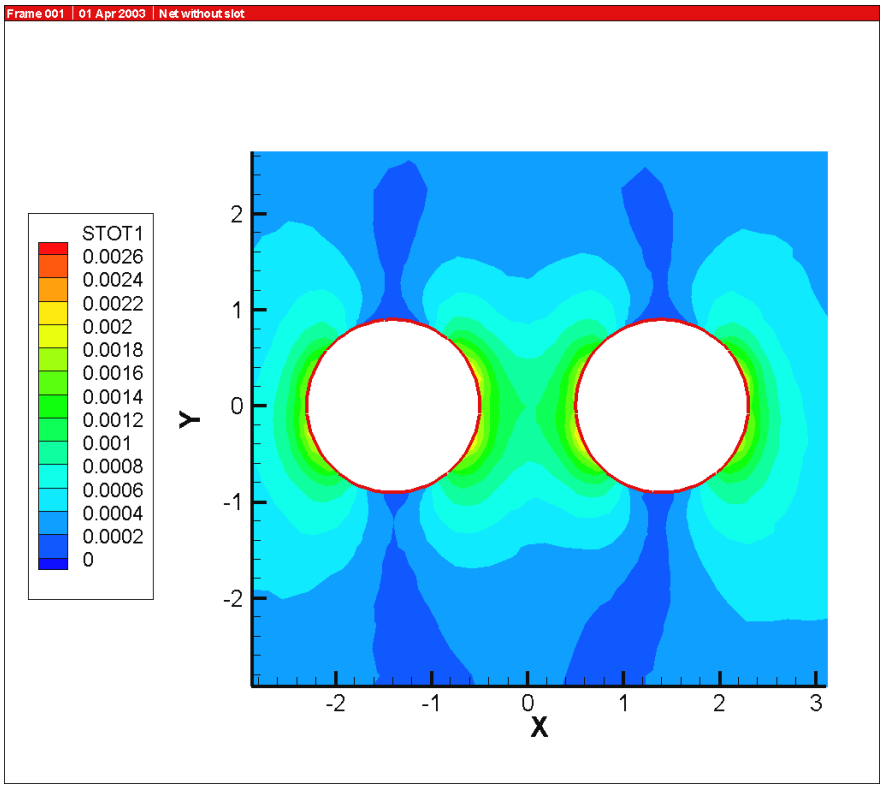

Figure G1. *Major principal strain before start heating. 0.5 m below the tunnel floor. Lowest Case.*

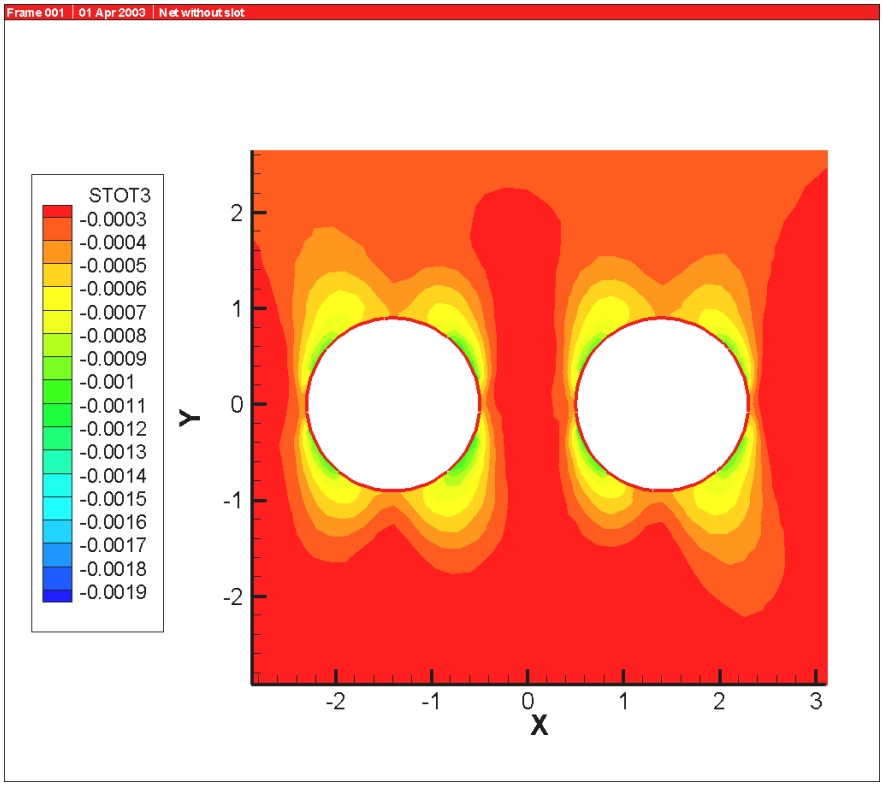

Figure G2. *Minor principal strain before start heating. 0.5 m below the tunnel floor. Lowest Case.*

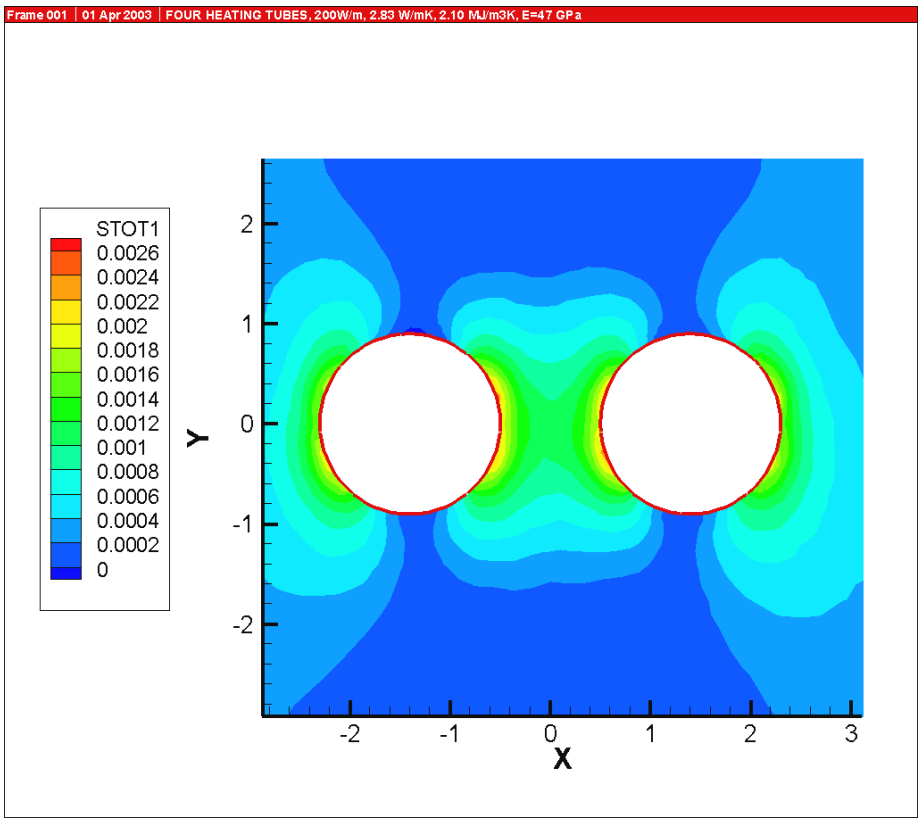

Figure G3. *Major principal strain after 30 days of heating. 0.5 m below the tunnel floor. Lowest Case.*

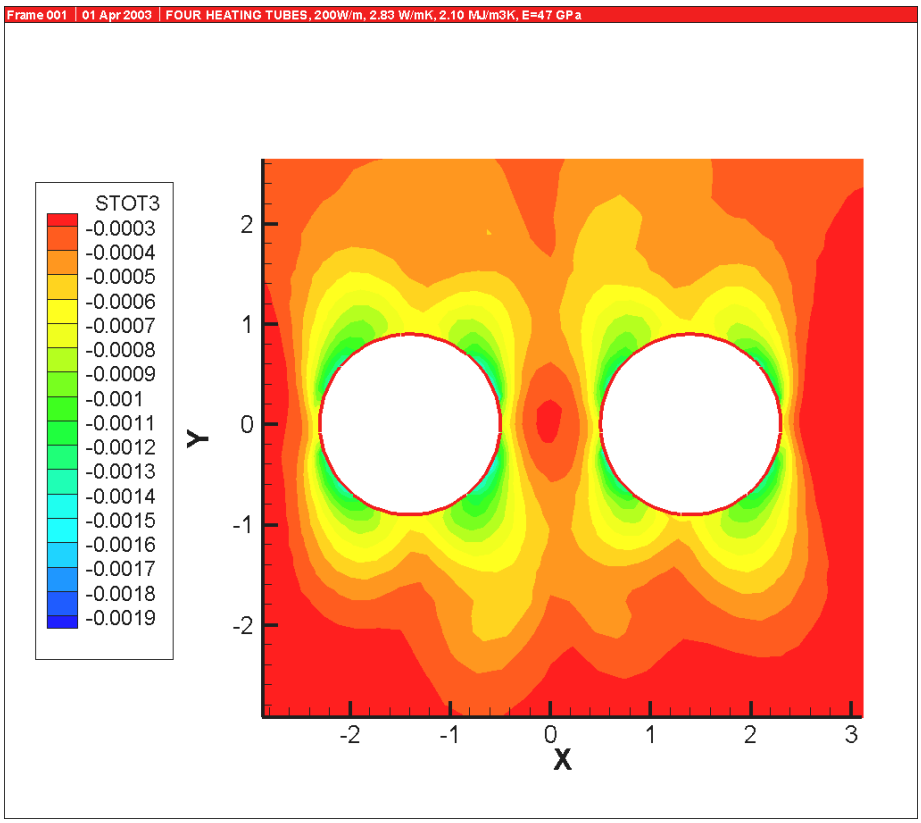

Figure G4. *Minor principal strain after 30 days of heating. 0.5 m below the tunnel floor. Lowest Case.*

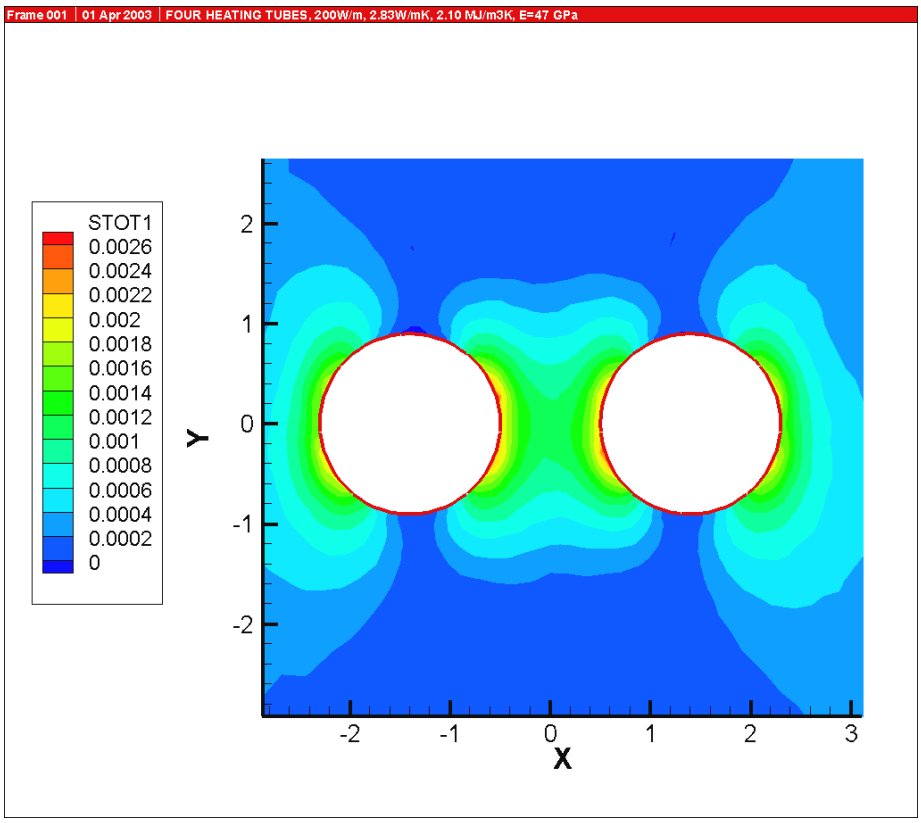

Figure G5. *Major principal strain after 60 days of heating. 0.5 m below the tunnel floor. Lowest Case.*

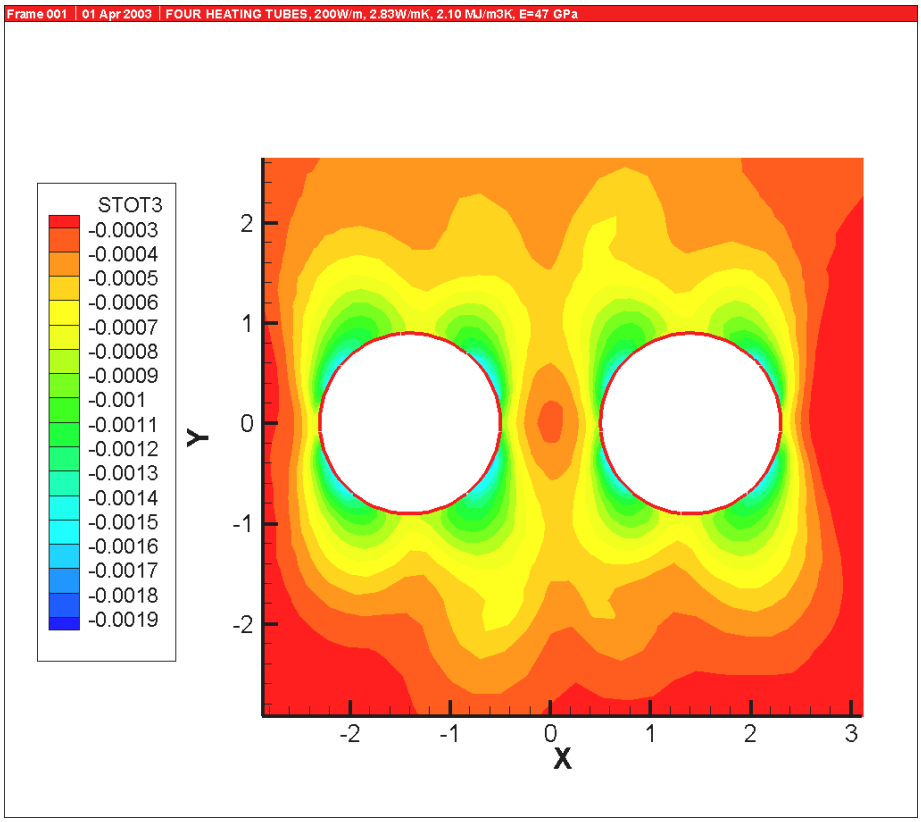

Figure G6. *Minor principal strain after 60 days of heating. 0.5 m below the tunnel floor. Lowest Case.*

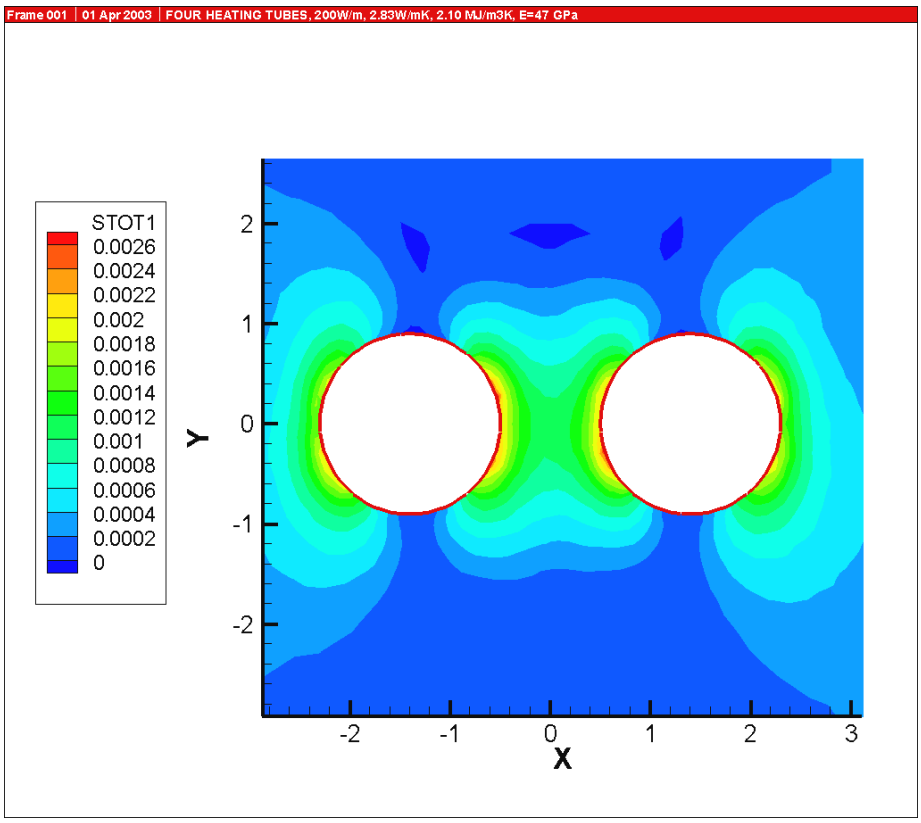

Figure G7. *Major principal strain after 90 days of heating. 0.5 m below the tunnel floor. Lowest Case.*

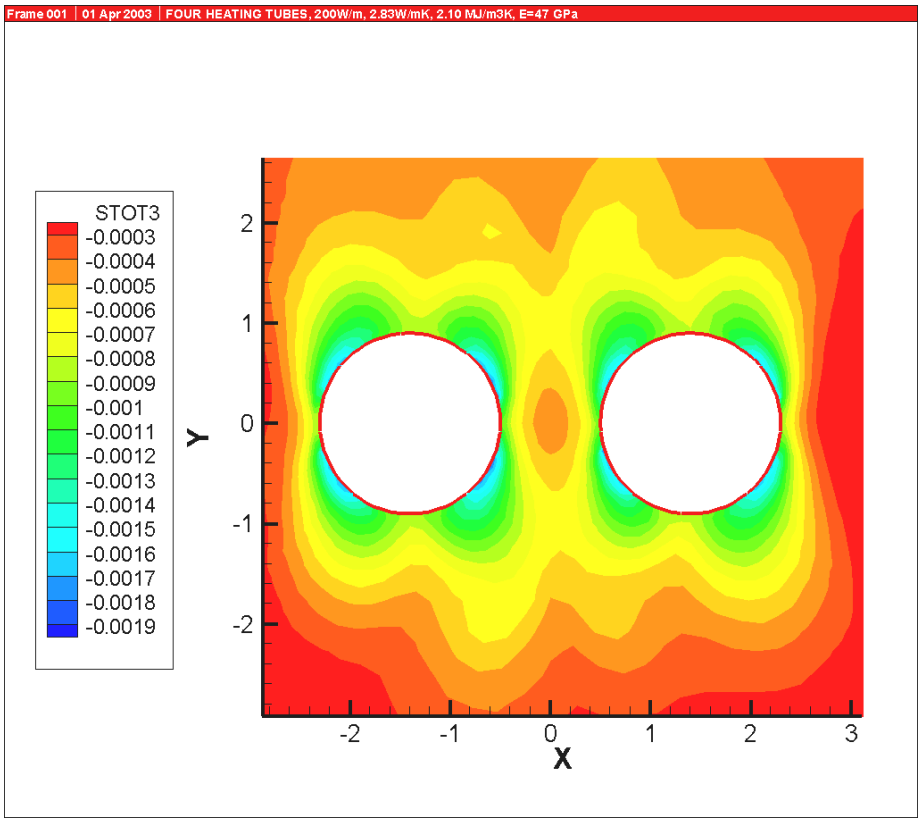

Figure G8. *Major principal strain after 90 days of heating. 0.5 m below the tunnel floor. Lowest Case.*

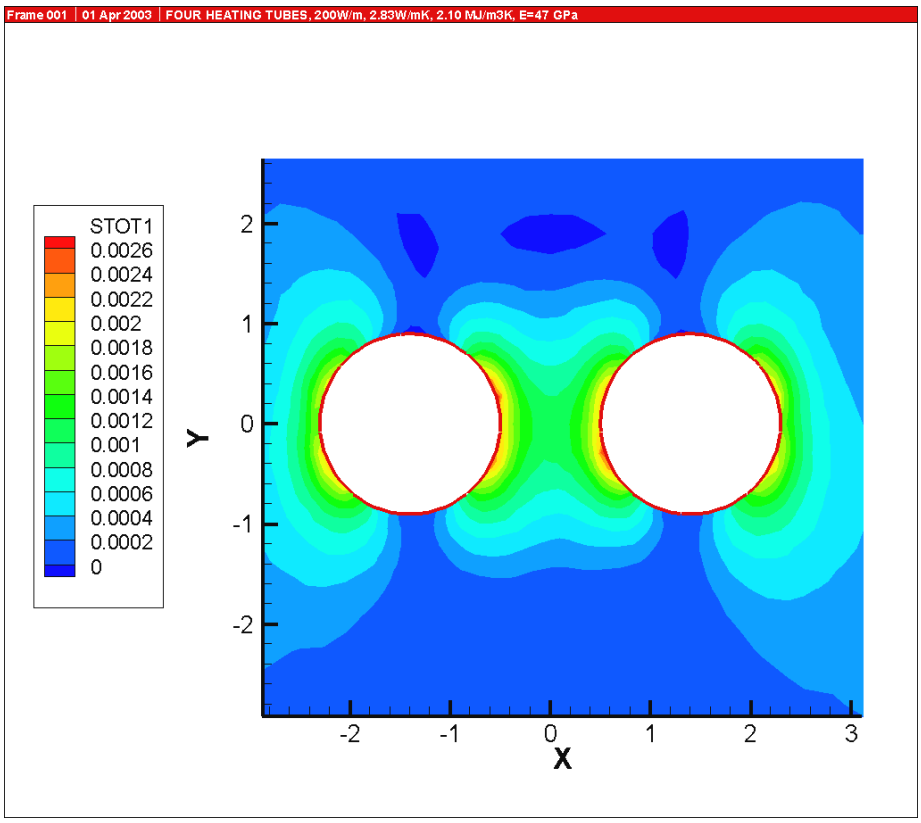

Figure G9. *Major principal strain after 120 days of heating. 0.5 m below the tunnel floor. Lowest Case.*

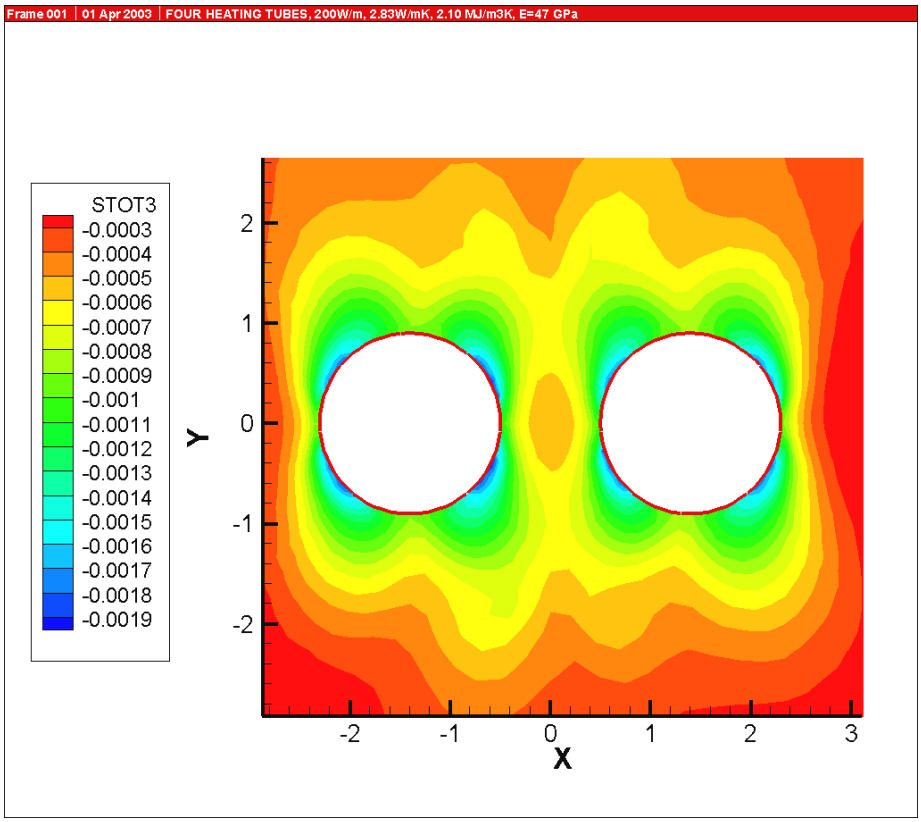

Figure G10. *Minor principal strain after 120 days of heating. 0.5 m below the tunnel floor. Lowest Case.*

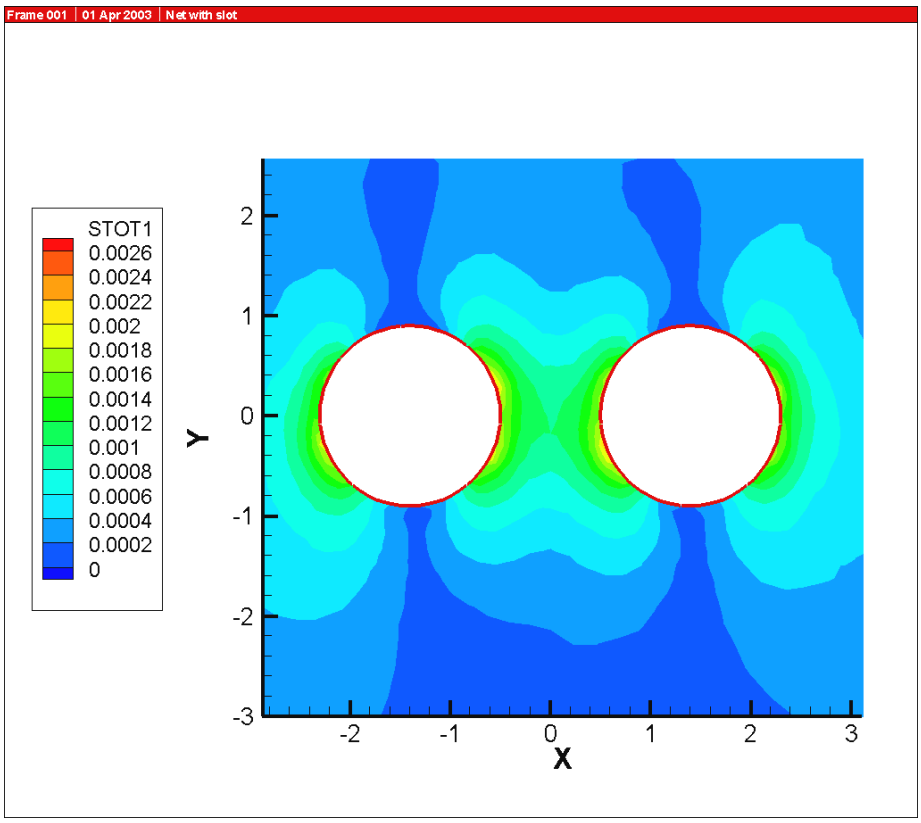

Figure G11. *Major principal strain before start heating. 0.5 m below the tunnel floor. Highest Case.*

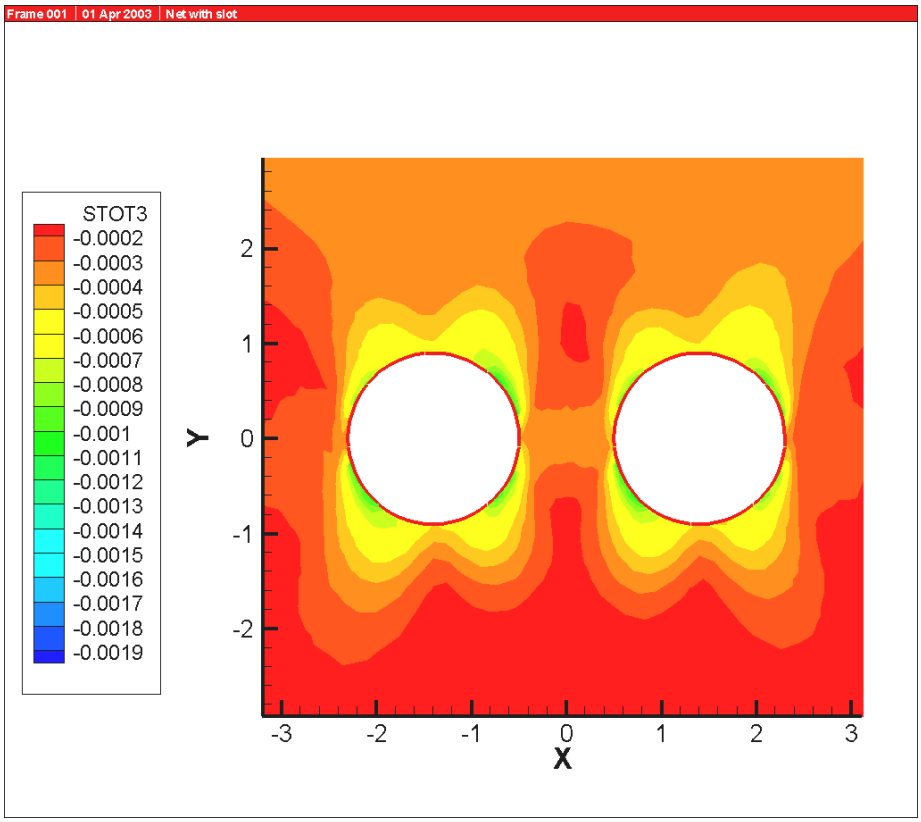

Figure G12*. Minor principal strain before start heating. 0.5 m below the tunnel floor. Highest Case.*

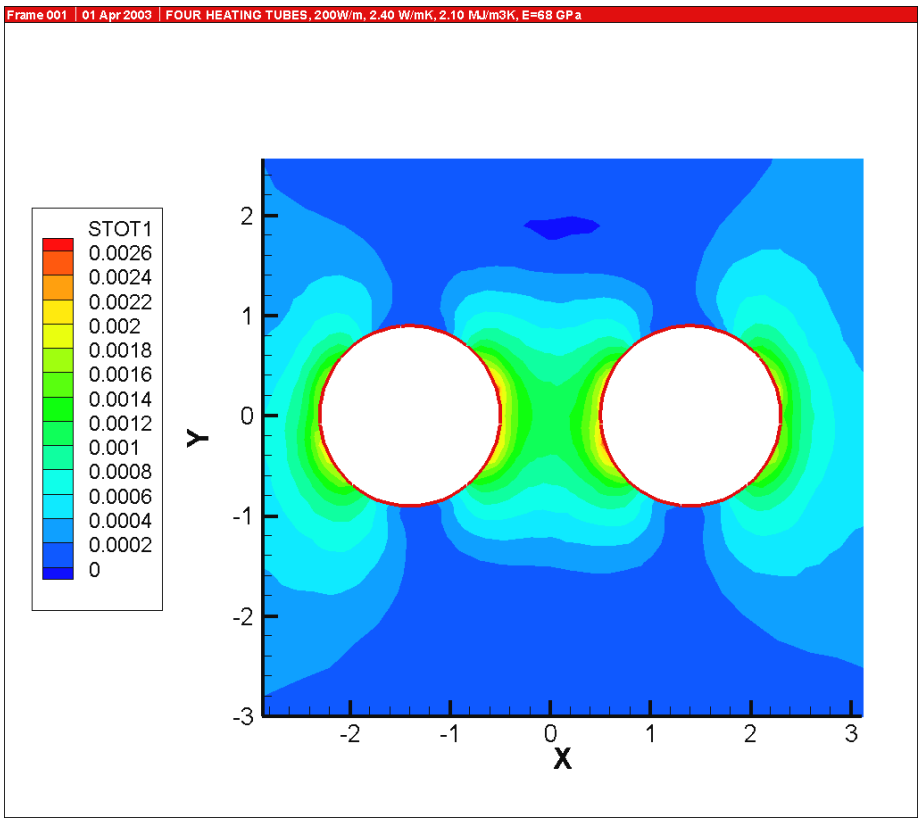

Figure G13. *Major principal strain after 30 days of heating. 0.5 m below the tunnel floor. Highest Case.*

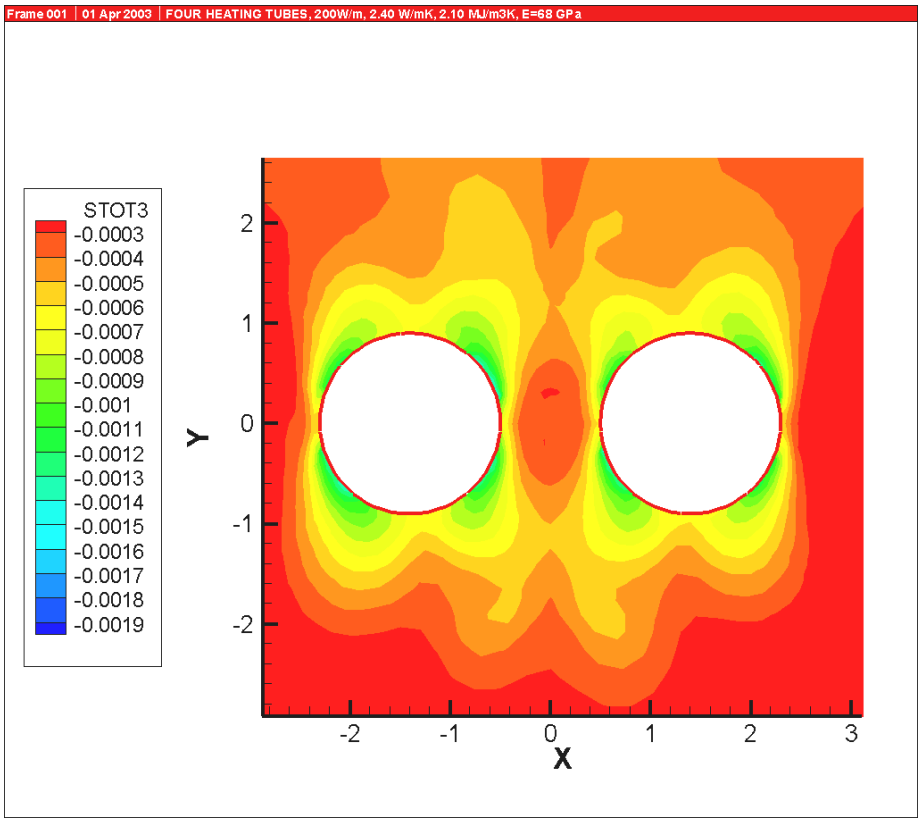

Figure G14. *Minor principal strain after 30 days of heating. 0.5 m below the tunnel floor. Highest Case.*

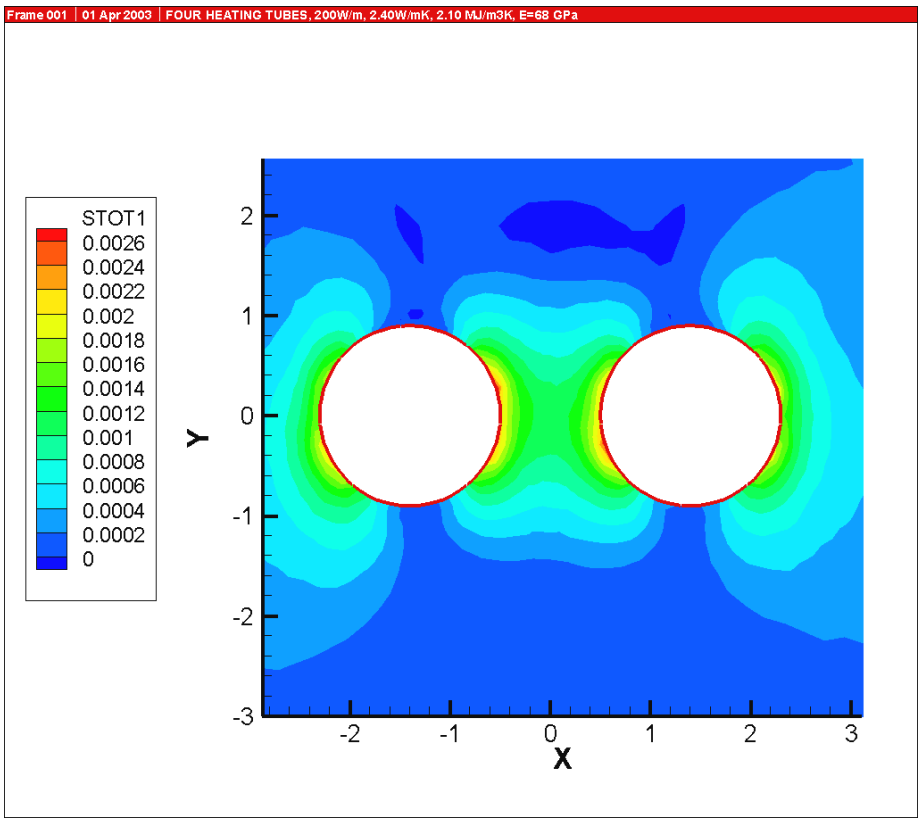

Figure G15. *Major principal strain after 60 days of heating. 0.5 m below the tunnel floor. Highest Case.*

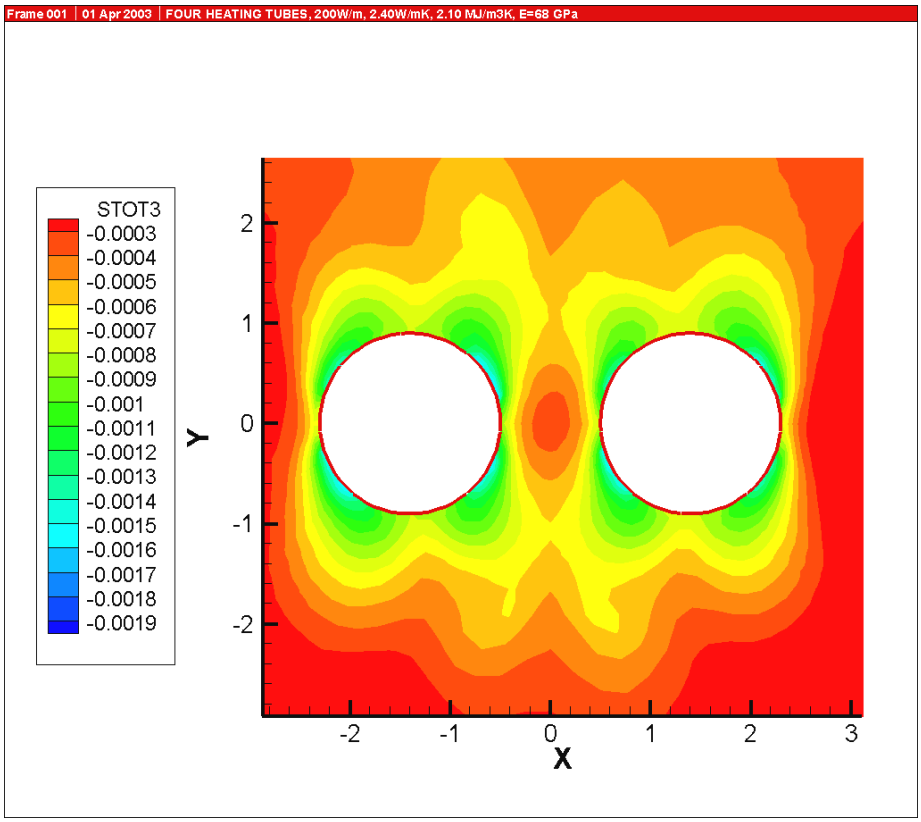

Figure G16. *Minor principal strain after 60 days of heating. 0.5 m below the tunnel floor. Highest Case.*

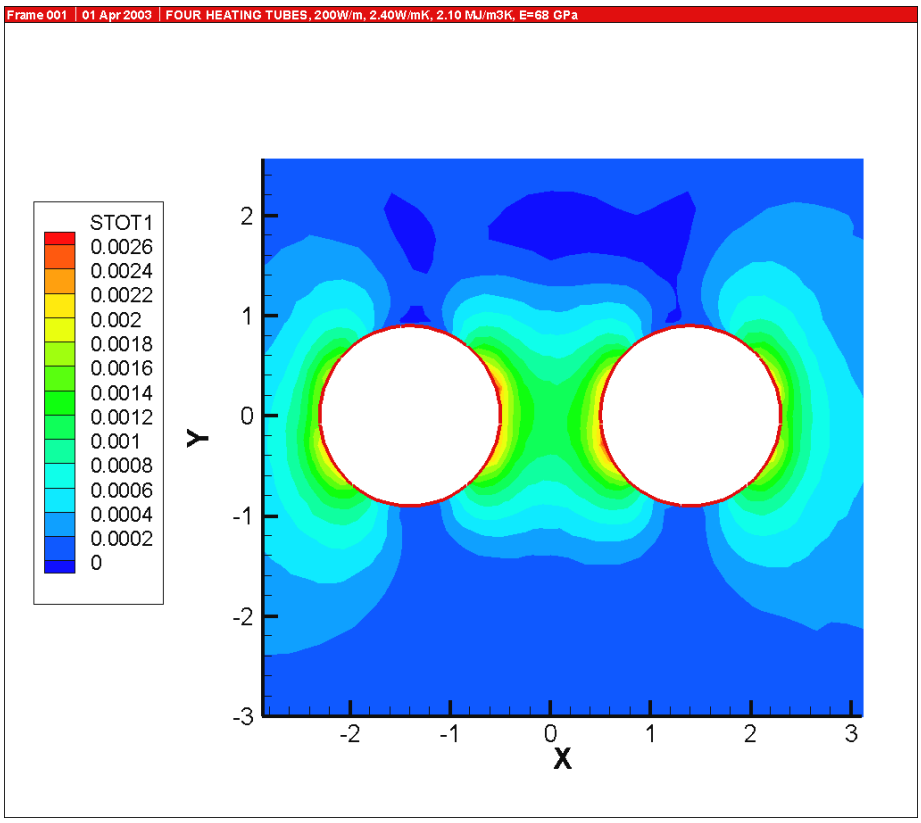

Figure G17. *Major principal strain after 90 days of heating. 0.5 m below the tunnel floor. Highest Case.*

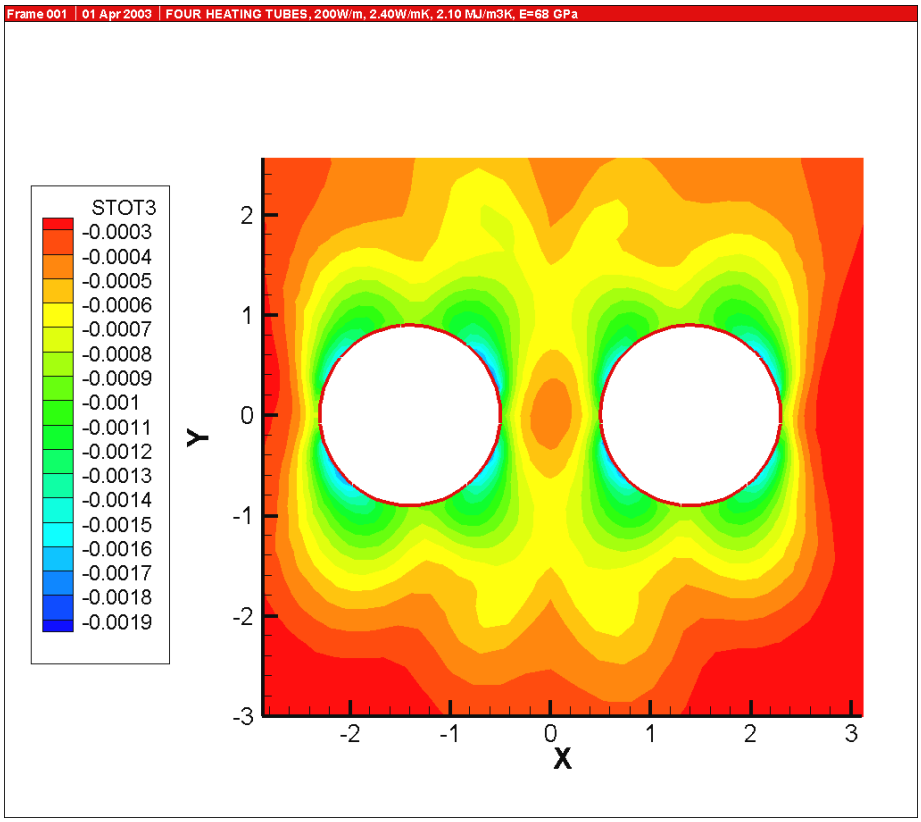

Figure G18 *Minor principal strain after 90 days of heating. 0.5 m below the tunnel floor. Highest Case.*

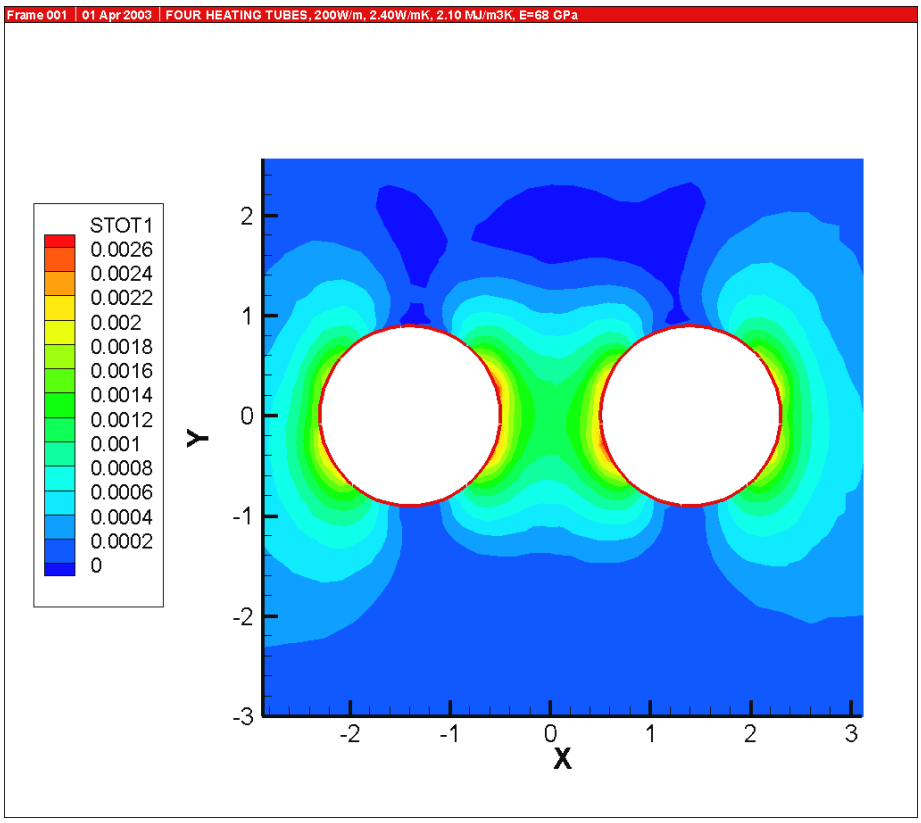

Figure G19. *Major principal strain after 120 days of heating. 0.5 m below the tunnel floor. Highest Case.*

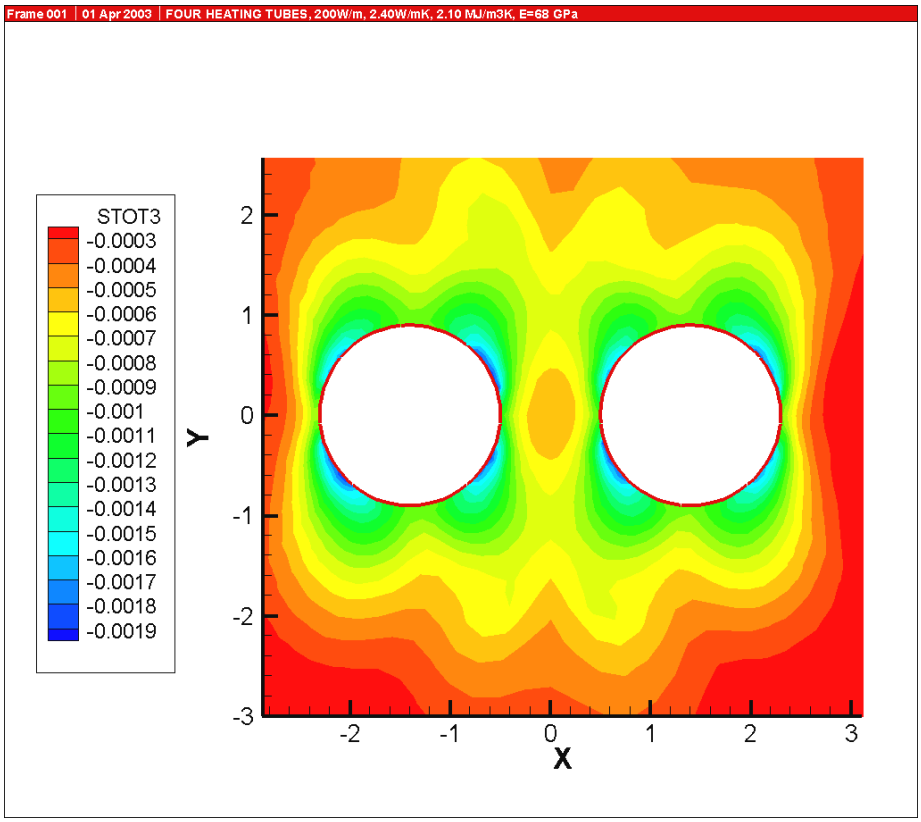

Figure G20. *Minor principal strain after 120 days of heating. 0.5 m below the tunnel floor. Highest Case.*

Appendix H: Vector deformation, vector and contour lines

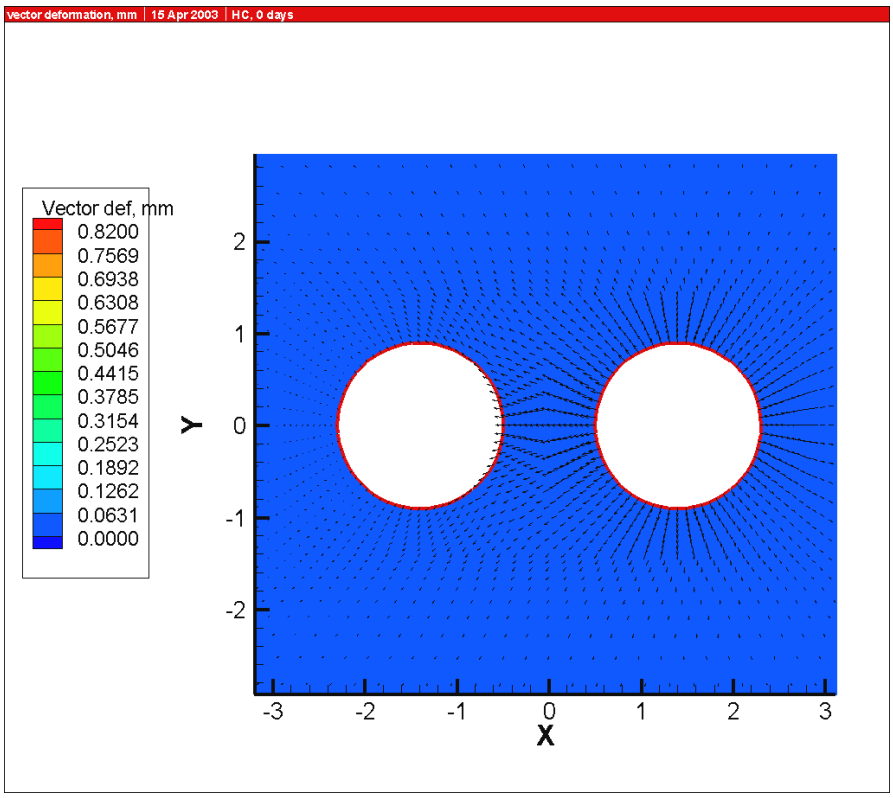

Figure 1. *Vector deformation (mm) for the highest case, before heating.*

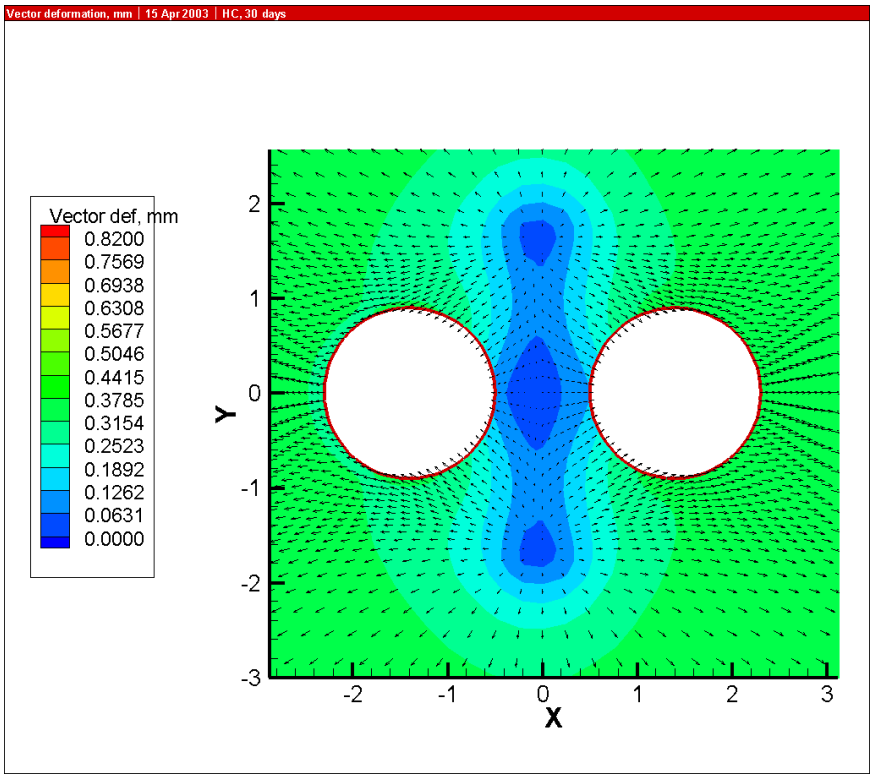

Figure 2 *Vector deformation (mm) for the highest case, 30 days of heating.*

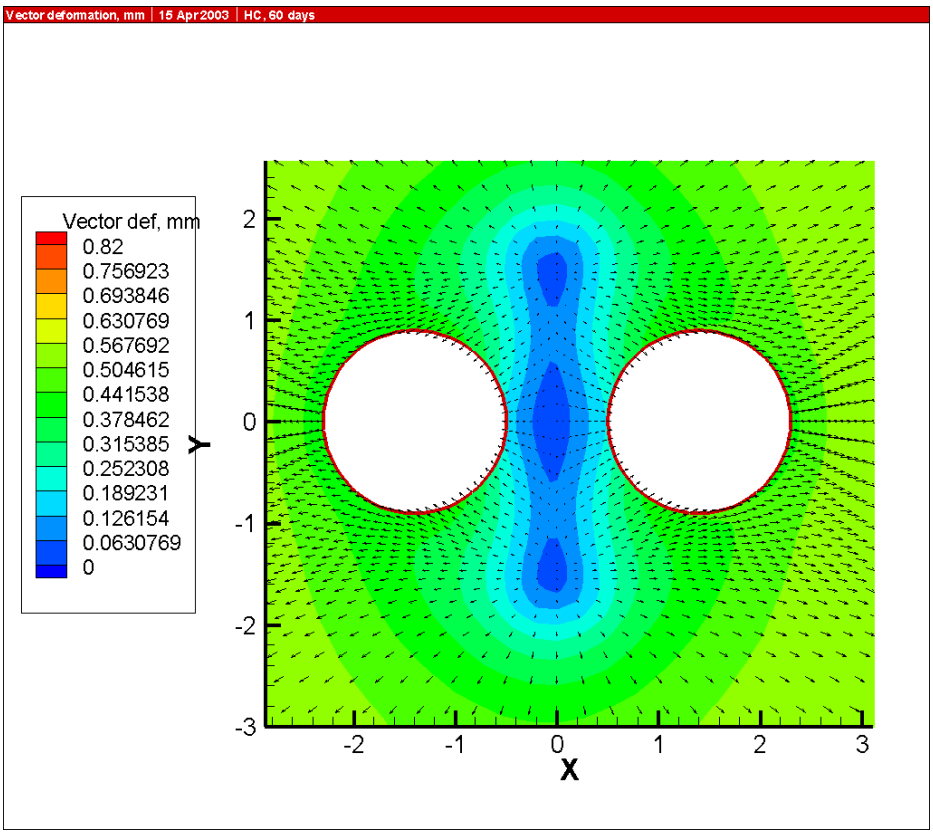

Figure 3 *Vector deformation (mm) for the highest case, 60 days of heating.*

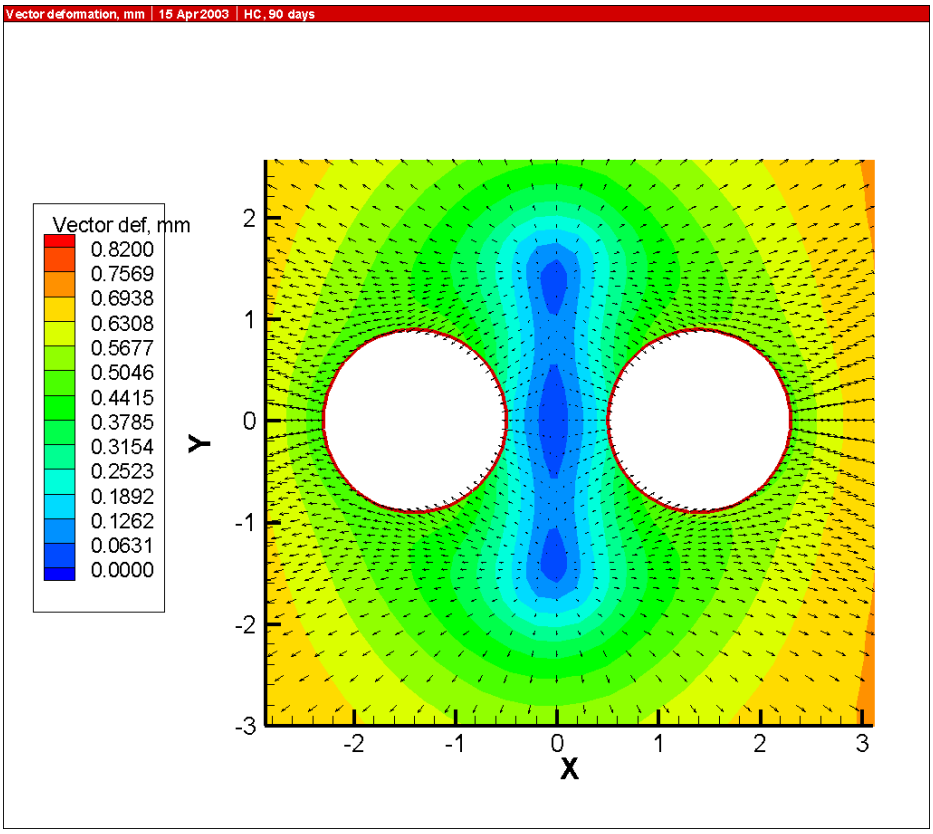

Figure 4 *Vector deformation (mm) for the highest case, 90 days of heating.*

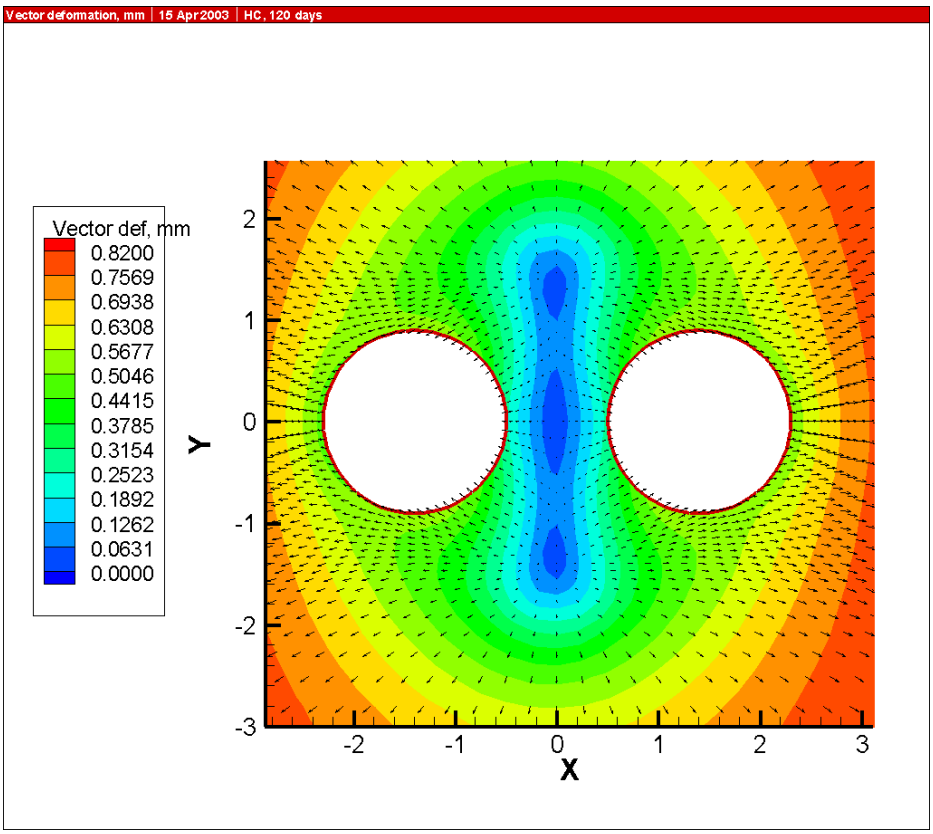

Figure 5. *Vector deformation (mm) for the highest case, 120 days of heating.*

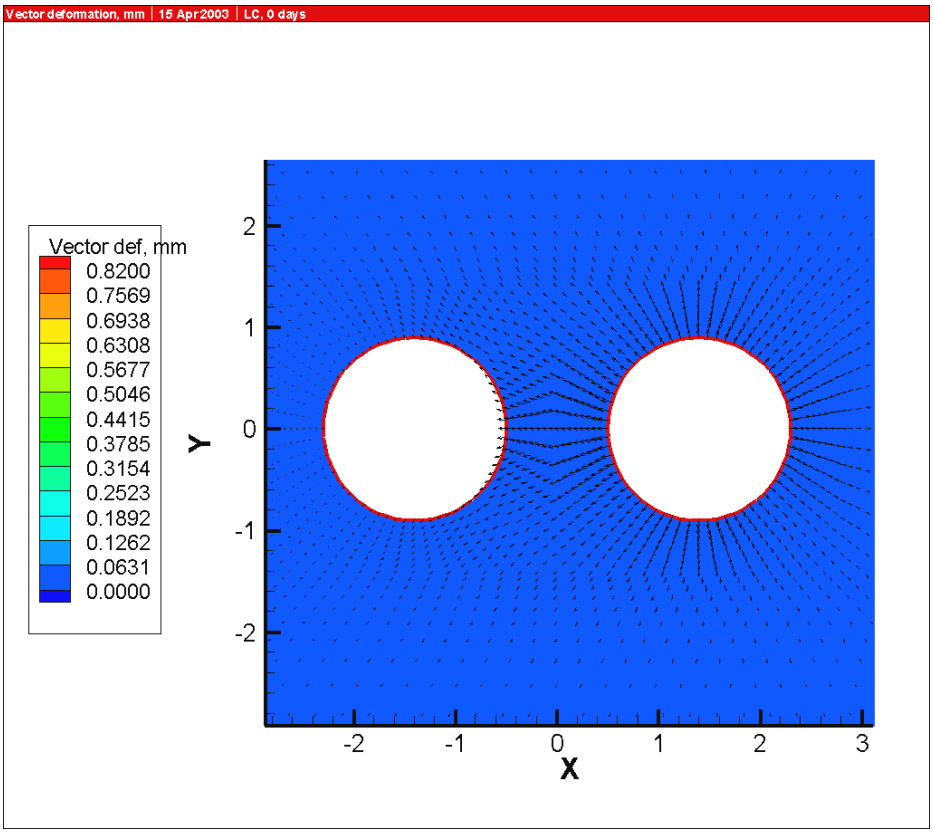

Figure 6 *Vector deformation (mm) for the lowest case, before heating.*

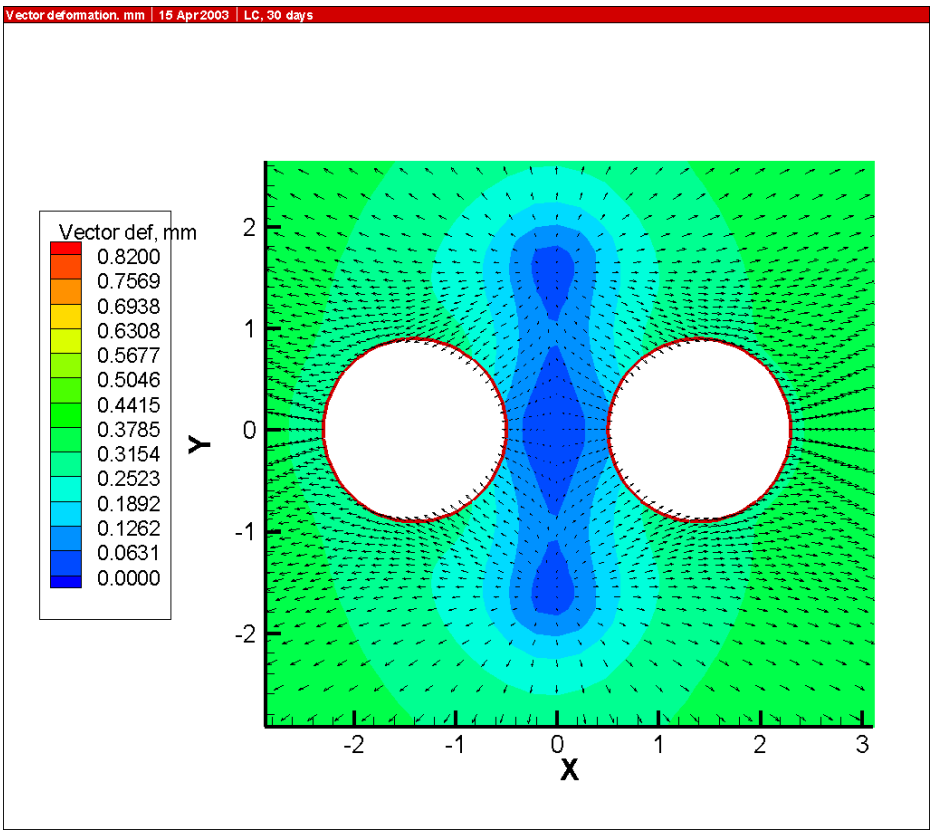

Figure 7 *Vector deformation (mm) for the lowest case, 30 days of heating.*

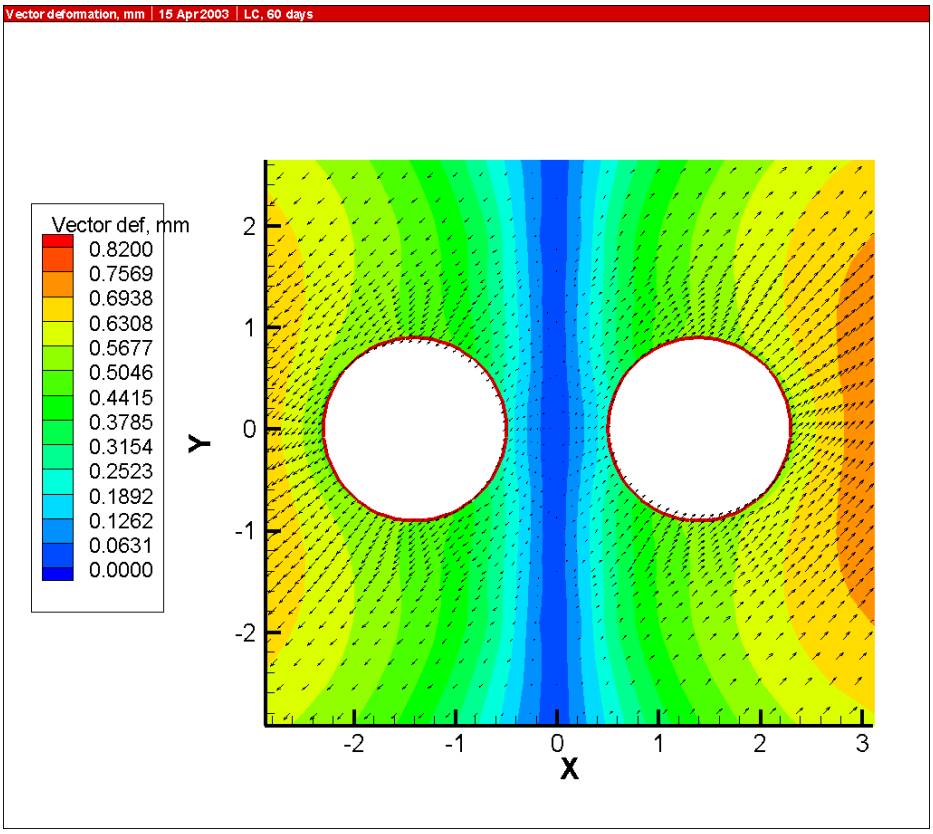

Figure 8 *Vector deformation (mm) for the lowest case, 60 days of heating.*

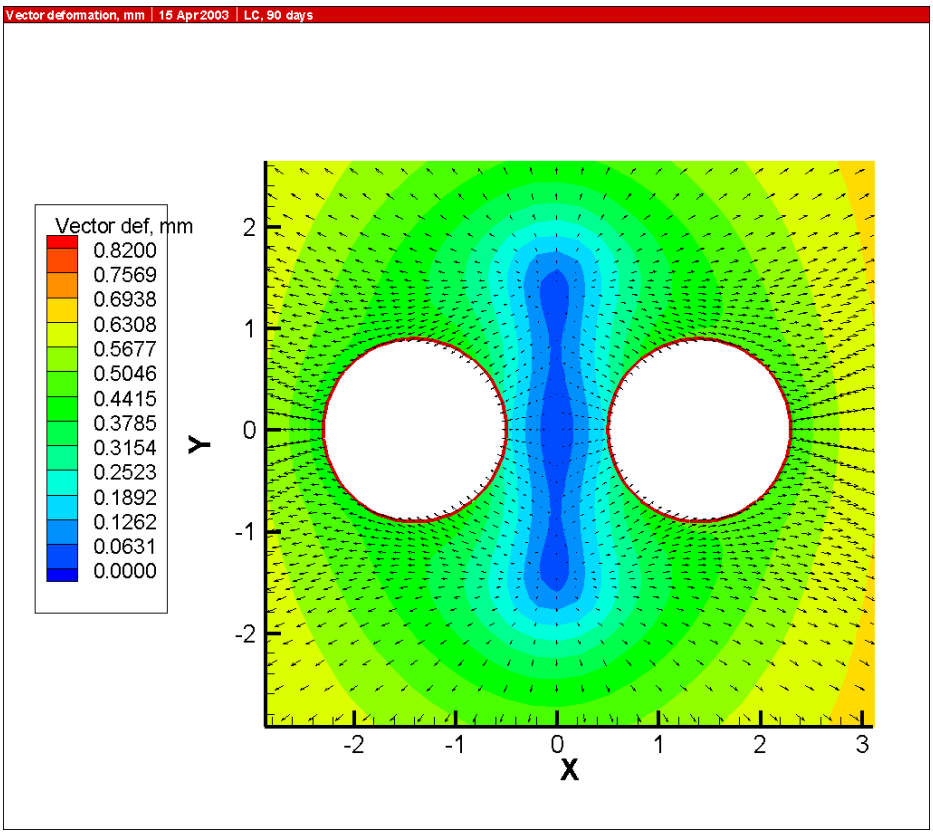

Figure 9 *Vector deformation (mm) for the lowest case, 90 days of heating.*

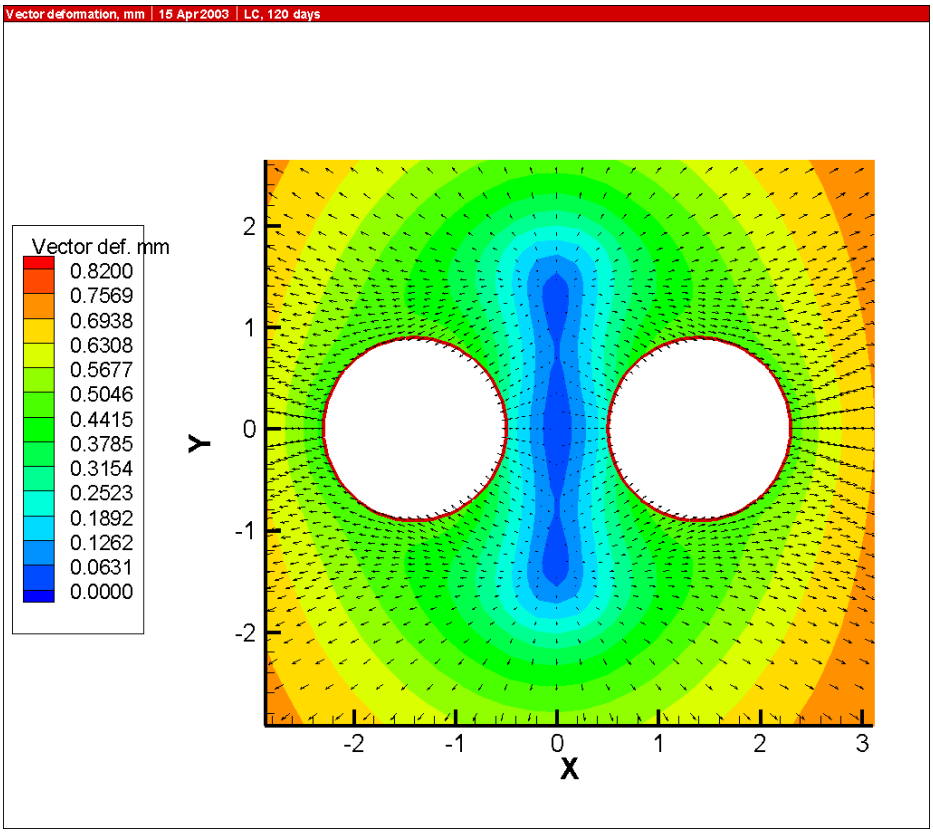

Figure 10 *Vector deformation (mm) for the lowest case,120 days of heating.*